NASA TECHNICAL MEMORANDUM

NASA TM X-72668

COPY NO.

NASA TM X-72668

FLOW VISUALIZATION STUDY OF CLOSE-COUPLED CANARD-WING AND STRAKE-WING CONFIGURATION

By Dennis D. Miner and Blair B. Gloss

March 3, 1975

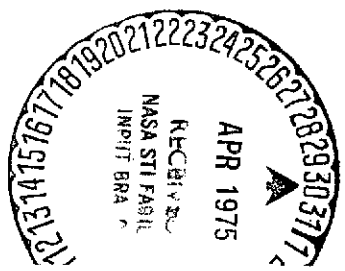

(NASA-TM-X-72668) FLOW VISUALIZATION STUDY OF CLOSE-COUPLED CANARD WING AND STRAKE WING CONFIGURATION (NASA) 115 p HC $5.25 CSCL 01A

N75-21247

Unclas
G3/02 18606

NATIONAL AERONAUTICS AND SPACE ADMINISTRATION

LANGLEY RESEARCH CENTER, HAMPTON, VIRGINIA 23665

1. Report No.	2. Government Accession No.	3. Recipient's Catalog No.
NASA TM X-72668		

4. Title and Subtitle	5. Report Date
FLOW VISUALIZATION STUDY OF CLOSE-COUPLED CANARD-WING AND STRAKE-WING CONFIGURATION	March 3, 1975
	6. Performing Organization Code
7. Author(s)	8. Performing Organization Report No.
Dennis D. Miner and Blair B. Gloss	
9. Performing Organization Name and Address	10. Work Unit No.
NASA Langley Research Center Hampton, Virginia 23665	505-11-21-02
	11. Contract or Grant No.
12. Sponsoring Agency Name and Address	13. Type of Report and Period Covered
National Aeronautics and Space Administration Washington, D. C. 20546	High No. TM X-
	14. Sponsoring Agency Code

15. Supplementary Notes

Final release of special information not suitable for formal publication.

16. Abstract

An investigation has been conducted in the Langley 1/8-scale V/STOL model tunnel to qualitatively determine the flow fields associated with semi-span close-coupled canard-wing and strake-wing models. Small helium filled bubbles were injected upstream of the models to make the flow visible. Photographs were taken over the angle-of-attack ranges of -10° to 40°.

17. Key Words (Suggested by Author(s)) (STAR category underlined)	18. Distribution Statement
Flow visualization Canard-wing Strake-wing	Unclassified-Unlimited

19. Security Classif. (of this report)	20. Security Classif. (of this page)	21. No. of Pages	22. Price*
Unclassified	Unclassified	115	$5.25

*Available from { The National Technical Information Service, Springfield, Virginia 22151
STIF/NASA Scientific and Technical Information Facility, P.O. Box 33, College Park, MD 20740

NATIONAL AERONAUTICS AND SPACE ADMINISTRATION

FLOW VISUALIZATION STUDY OF CLOSE-COUPLED CANARD-WING AND STRAKE-WING CONFIGURATION

By Dennis D. Miner and Blair B. Gloss

SUMMARY

An investigation has been conducted in the Langley 1/8-scale V/STOL model tunnel to qualitatively determine the flow fields associated with semi-span close-coupled canard-wing and strake-wing models. Small helium filled bubbles were injected upstream of the models to make the flow visible. Photographs were taken over the angle of attack range of -10° to 40°.

The results of this study indicate that the presence of a canard above or in the wing chord plane enhances the wing's leading edge vortex and delays the stall of the wing. At positive angles of attack, the wake of the canard located above the wing chord plane passes above the wing; however, over the same angle of attack range, the wing is in or above the wake of the canard located below the wing chord plane. Also, for the strake-wing configuration at angles of attack greater than 18°, there are three vortex systems associated with this model.

INTRODUCTION

Currently, NASA is conducting studies on devices, such as the close-coupled canard-wing and strake-wing combinations, which improve the performance of highly maneuverable aircraft at high angles of attack (Refs. 1, 2, 3). The data from these studies has been limited primarily to force data, with some theoretical analysis. Although the fighter type wing planforms, because of their moderate sweep angles, generally do not develop appreciable vortex lift the results of references 1 and 3 have indicated the presence of vortex lift on the wing in the presence of a canard. The wing-strake data of reference 2 has indicated that, in addition to the strong vortex lift generated on the strake, a favorable interference on the wing lift characteristics. As a result, this cursory flow visualization study was initiated to ascertain the general nature of the flow fields associated with the canard, strake, wing configurations.

This study used semi-span canard-wing and strake-wing models (scaled versions of those models used in Refs. 1, 2, and 3) mounted on a reflection plane. Helium filled soap bubbles were injected into the tunnel flow upstream of the model, and as these small bubbles passed through the flow field, photographs were taken. The tests were conducted in the Langley 1/8-scale V/STOL model tunnel at a dynamic pressure of approximately 1.5 lbf/ft^2. Angles of attack were from -10 to 40°.

MODEL DESCRIPTION

The canard-wing model investigated is shown in Figure 1 and the strake-wing model is shown in Figure 2. The same wing is used on both models. The model

planforms studied were scaled down versions of those used in References 1, 2, and 3. The canard and wing were constructed from 0.25 inch thick plexiglass and the strake was made of 0.125 inch thick brass. All models were uncambered with sharp beveled edges; the wing and canard had a 1/2" bevel and the strake had a slight bevel. All three components were painted glossy black to produce the best contrast between model and soap bubbles.

The model configurations studied were: (1) canard alone; (2) wing alone; (3) canard located above the wing chord plane in the presence of the wing (high canard); (4) canard located in the wing chord plane in the presence of the wing (mid canard); (5) canard located below the wing chord plane in the presence of the wing (low canard); (6) strake and wing. For a detailed definition of the vertical positions of the canard see Figure 3.

APPARATUS AND TEST PROCEDURES

The present investigation was conducted in the Langley 1/8-scale V/STOL model tunnel. Figure 4 shows two views of the tunnel test section. The flow field was visualized by injecting small, neutrally bouyant, helium filled, soap bubbles into the freestream forward of the model. The bubble head (that piece of equipment from which the bubbles eminated) was attached to a thin dowel rod so that the bubbles could be directed to the desired flow field region. The source of light was a high-intensity lamp mounted downstream of the model and directed upstream. The lamp has louvers to help "focus" the light beam. The camera used in this study was a Hasselblad, model 500 EL/M, 70 mm. The film used was Kodak Tri-X Pan, 70 mm., black and white, which had an ASA rating of 400. A development process was used which pushed the ASA rating to approximately

1000. This helped to heighten the contrast between the model and the bubbles. The best camera setting found for this test was a shutter speed of 1/8 second and a 5.6 f-stop. At this speed and setting, the bubbles produced streaks on the photographic film as they passed through the flow field. Since all models had sharp leading edges, the flow field about the models was probably not significantly affected by variations in tunnel velocity, i.e. Reynolds number; so the tunnel was operated at a dynamic pressure of approximately 1.5 lbf/ft^2 which was found to give the best photographic results. Photographs were taken of the models at angles of attack from -10 to 40 degrees.

DISCUSSION OF RESULTS

Figures 5-73 present photographs of the flow fields of the canard wing configurations and Figures 74-102 the strake-wing configuration. It should be noted that the helium bubbles injected into the flow field are generally neutrally buoyant whose average diameter was approximately 0.1 inch. Thus, if the flow field details were too small, for example the leading edge vortex at the planform apex, the bubbles would not show the detail because of their physical size.

There are photographs at low angles of attack that show no leading edge vortex, only a slight ripple of the flow near the leading edge. The conclusion that no vortex exists should not be drawn without further examination since the vortex might be too small or weak to trap a soap bubble.

Occasionally, the light reflected from the white picture identification numbers is reflected from the glossy wing leading edge. (See Figure 18 for an example). Although it is readily seen that it is not a bubble streak, the

reader should be alerted to this photographic phenomena. Also the camera angle relative to the models is not always the same for all configurations and angles of attack.

In the following, high canard, mid canard, and low canard refer to the canard position relative to the wing chord plane.

I) Canard-Wing Configuration

a) ALPHA = -10°: Figures 5-14 present the canard-wing configuration at -10° angle of attack. It should be noted that, since the canard and wing have no camber, twist, or dihedral the top view of the flow field at -10° angle of attack is also the bottom surface flow field for the model at a positive 10° angle of attack. The photographs for all the configurations at this angle of attack show no spanwise flow on the upper surface of the model. Figure 9 (high canard) shows that the wing is in the canard's wake at -10° angle of attack.

b) ALPHA = 0°: Figures 15 and 16 are photographs of the mid and low canard-wing configurations. These pictures are typical of all configurations at 0° angle of attack.

c) ALPHA = 10°: The configurations at an angle of attack of 10° are presented in Figures 17-27. The canard alone picture (Fig. 17) shows a fairly streamwise flow field. The bubble streaks show no indication of leading edge vortex formation. However, as mentioned earlier, a vortex may exist, but it may too small and weak to be detected by the soap bubbles. The bubble streaks in Figures 18 and 19 (wing alone) indicate that the flow has separated all along the leading edge. Note the rippling of the bubble

streaks near the leading edge. Comparing the photograph in Figure 17 (canard alone) with those in Figures 20, 23 and, 25 (high, mid, low canards respectively), it is clear that the wing up wash has enhanced the leading edge vortex of the canard. Again note the rippling of the bubble streaks near the leading edge. It is felt that the canard leading edge vortex (as depicted in Figures 20, 23, & 25) does not have enough strength to entrain the soap bubbles; thus there is no visualization of the vortex details. A comparison of Figures 18 and 19 (wing alone) with Figures 21, 24 and 26 (wing in the presence of the high, mid, and low canard, respectively) show two things: (1) no large flow changes on the wing due to the canard at this angle of attack, 10°; (2) bubbles have entered the leading edge vortex flow field of the wing for the high and low canard configurations which may indicate a stronger vortex system for these two configuration than for the wing alone configuration. Comparing Figures 22 and 27 it is clear that the canard wake flows above the wing for the high canard configuration and below the wing for the low canard configuration.

d) ALPHA = 12°: Figures 28 and 29 are presented to show that in general the vortex systems for the canard and wing become visible at this angle of attack. The leading edge vortex has not burst on the wing till approaching the wing trailing edge (Figure 29), however it appears that the canard vortex (Figure 28) has burst near mid-span at 1/4 chord. Leading edge vortex bursting is believed to have occurred when the vortex appears to grow in radial size rather abruptly.

e) ALPHA = 15°: Figures 30-39 present the photographs of the canard-wing configurations at 15° angle of attack. In comparing Figure 30 (canard alone) to the high, mid, and low canard pictures of figures 32, 35, and 37

respectively, it appears that the canard vortex is strengthened when the canard is in the presence of the wing. The canard leading edge vortices shown in all these photographs seem to be bursting half way between the root and tip. The leading edge vortex on the wing alone (Figure 31) is quite strong but bursts soon after forming. The addition of the high or mid canard (Figs. 33 and 36 respectively) noticeably delays the vortex bursting on the wing. But for the low canard (Figure 38) the leading edge vortex appears to start forming near mid span but bursts very soon after. Figures 34 and 39 again show that the high canard wake passes over the wing and that the wing is in the wake of the low canard.

f) ALPHA = 18°: The photographs showing several canard-wing configurations at 18° angle of attack are presented in Figures 40-43. In general, these flow fields show very few differences from the flow fields of these configurations at an angle of attack of 15°.

g) ALPHA = 20°: Figures 44-54 show the flow fields of the canard-wing combinations at 20° angle of attack. Comparing the canard alone, high canard, mid canard, and low canard pictures (Figures 44, 46, 49 and 52, respectively), it is seen that the leading edge vortex on the canard in the low position (Figure 52) appears to burst noticeably closer to the canard apex than the other canard configurations. The leading edge vortex on the wing alone, Figure 45, bursts considerably closer to the wing apex than the vortex on the wing in the presence of the high canard (Figure 47) or of the mid canard (Figure 50). The wing in the presence of the low canard (Figure 53) still has a small vortex forming near mid span. Figures 48, 51, and 54 are side views of the high, mid, and low canards in the presence of the wing and show the same canard wake trends established at lower angles of attack.

h) ALPHA = 25°: Figures 55 and 56 show the vortex flow field on the canard alone and on the wing with the mid canard.

i) ALPHA = 30°: The canard-wing models at an angle of attack of 30° are presented in Figures 57-65. Figure 57 shows the canard alone with the leading edge vortex bursting very close to the canard apex. The wing alone (Figure 58) appears to be completely stalled at this angle of attack. With the addition of a high or mid canard (Figs. 60 and 62, respectively) the positive influence of the canard on the wing is readily seen. In both cases the wing has a leading edge vortex, bursting close to the apex. The flow field of the wing in the presence of a high or mid canard is better organized than the flow field on the wing alone. However, both the canards, high and mid locations (Figures 59 and 61), are close to being stalled. For the low canard case (Figures 63 and 64), the canard is nearly stalled and the wing again has very disorganized flow with a short mid-span vortex. Figure 65 (wing with low canard) shows the flow being turned by the upwash of the wing. This appears to produce an increase in effective angle of attack and stalls the wing sooner.

j) ALPHA = 40°: Figures 66-73 present the canard-wing models at 40° angle of attack. At this angle all canards and wings are stalled.

II) Strake-Wing Configuration

a) ALPHA = -10°: Figure 74 shows the strake-wing configuration at -10° angle of attack. The flow is streamwise with no apparent sidewash disturbances.

b) ALPHA = 0°: At 0° angle of attack (Figure 75), the flow field is very smooth with no spanwise flow.

c) ALPHA = 10°: As with the wing alone photographs (Figures 18 and 19) at 10° angle of attack, the wing with the strake has a slight disturbance along the wing leading edge (Figure 76). Again, there probably is a small, weak leading edge vortex that cannot trap a helium bubble so the bubble streaks just flow over the vortex. However, Figure 77 shows that a strake vortex has been formed. A side view of the strake-wing is presented in Figure 78.

d) ALPHA = 12°: At 12° angle of attack (Figure 79) the strake vortex becomes stronger and a wing leading edge vortex develops just outbound of the kink (where the strake meets the leading edge of the wing). This vortex appears to be bursting near the trailing edge of the wing.

e) ALPHA = 15°: Figures 80 and 81 present photographs of the strake-wing configuration at 15° angle of attack. A wing leading edge vortex is formed but it appears to be bursting further upstream than this vortex did at 12° angle of attack. Also a still tighter strake vortex is present than was present at 12° angle of attack.

f) ALPHA = 18°: At 18° angle of attack, a secondary wing leading edge vortex has appeared along with the vortex that developed at lower angles of attack (Figure 82). This secondary vortex was not expected; however, it appears to be very weak. A tight primary vortex is displayed in Figure 83. Figure 84 is a photograph of the strengthening strake vortex. No bursting of this vortex system occurs until higher angles of attack are reached. Another side view is provided by Figure 85.

g) ALPHA = 20°: Figures 86-90 present the strake-wing at 20° angle of attack. Figures 86 and 87 show the main wing vortex and Figures 88-90 show both the primary and secondary wing leading edge vortex systems. The

secondary leading edge vortex is weaker than the main vortex and sometimes gets wrapped up in it (Figure 89).

h) ALPHA = 25°: Figures 91-94 present several views of the strake-wing vortices. Figure 91 shows the main wing vortex bursting earlier than when the model was at 20° angle of attack. Figure 94 shows the tight core of the strake vortex created at these higher angles of attack.

i) ALPHA = 30°: The angle of attack of 30° for the strake-wing is shown in Figures 95-99. The wing primary vortex is bursting soon after forming but the secondary wing leading edge vortex is still present (Figure 97). Figure 99 shows the strake vortex bursting near the wing mid-root chord.

j) ALPHA = 34°: A photograph of the strake vortex is presented in Figure 100. This picture shows a good example of vortex bursting.

k) ALPHA = 40°: At 40° angle of attack, Figure 101 shows the wing is now stalled. The strake vortex (Figure 102) is now bursting near the wing's leading edge.

CONCLUDING REMARKS

Semi-span, close-coupled canard-wing and strake-wing models were mounted in the Langley 1/8-scale V/STOL model tunnel to qualitatively determine the flow field about these models. Small helium filled soap bubbles were injected into the flow upstream of the models to make the flow field visable. Photographs were taken over the angle of attack range of -10° to 40° at 0° sideslip. Some of the major results are outlined below:

1. The presence of a canard above or in the wing chord plane enhances the wing's leading edge vortex and delays wing stall.

2. At positive angles of attack the wake of the canard location above the wing chord plane passes over the wing, however, over the same angle of attack range, the wing is in or above the wake of the canard located below the wing chord plane.

3. For angles of attack greater than 18°, there are three separate vortex systems attached to the strake-wing configuration: strake leading edge vortex, a primary wing leading edge vortex emitting from the kink, and a secondary wing leading edge vortex.

REFERENCES

1. Gloss, Blair B.: Effect of Canard Location and Size on Canard-Wing Interference and Aerodynamic-Center Shift Related to Maneuvering Aircraft at Transonic Speeds. NASA TN D-7505; 1974.

2. Henderson, William P. and Huffman, Jarrett K.: Effect of Wing Design on the Longitudinal Aerodynamic Characteristics of a Wing-Body Model at Subsonic Speeds. NASA TN D-7099, 1972.

3. Gloss, Blair B.: The Effect of Canard Leading-Edge Sweep and Dihedral Angle on the Longitudinal and Lateral Aerodynamic Characteristics of a Close-Coupled Canard-Wing Configuration. NASA TN D-7814, 1974.

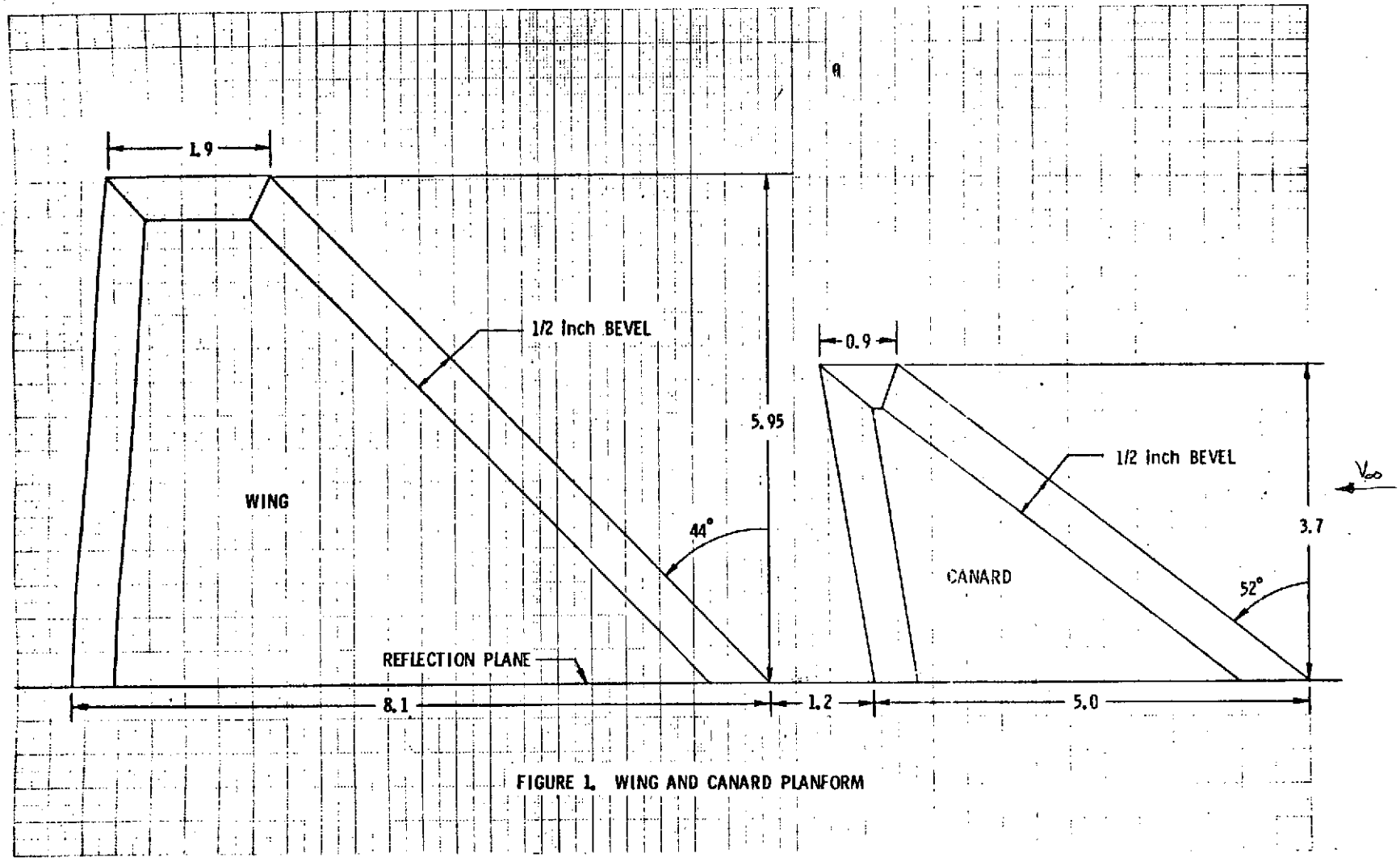

FIGURE 1. WING AND CANARD PLANFORM

X	Y
STA. 0.0	0.000
1.0	.150
2.0	.275
3.0	.400
4.0	.525
5.0	.700
6.0	.800
6.4	.875
6.8	.950
7.2	1.050
7.6	1.100
8.0	1.175
9.0	1.275
10.0	1.350
10.5	1.400

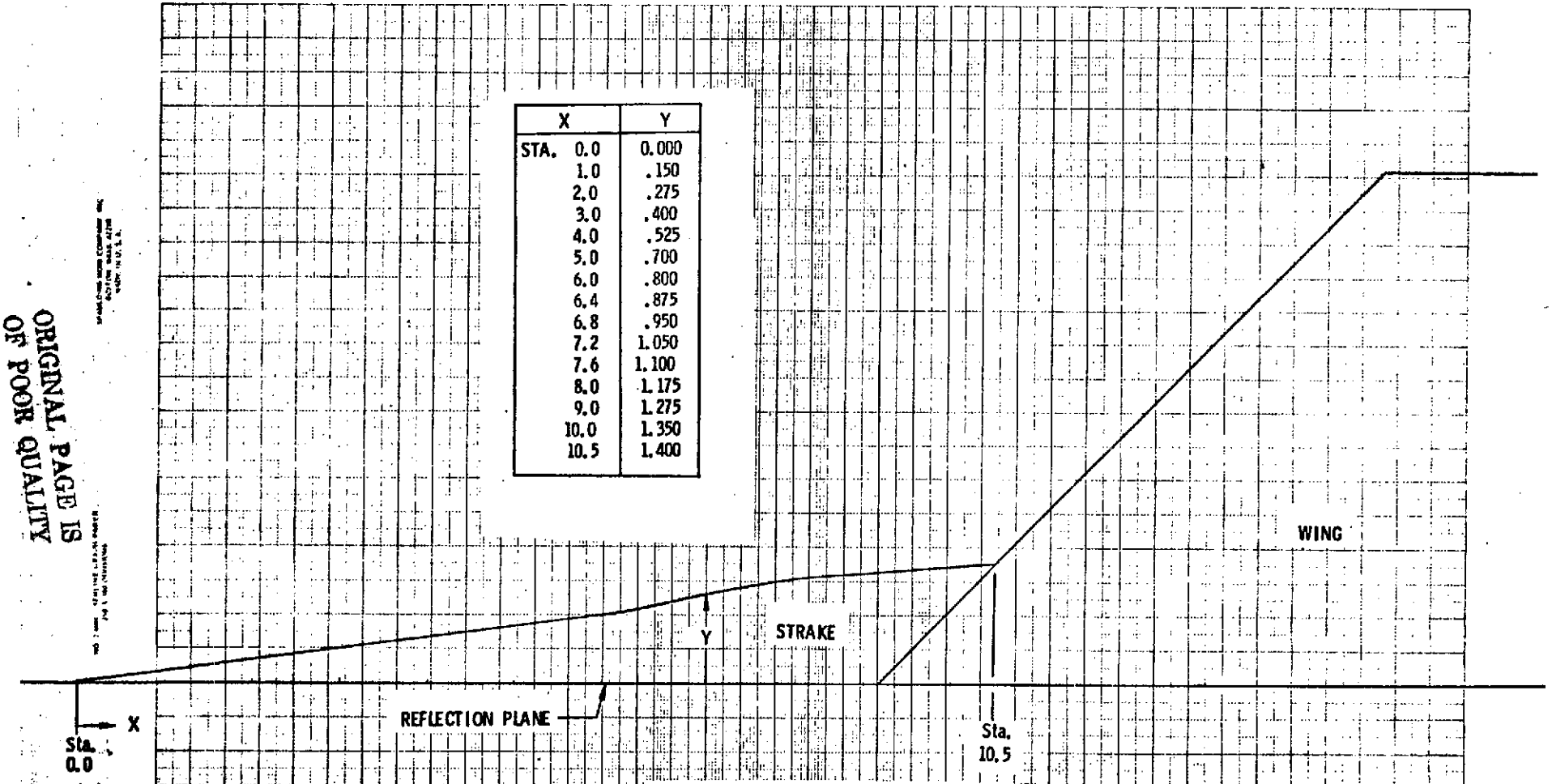

FIGURE 2. WING - STRAKE COMBINATION

FIGURE 3. WING - CANARD CONFIGURATIONS

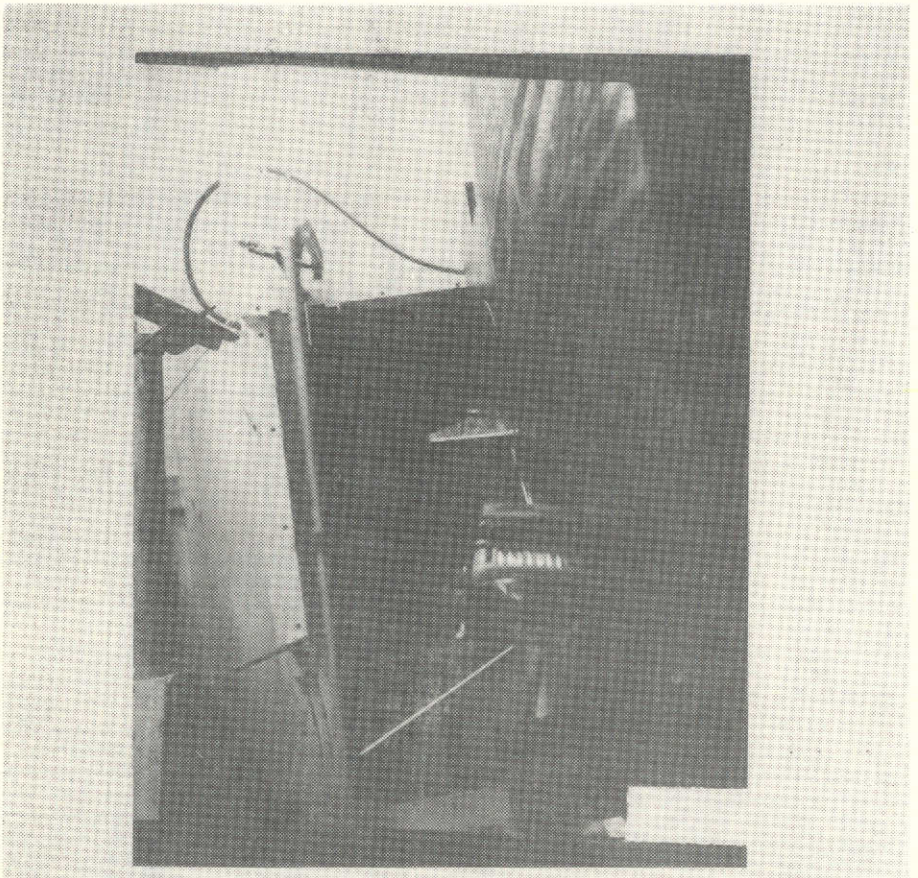

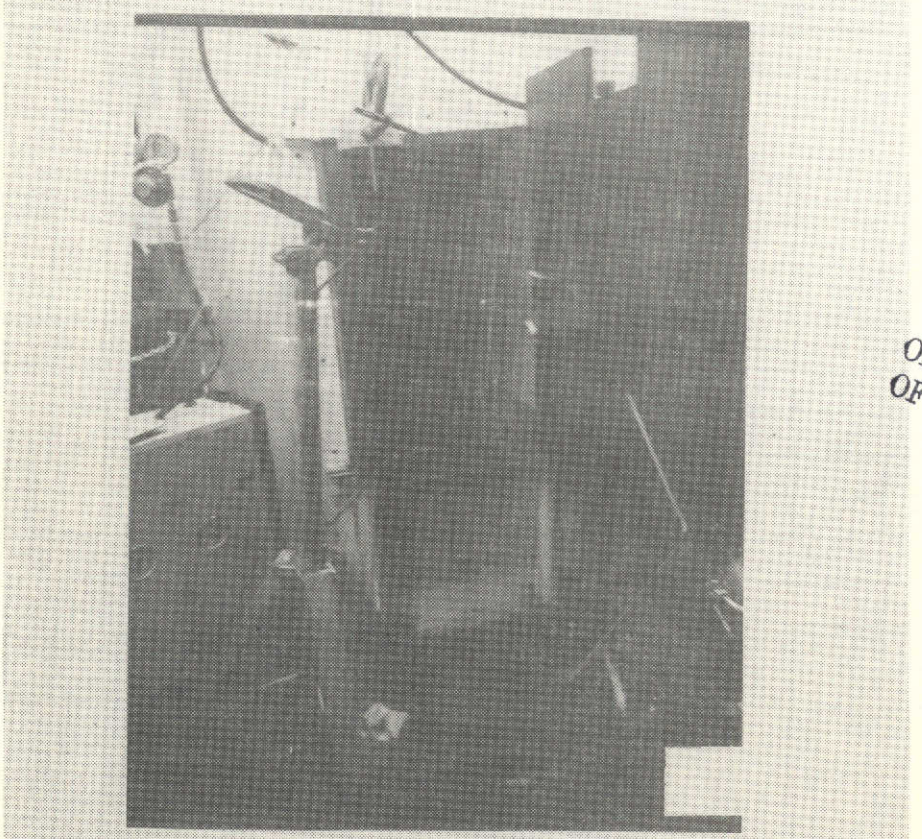

FIGURE 4. TWO VIEWS OF TUNNEL SET-UP

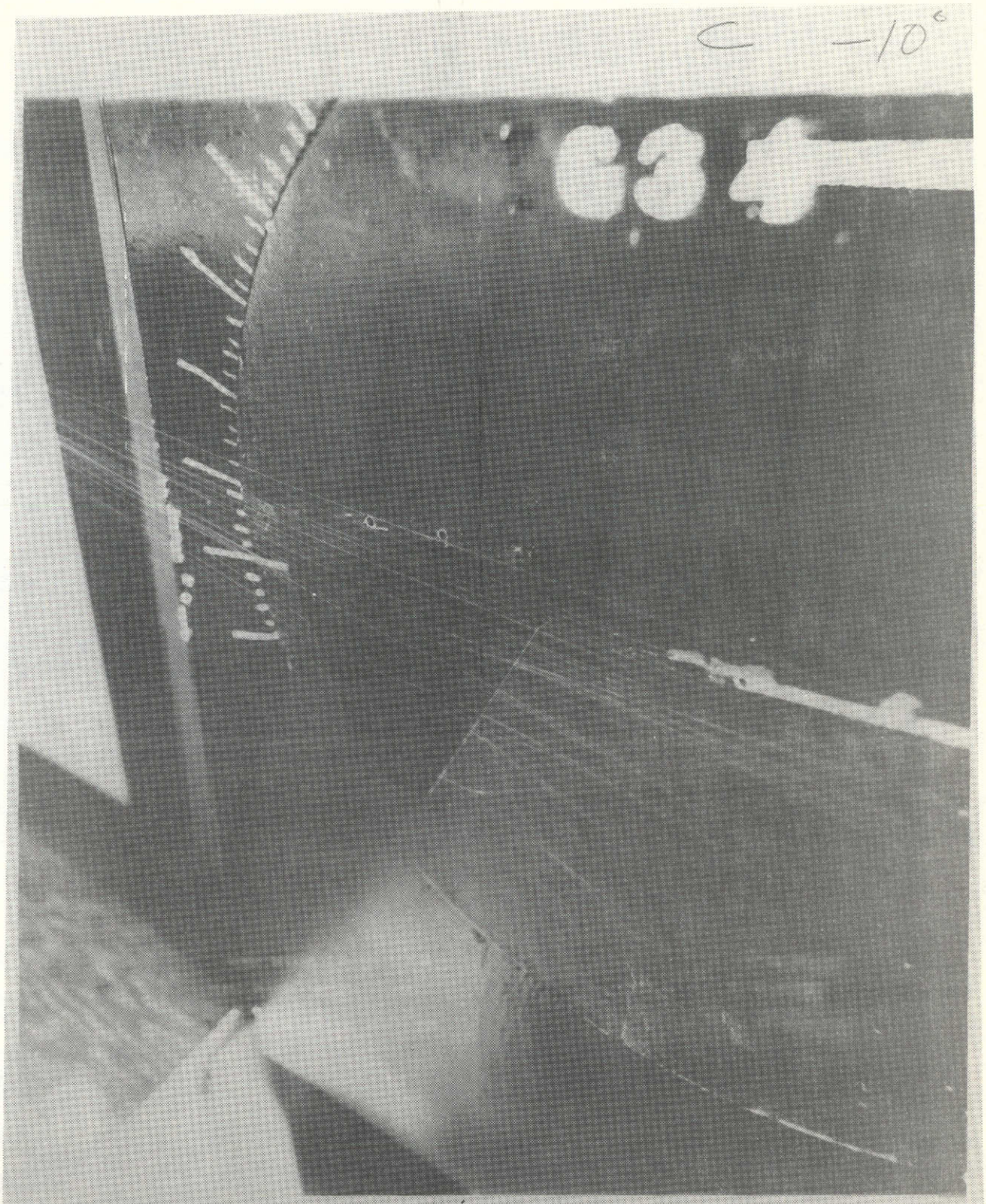

Figure 5. Canard alone at -10° angle of attack.

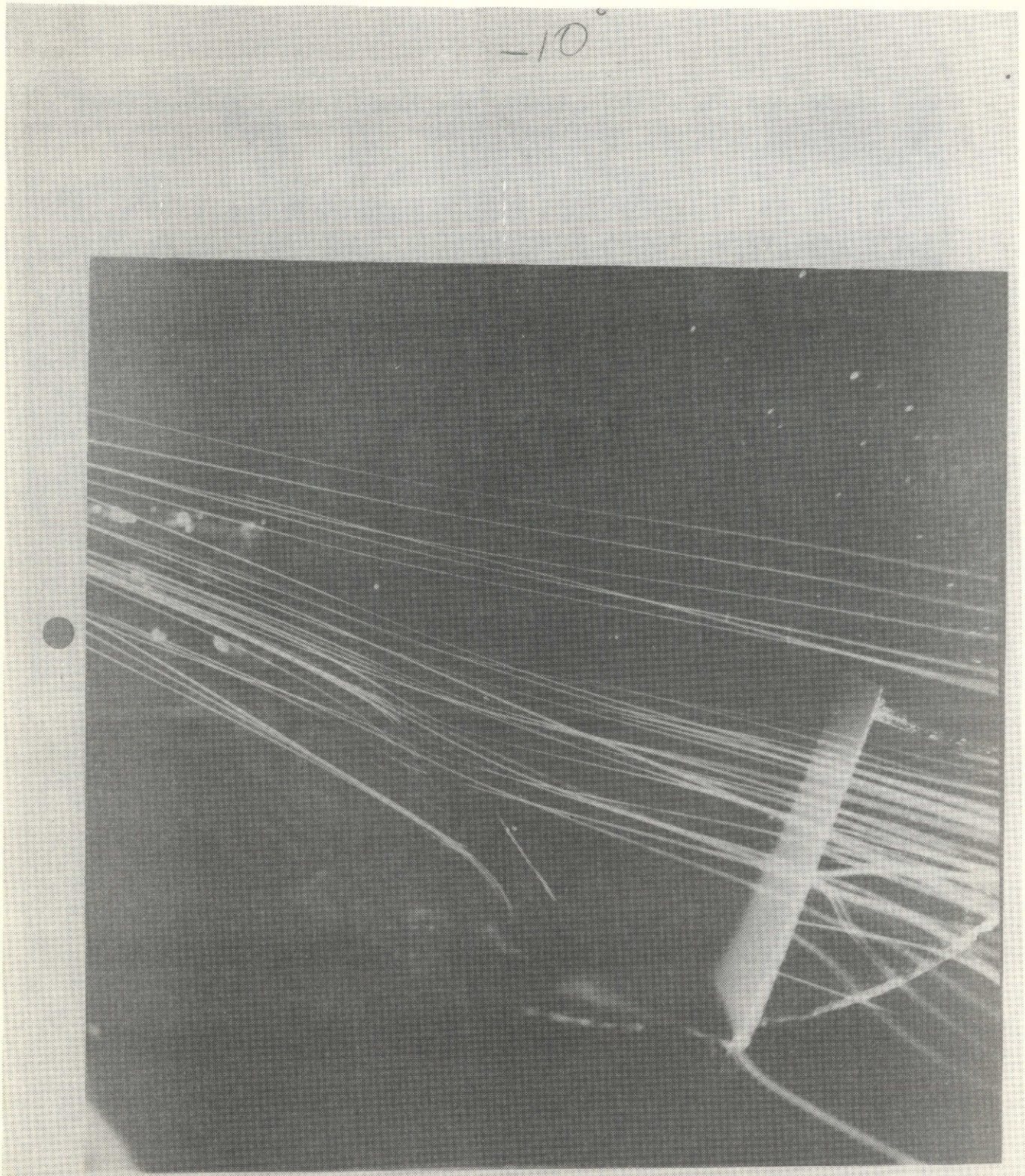

Figure 6. Wing alone at -10° angle of attack.

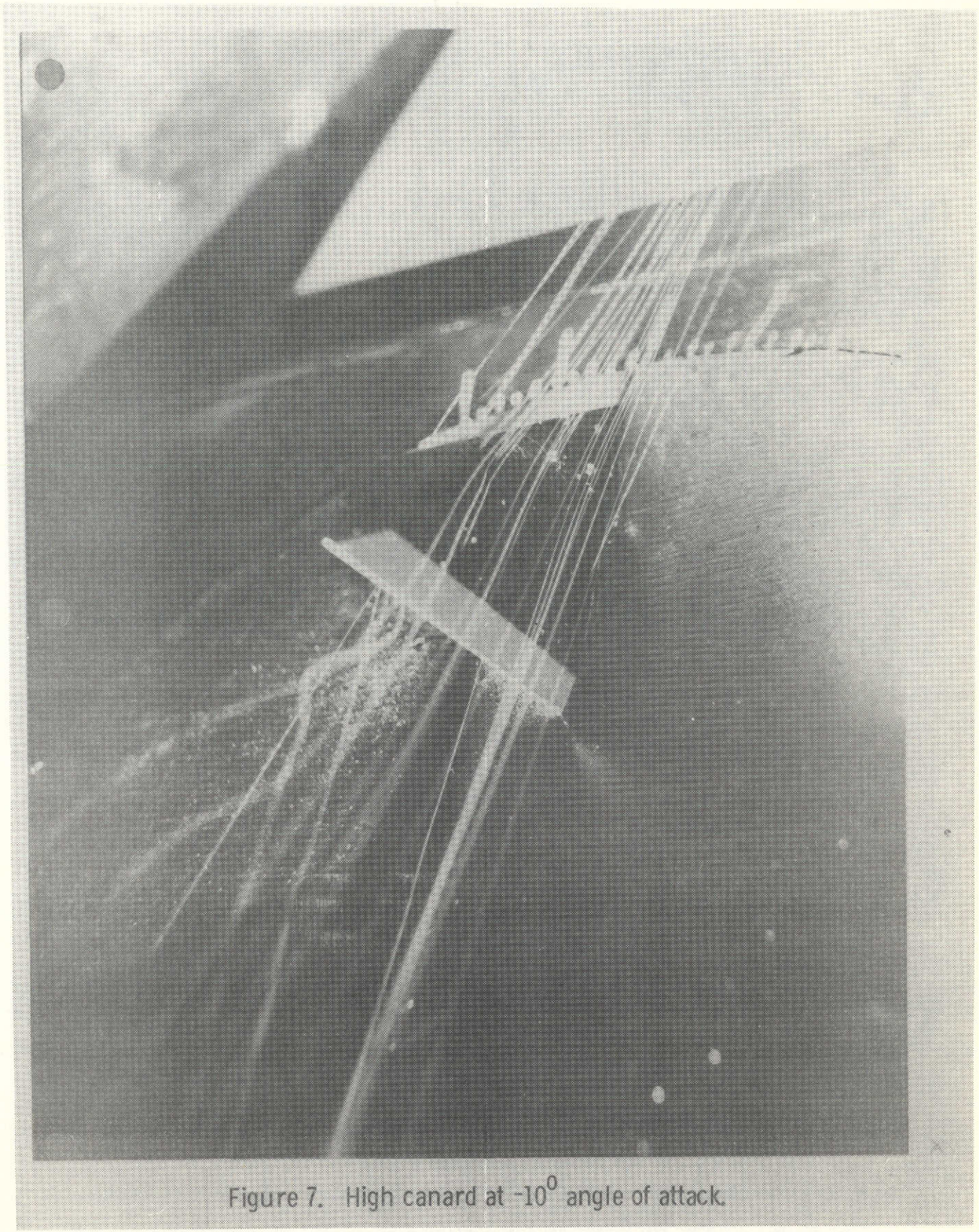

Figure 7. High canard at -10^{0} angle of attack.

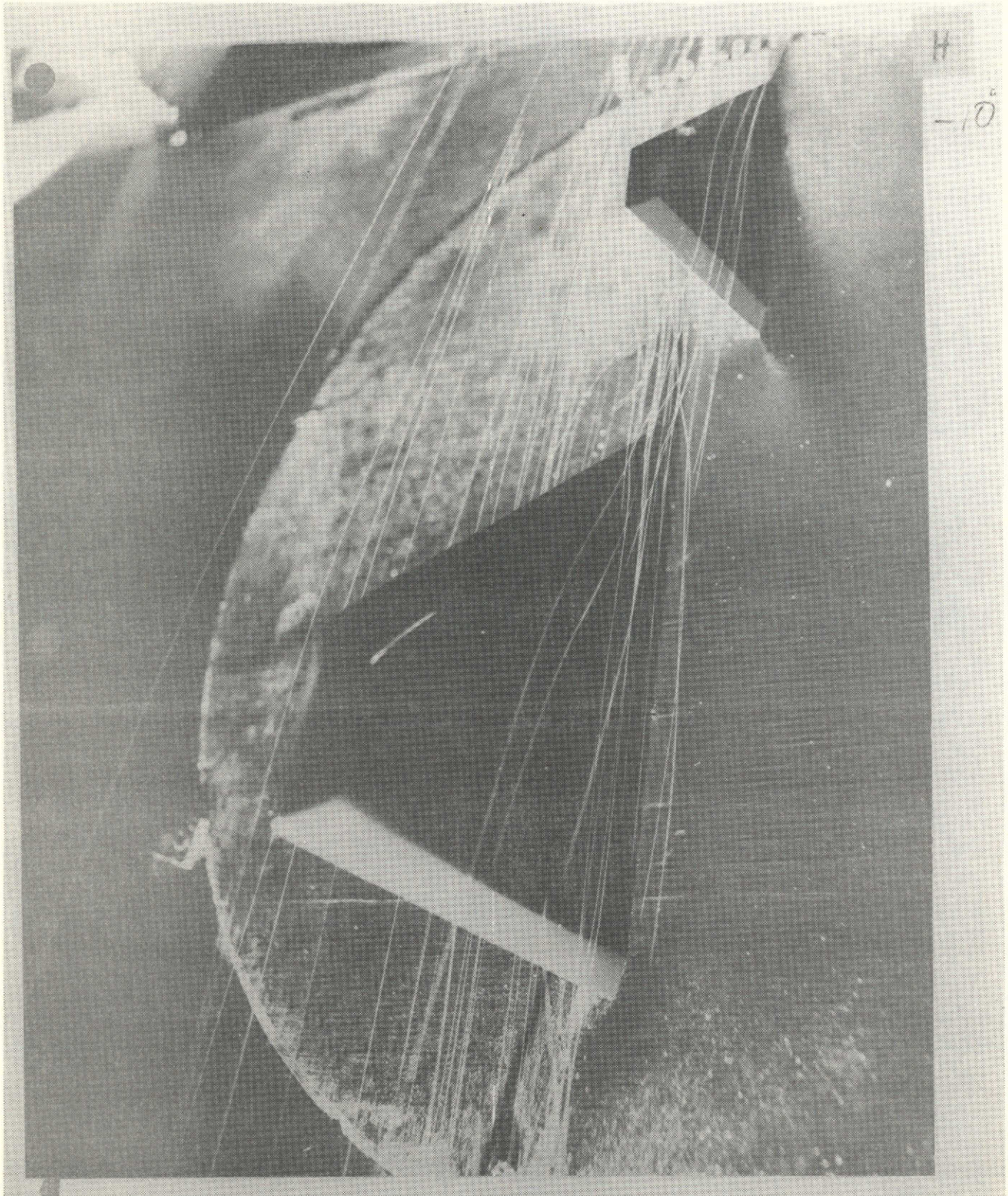

Figure 8. Wing in the presence of the high canard at -10° angle of attack.

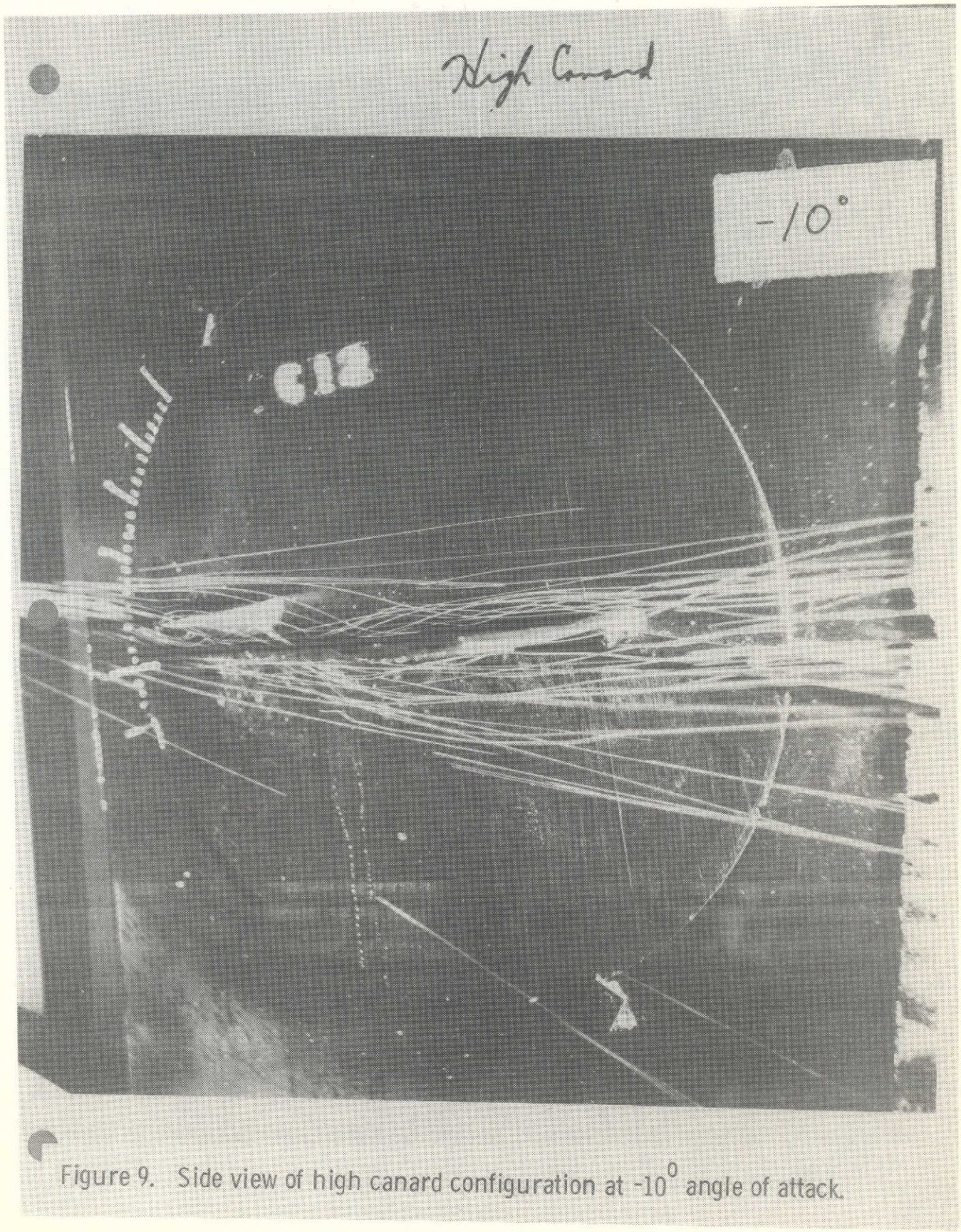

Figure 9. Side view of high canard configuration at -10^{0} angle of attack.

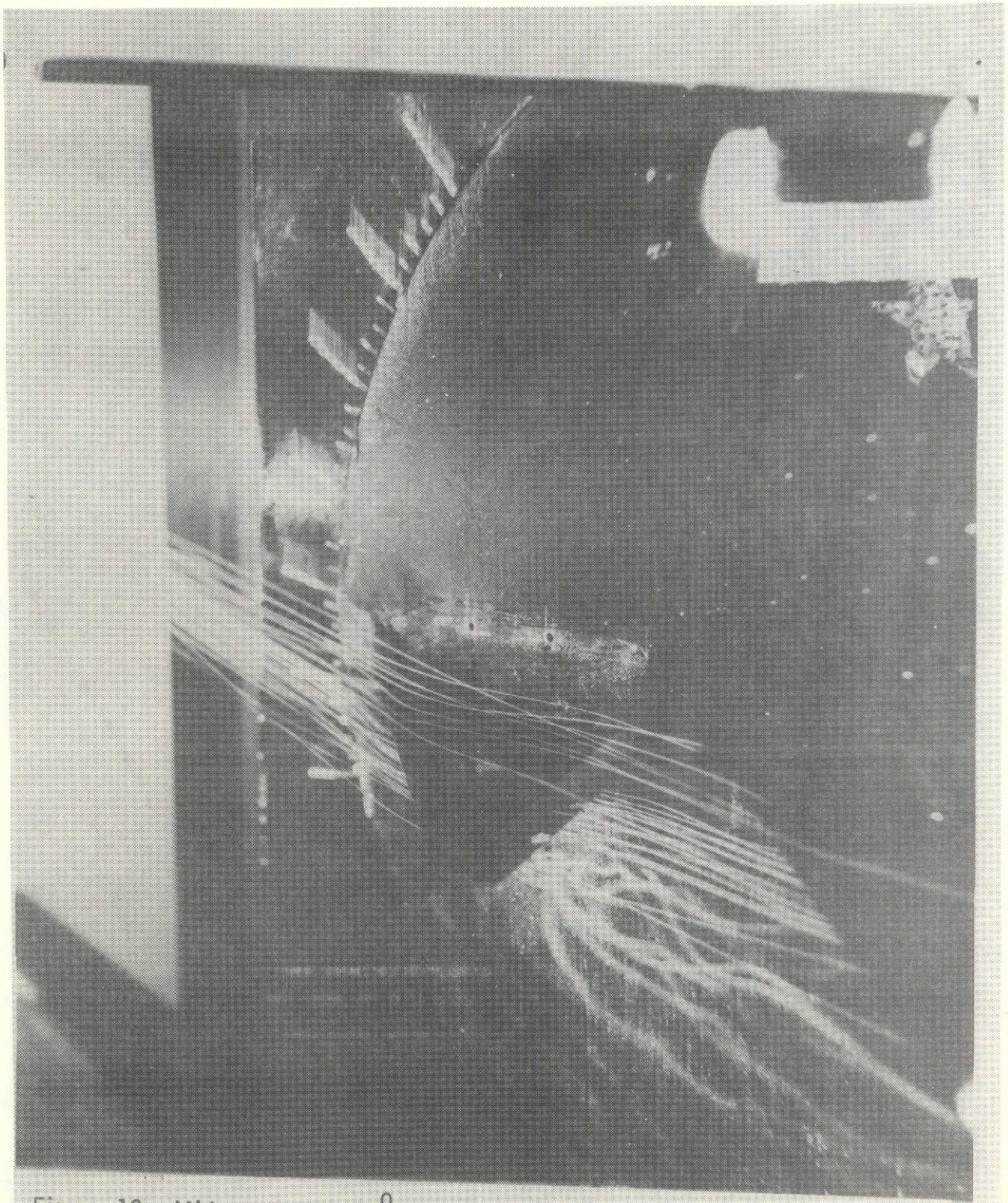

Figure 10. Mid canard at -10^{0} angle of attack.

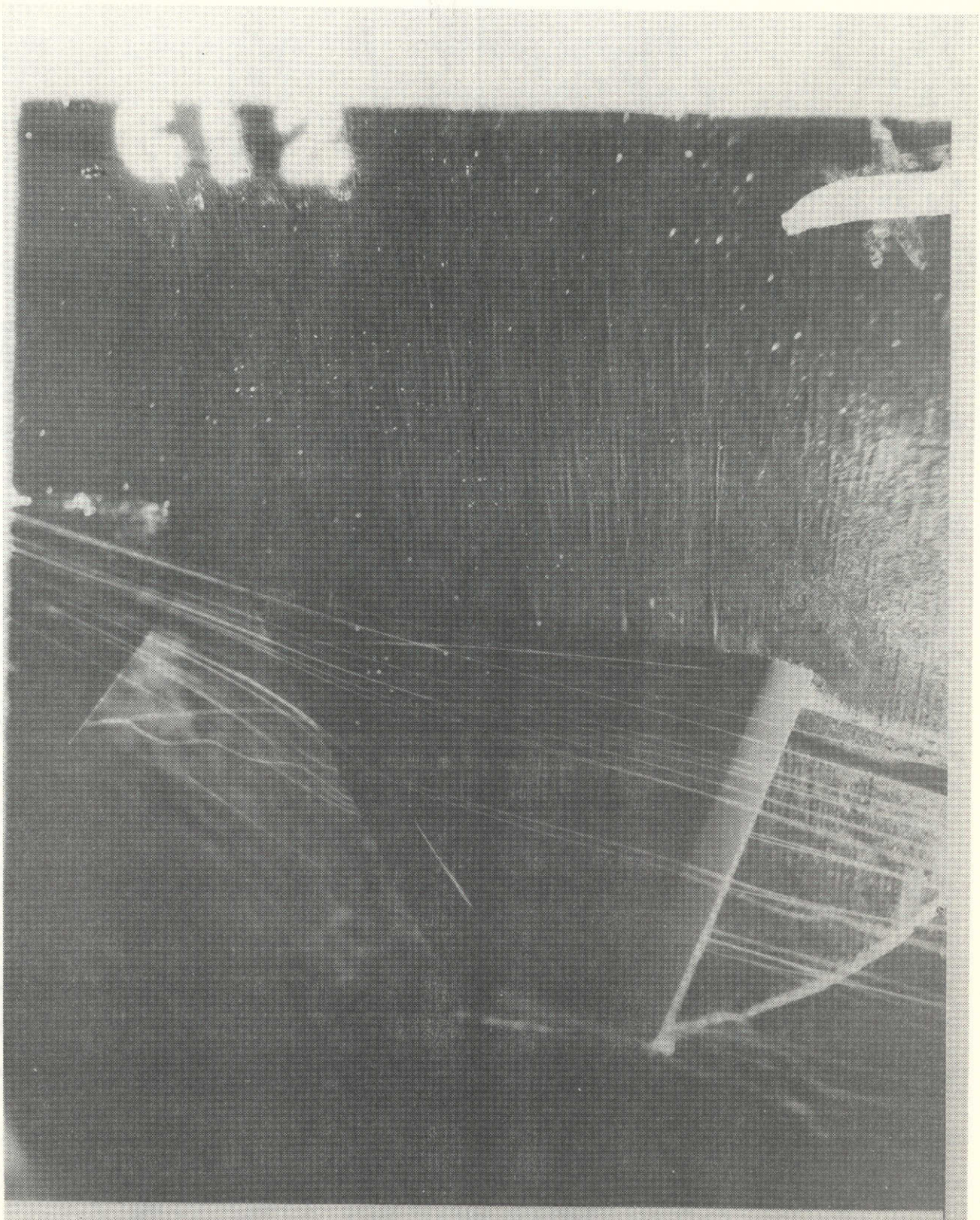

Figure 11. Wing in the presence of the mid canard at -10^{0} angle of attack.

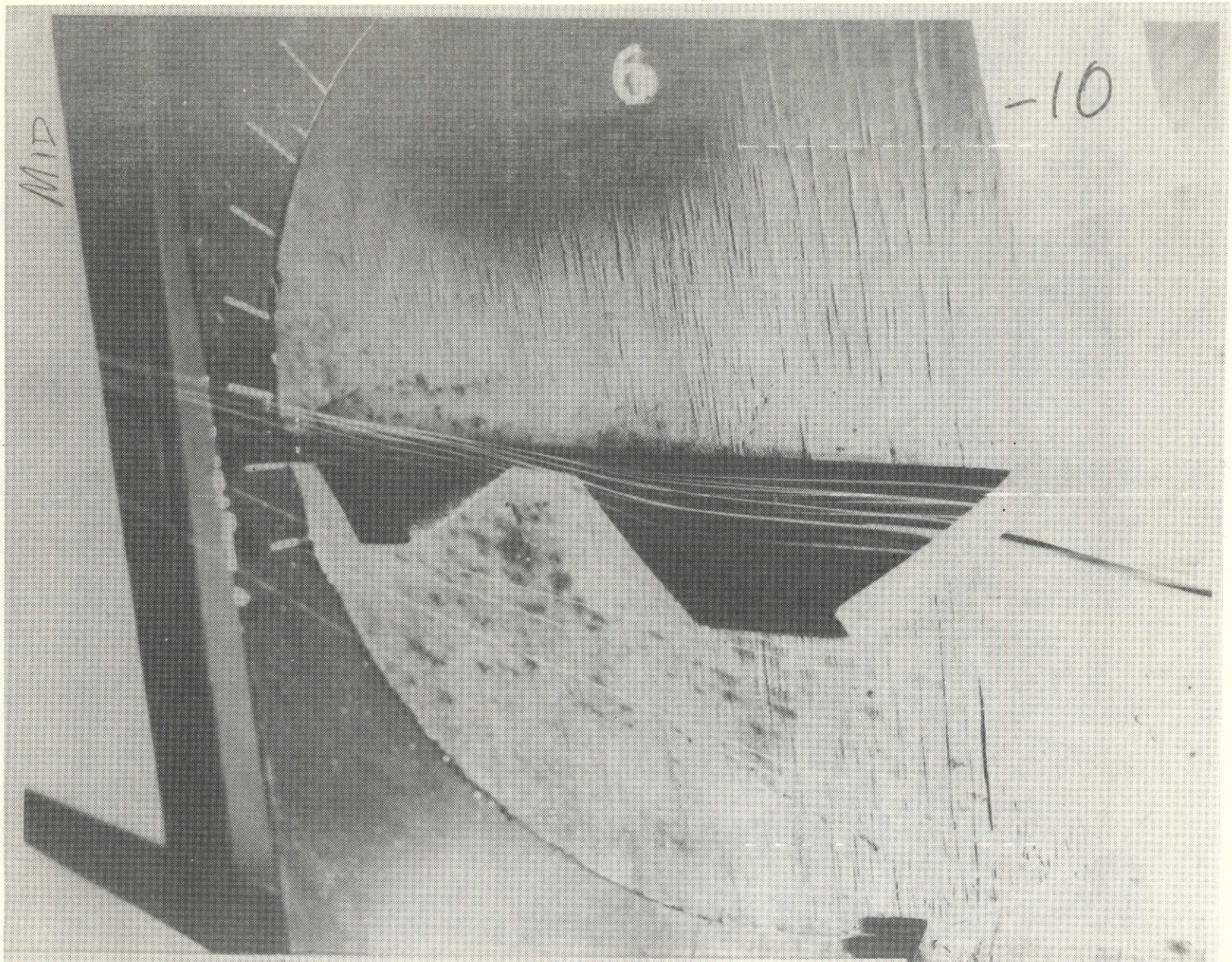

Figure 12. Wing in the presence of the mid canard at -10^0 angle of attack.

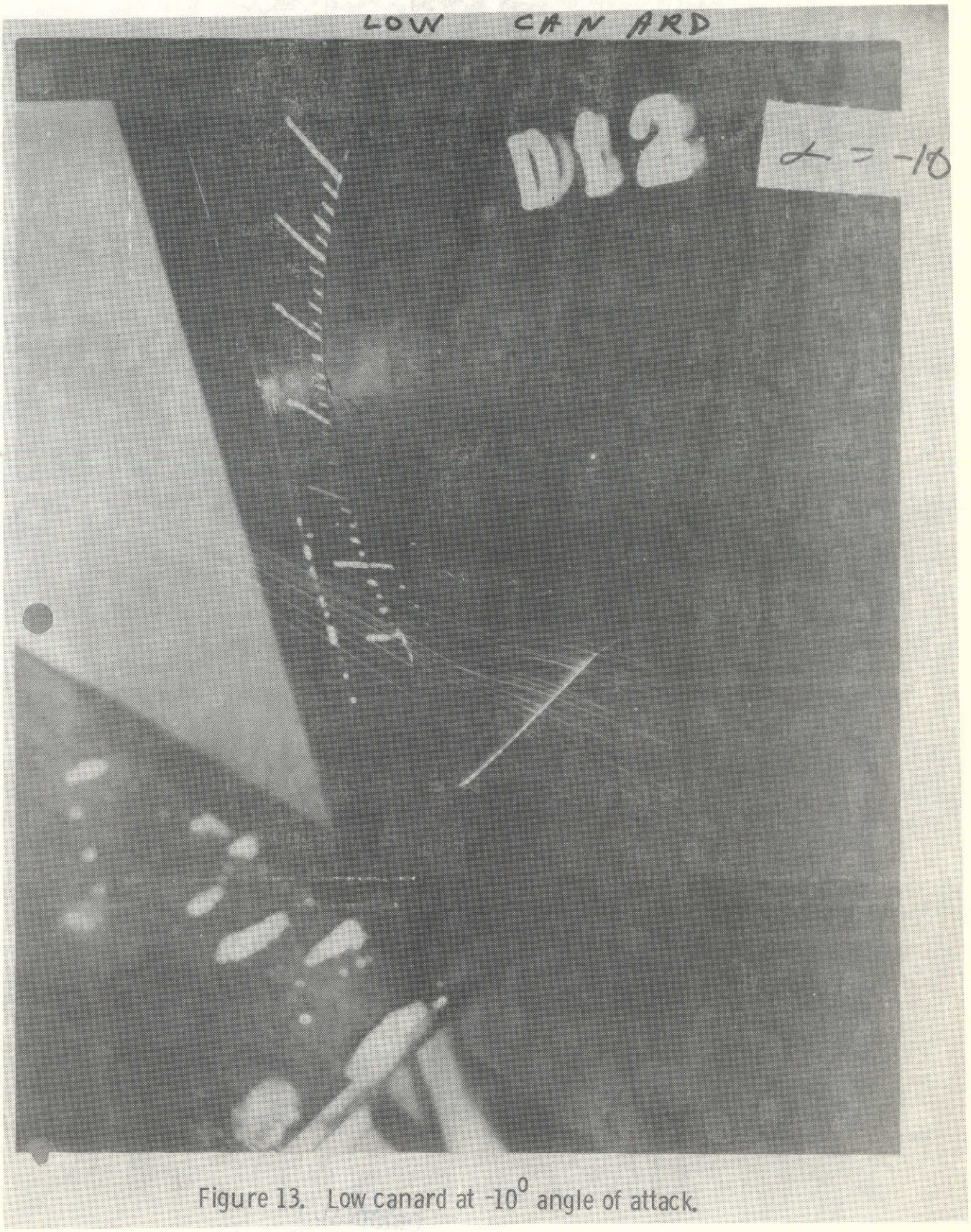

Figure 13. Low canard at -10^{0} angle of attack.

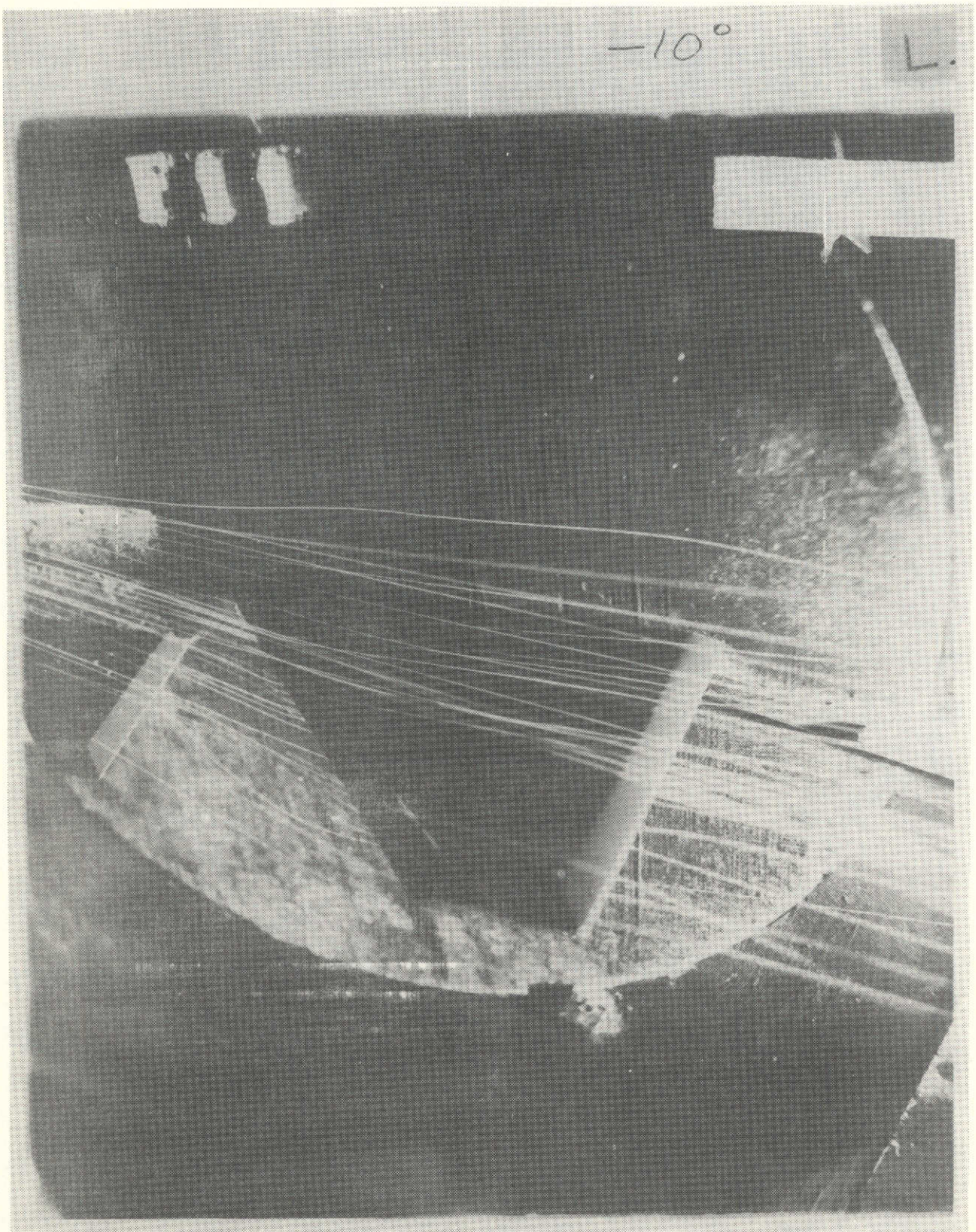

Figure 14. Wing in the presence of the low canard at -10^{0} angle of attack.

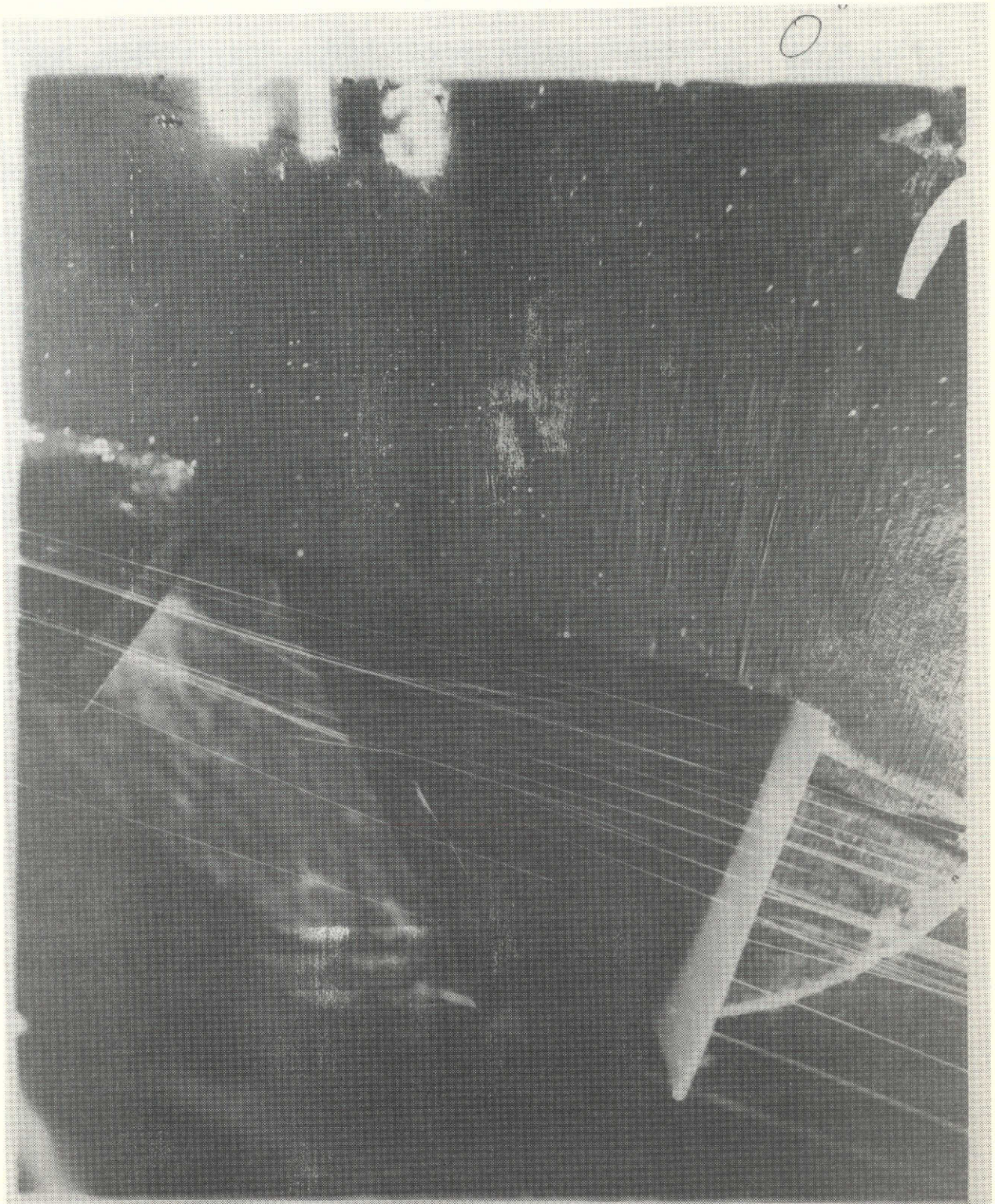

Figure 15. Wing in the presence of the mid canard at 0^{o} angle of attack.

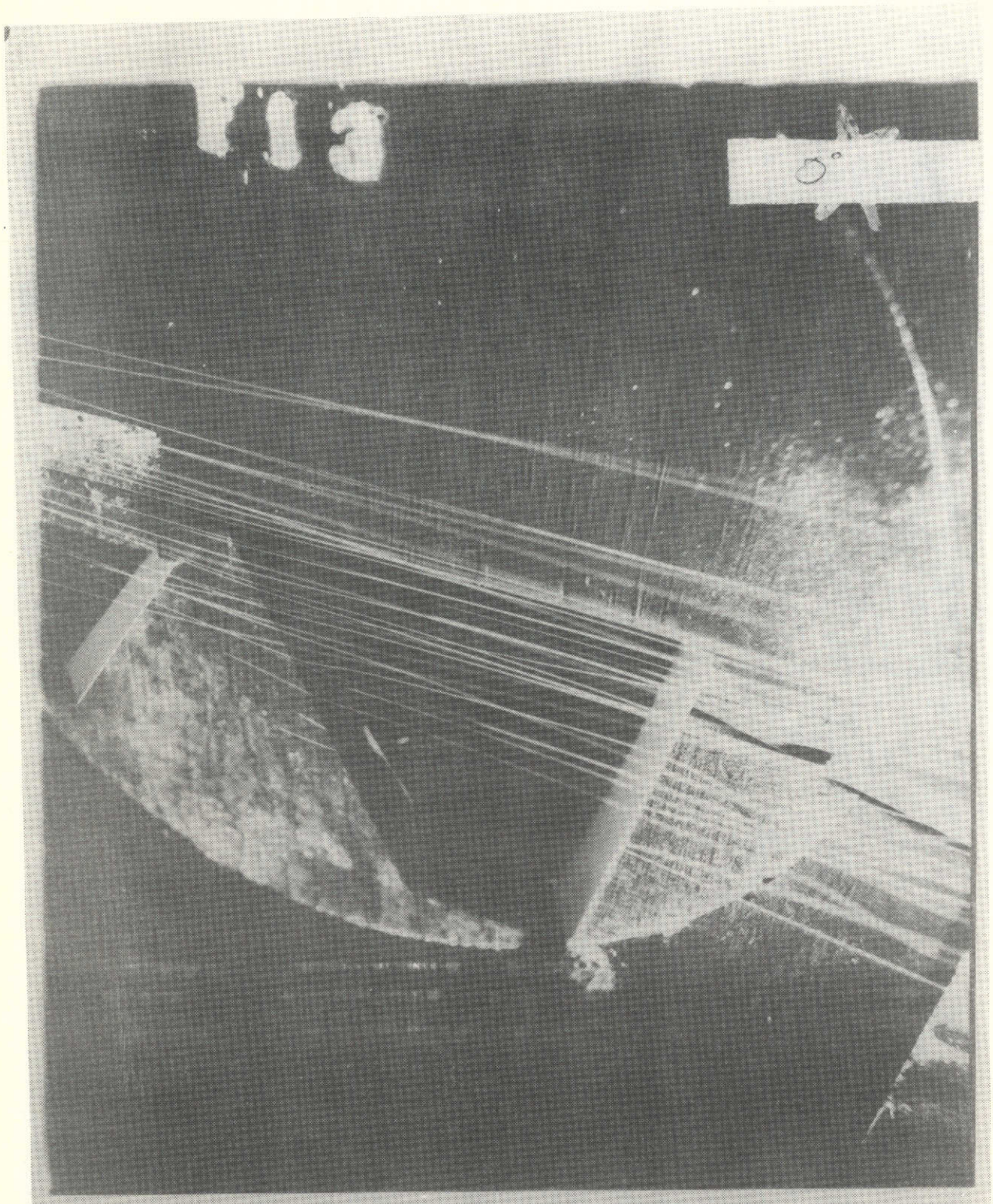

Figure 16. Wing in the presence of the low canard at 0^{0} angle of attack.

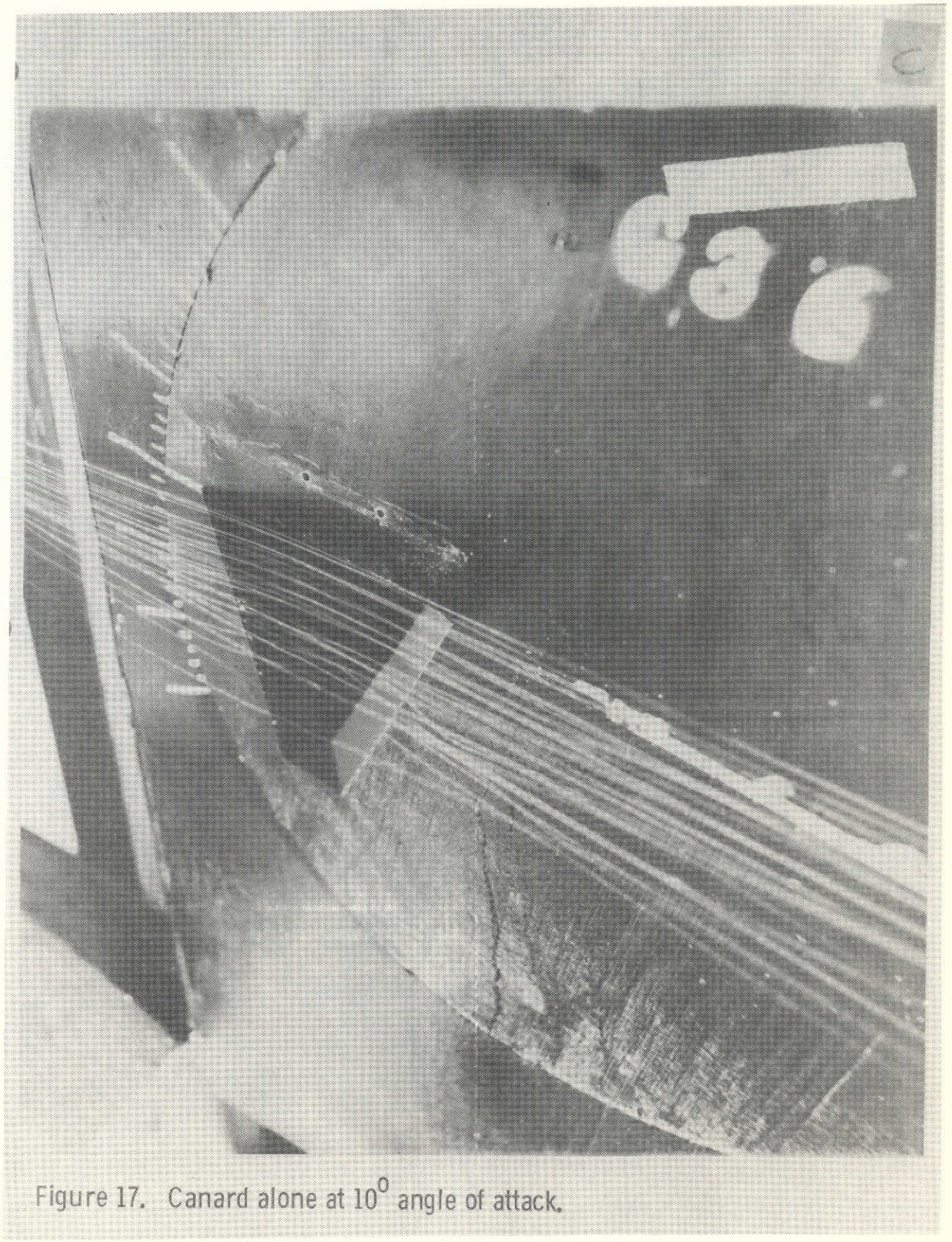

Figure 17. Canard alone at 10^{o} angle of attack.

Figure 18. Wing alone at 10^{0} angle of attack.

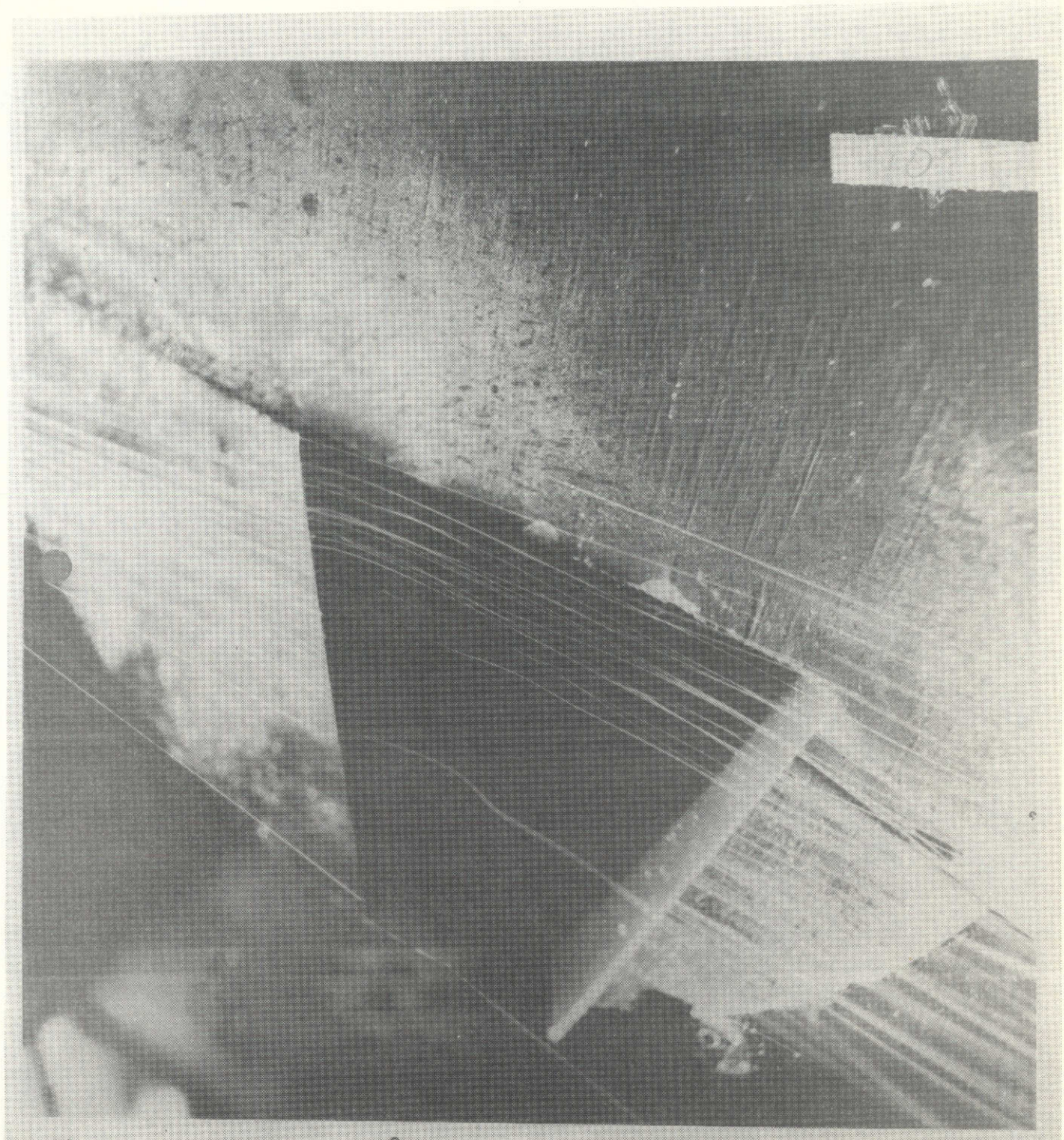

Figure 19. Wing alone at 10^{o} angle of attack.

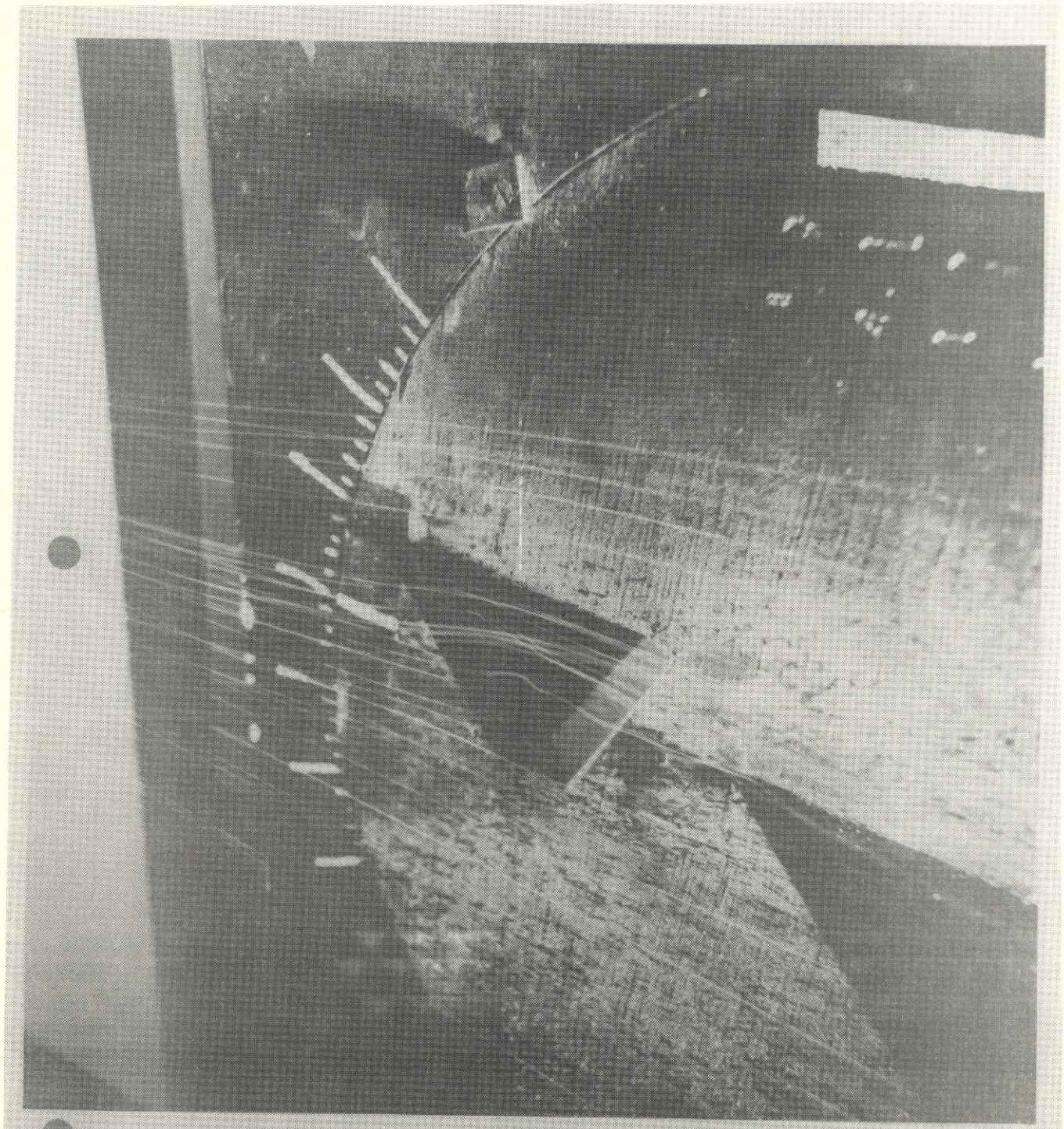

Figure 20. High canard at 10^{0} angle of attack.

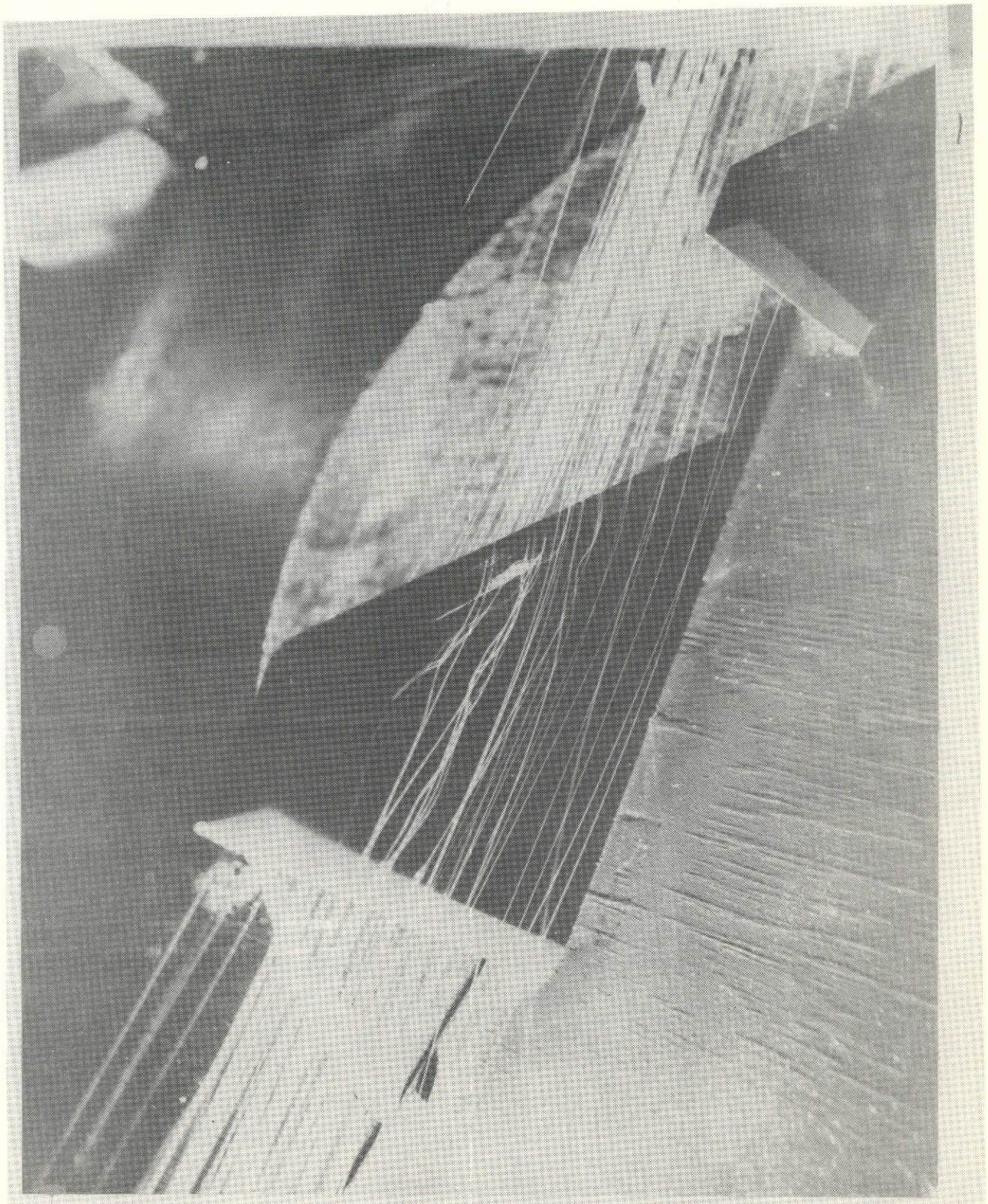

Figure 21. Wing in the presence of the high canard at 10^{0} angle of attack.

Figure 22. Side view of the high canard configuration at 10^{0} angle of attack.

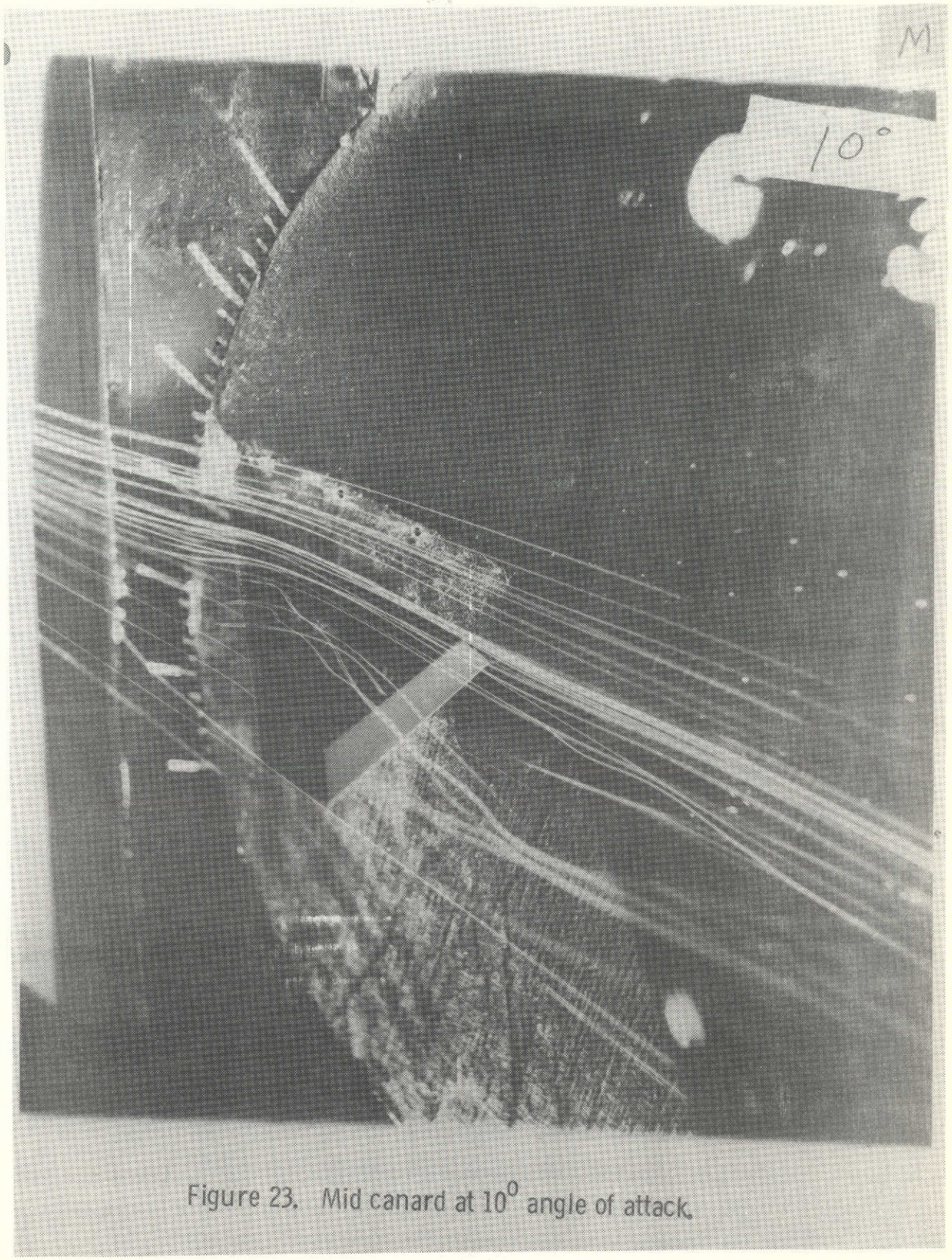

Figure 23. Mid canard at 10^0 angle of attack.

Figure 24. Wing in the presence of the mid canard at 10^{0} angle of attack.

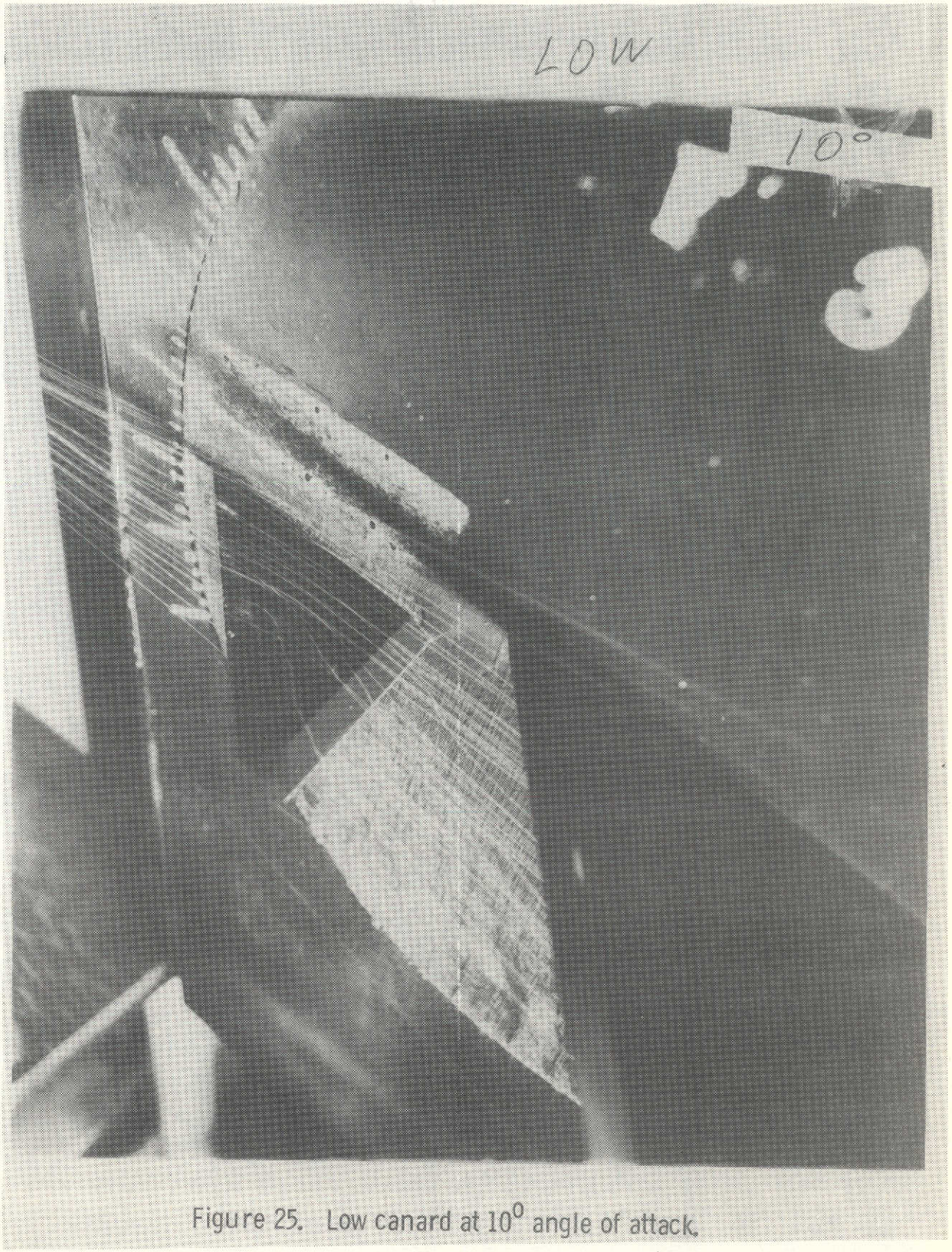

Figure 25. Low canard at 10^{0} angle of attack.

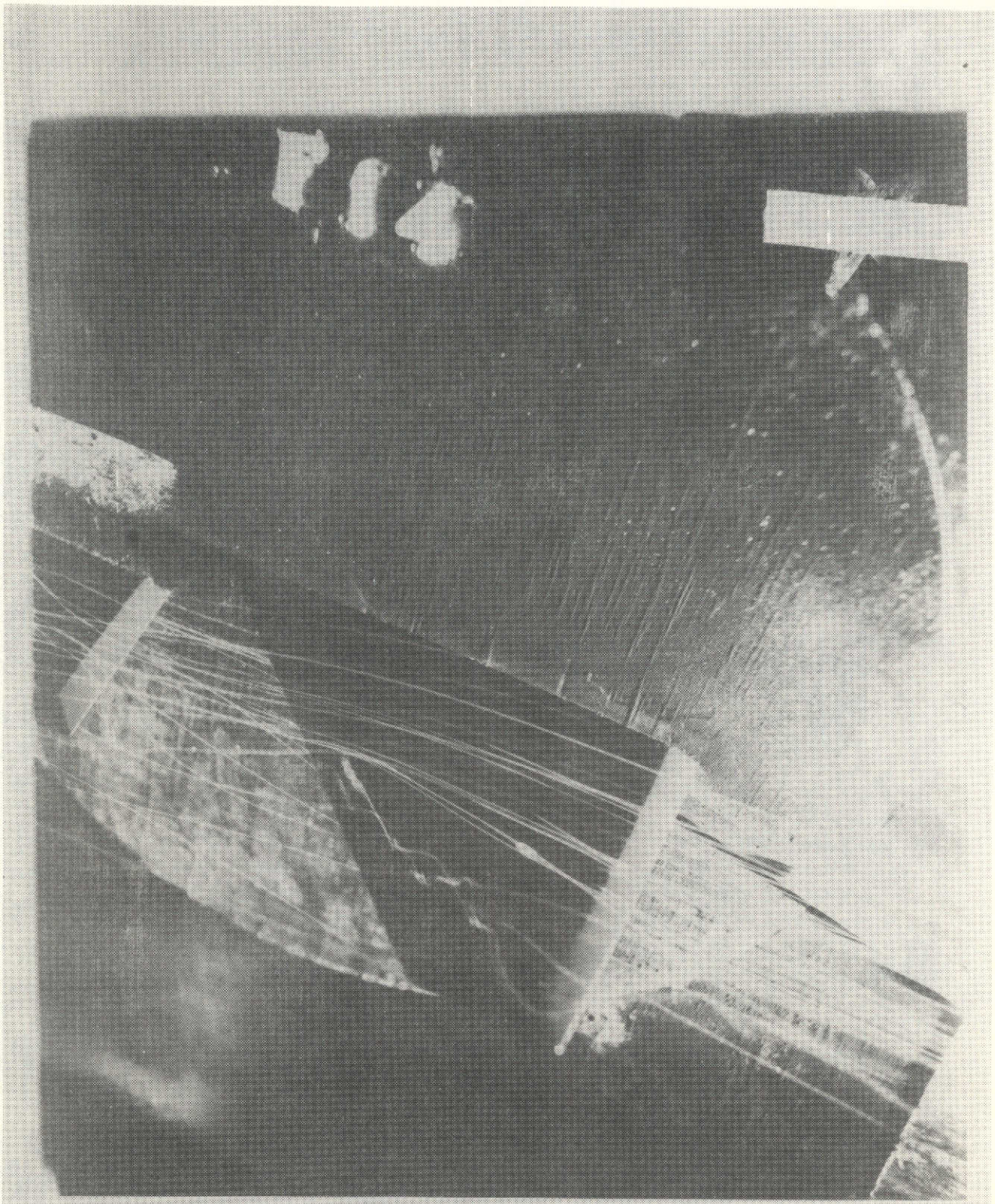

Figure 26. Wing the presence of the low canard at 10^{0} angle of attack.

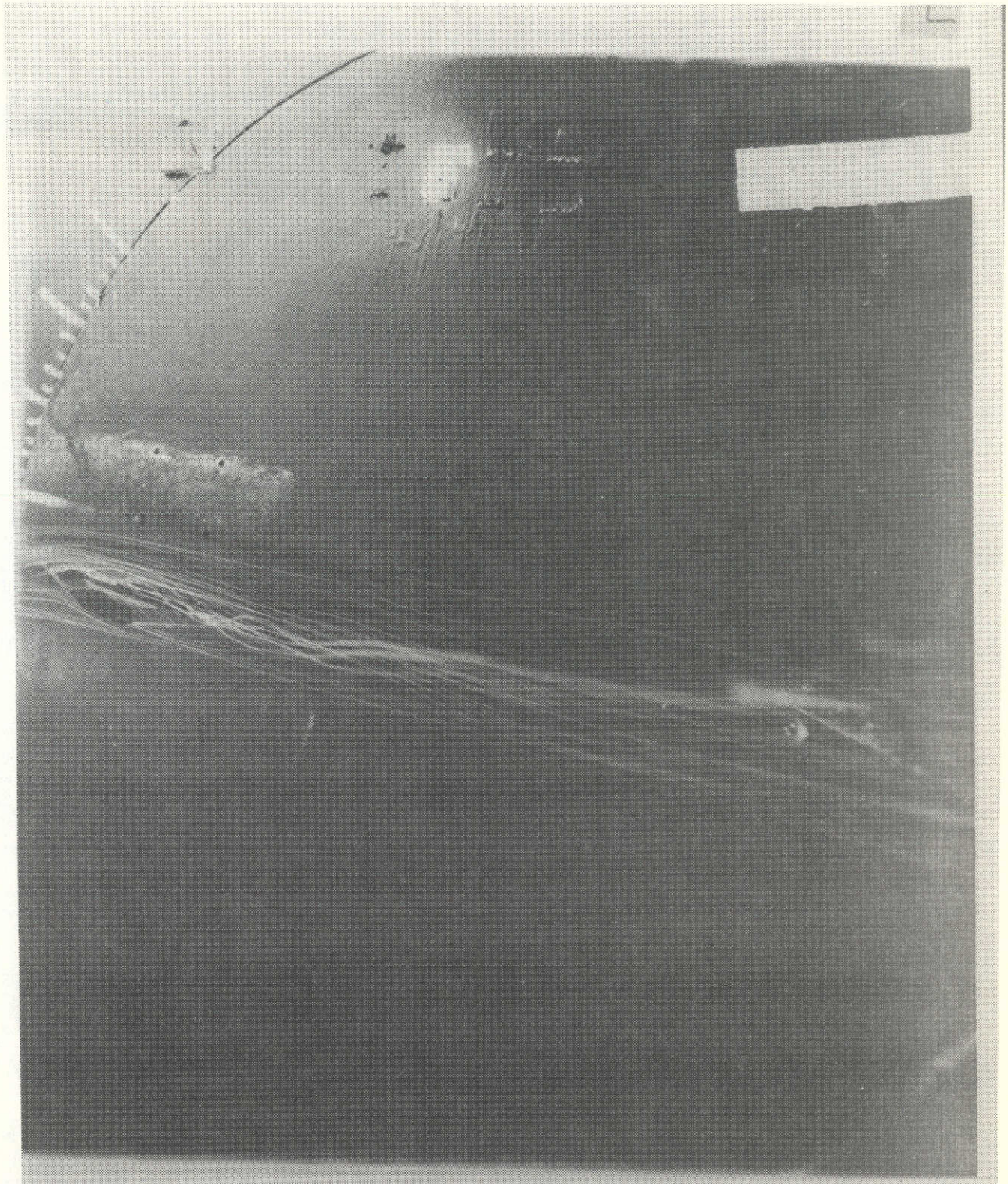

Figure 27. Side view of the low canard configuration at 10^{0} angle of attack.

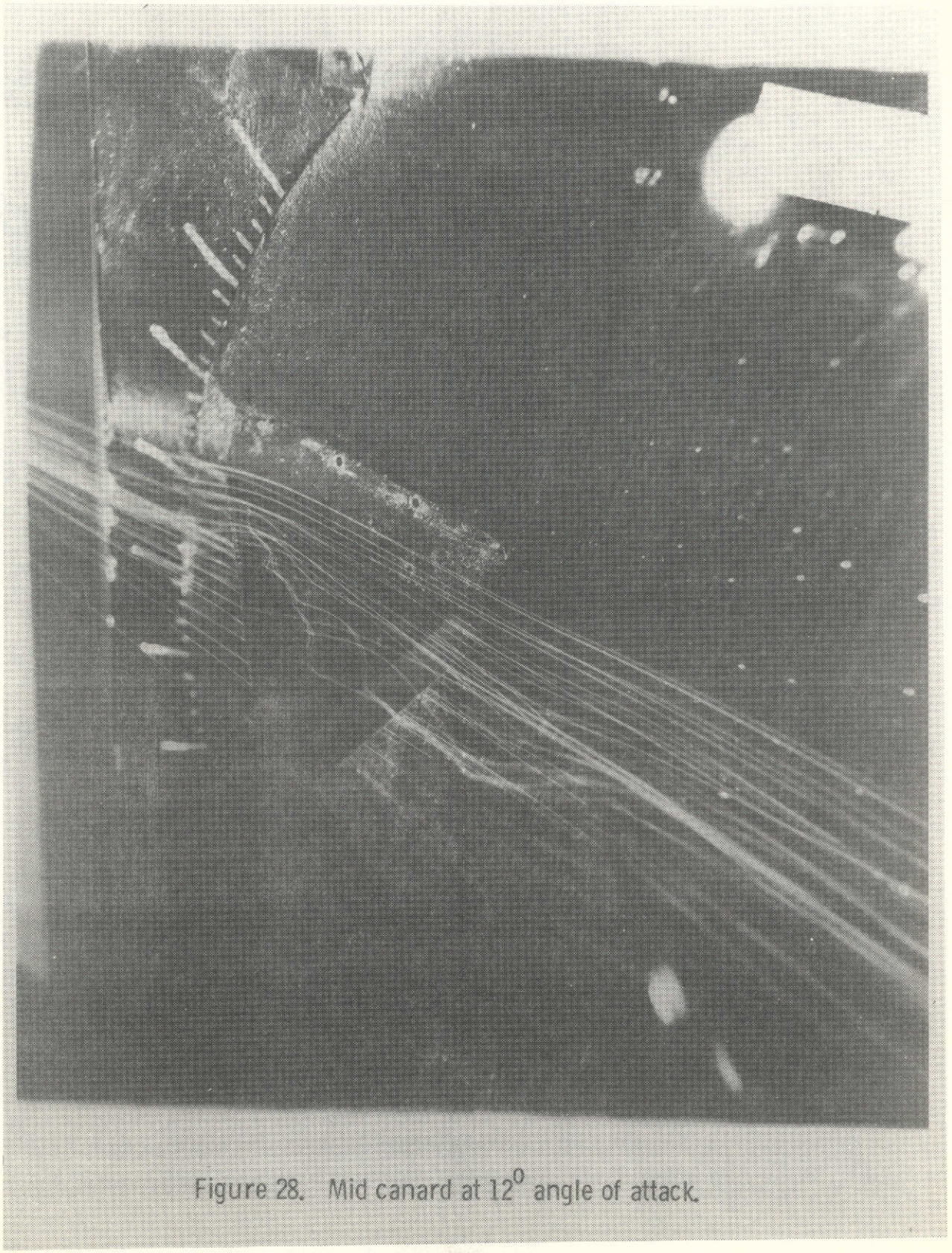

Figure 28. Mid canard at 12^0 angle of attack.

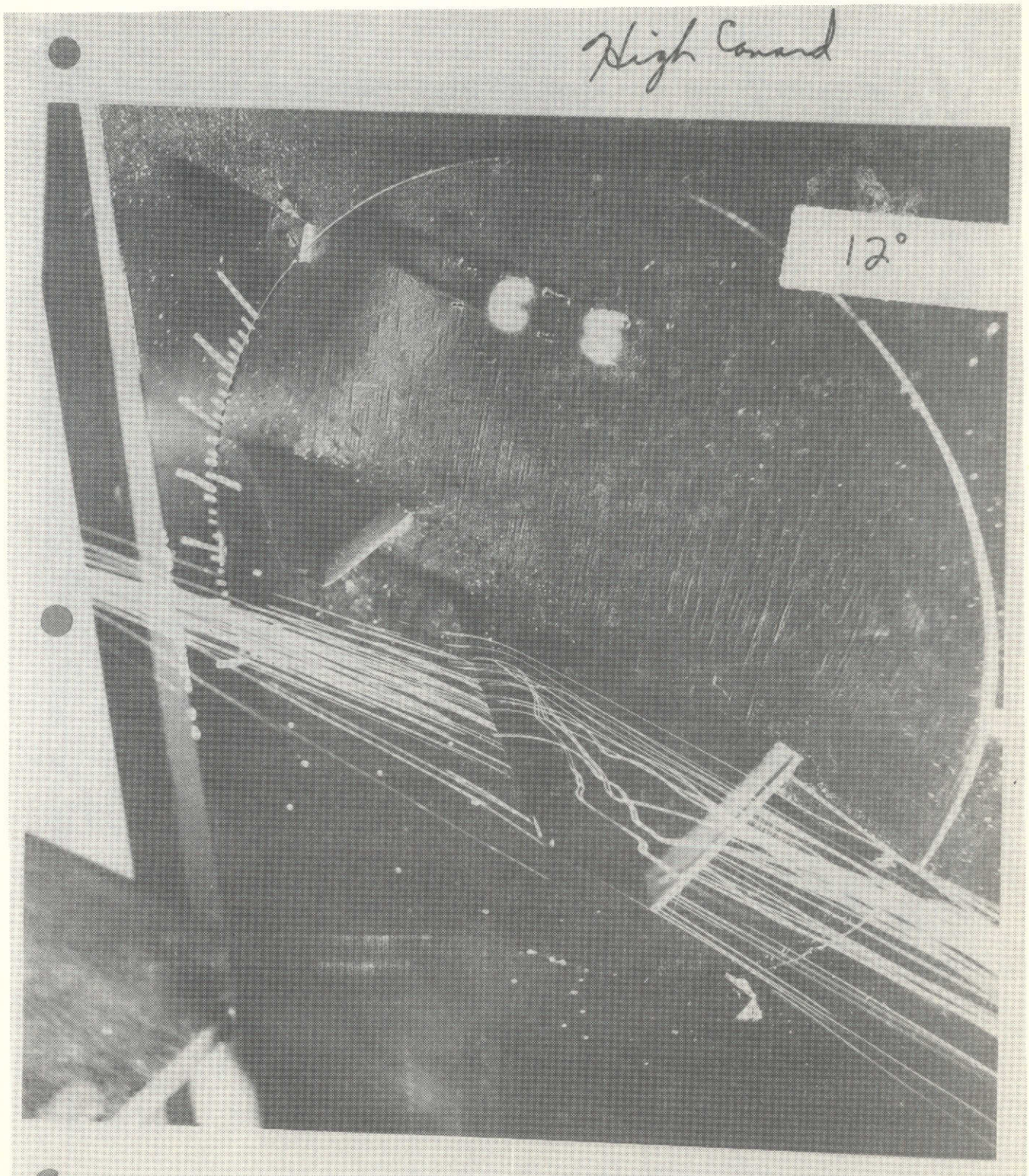

Figure 29. Wing in the presence of the high canard at 12^{0} angle of attack.

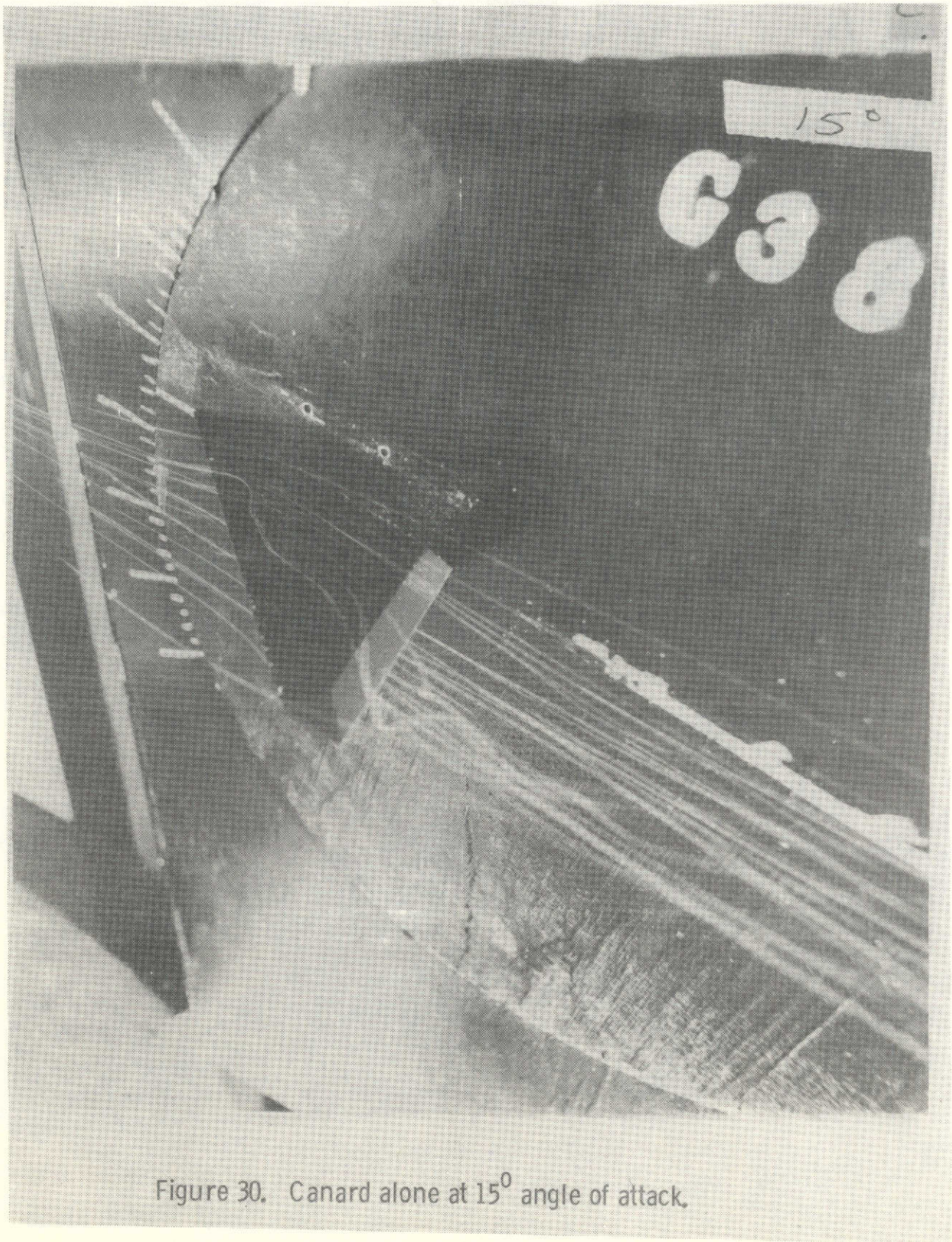

Figure 30. Canard alone at 15^{0} angle of attack.

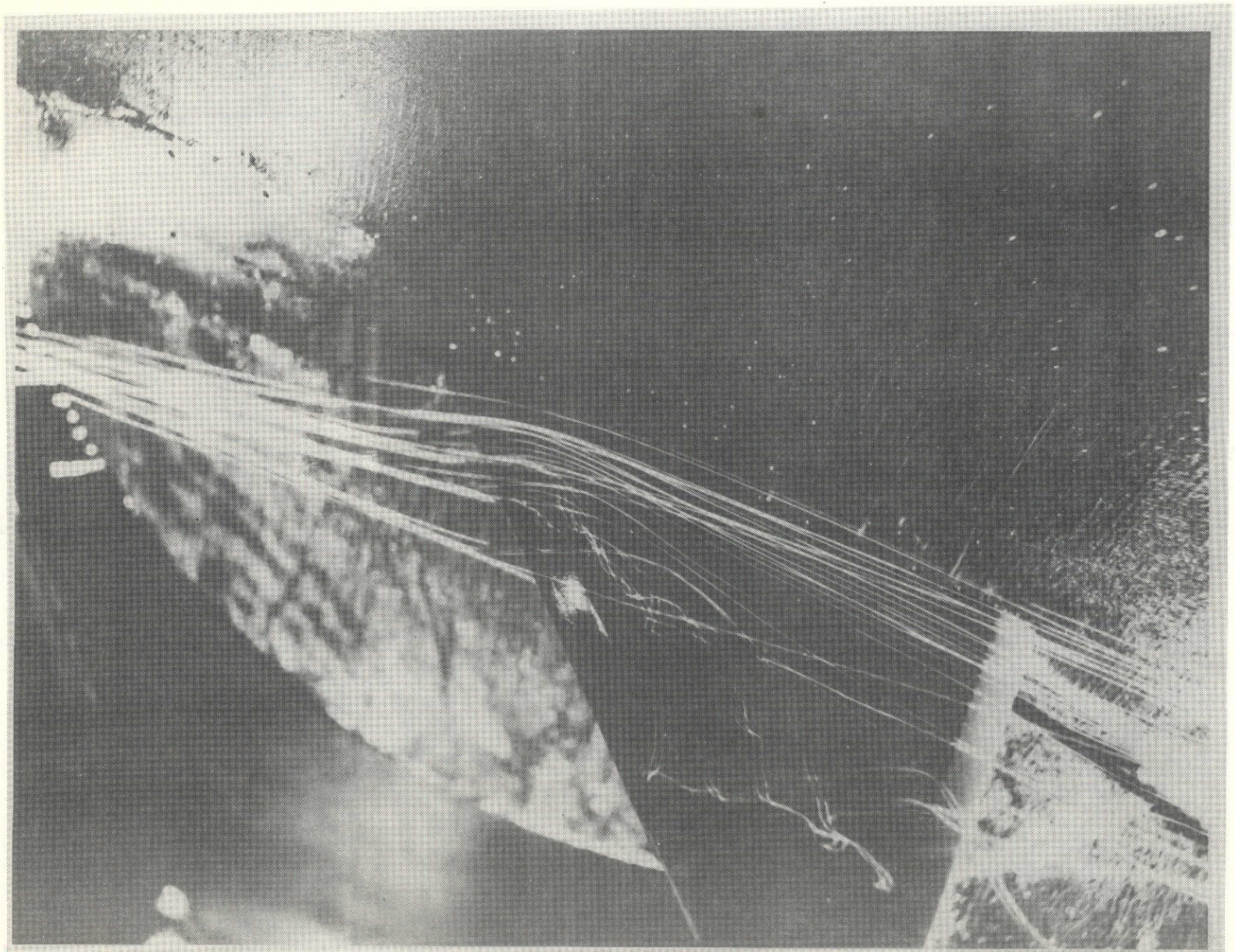

Figure 31. Wing alone at 15^{o} angle of attack.

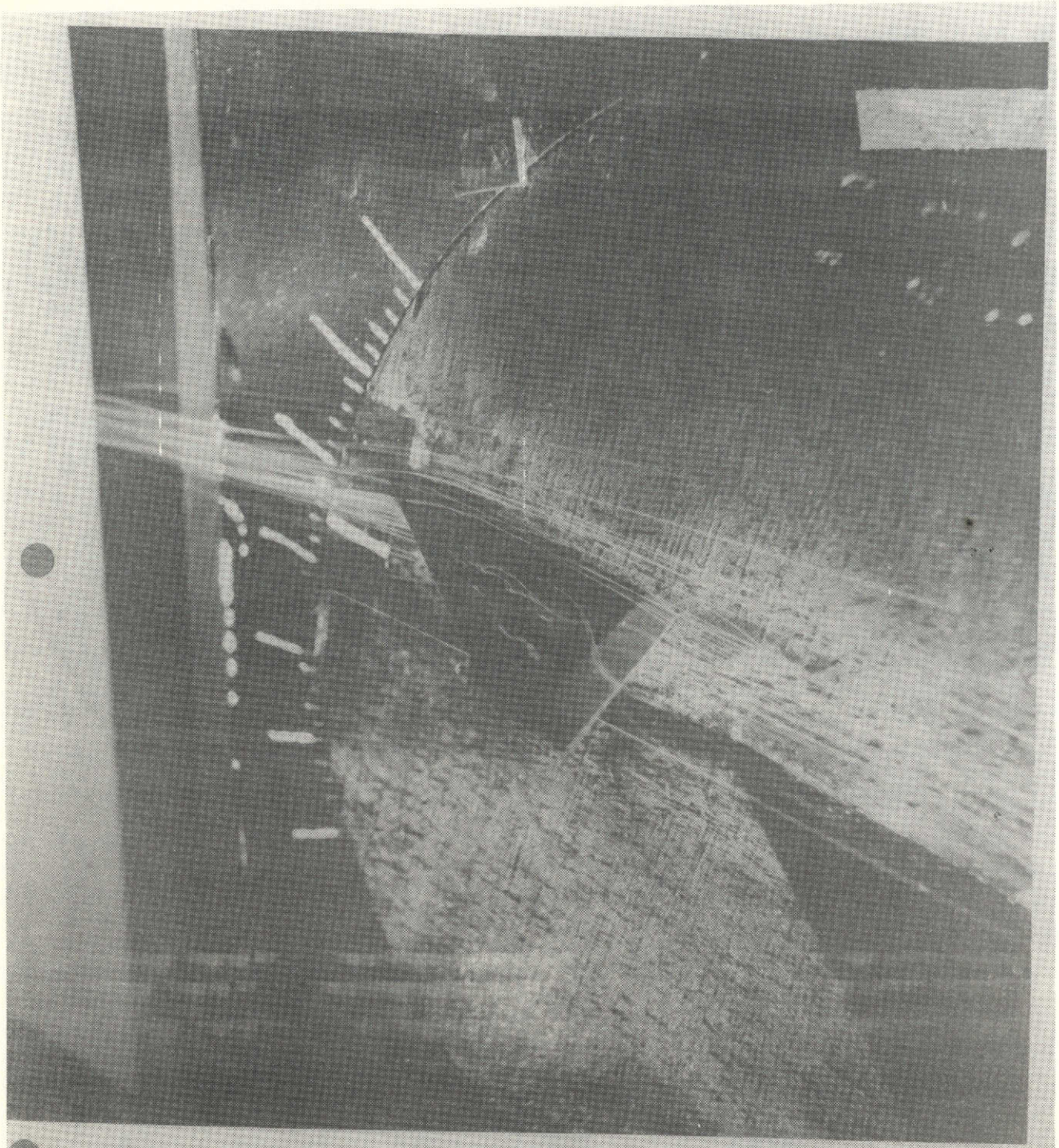

Figure 32. High canard at 15^{0} angle of attack.

Figure 33. Wing in the presence of the high canard at 15^{0} angle of attack.

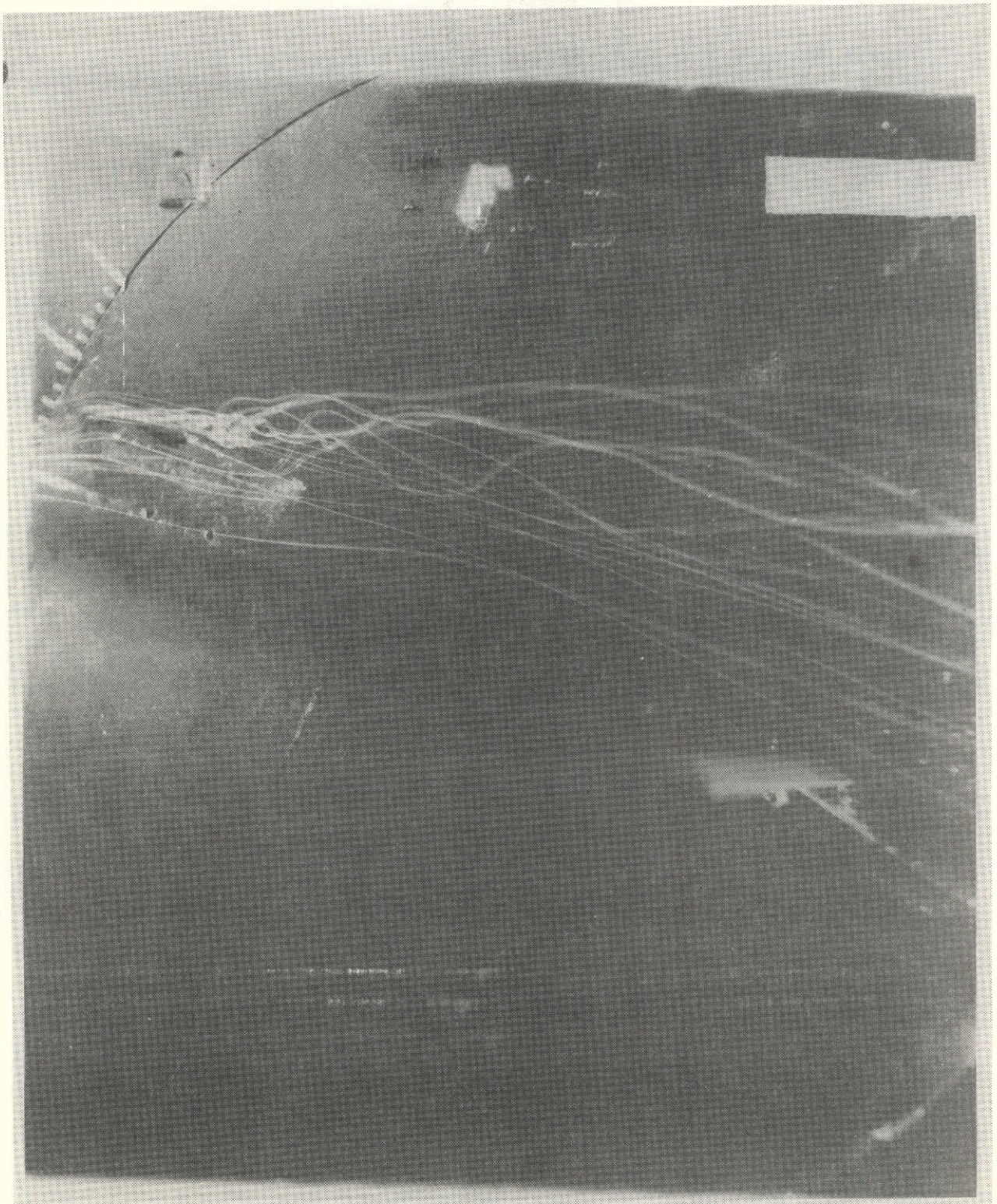

Figure 34. Side view of the high canard configuration at 15^{0} angle of attack.

Figure 35. Mid canard at 15^{0} angle of attack.

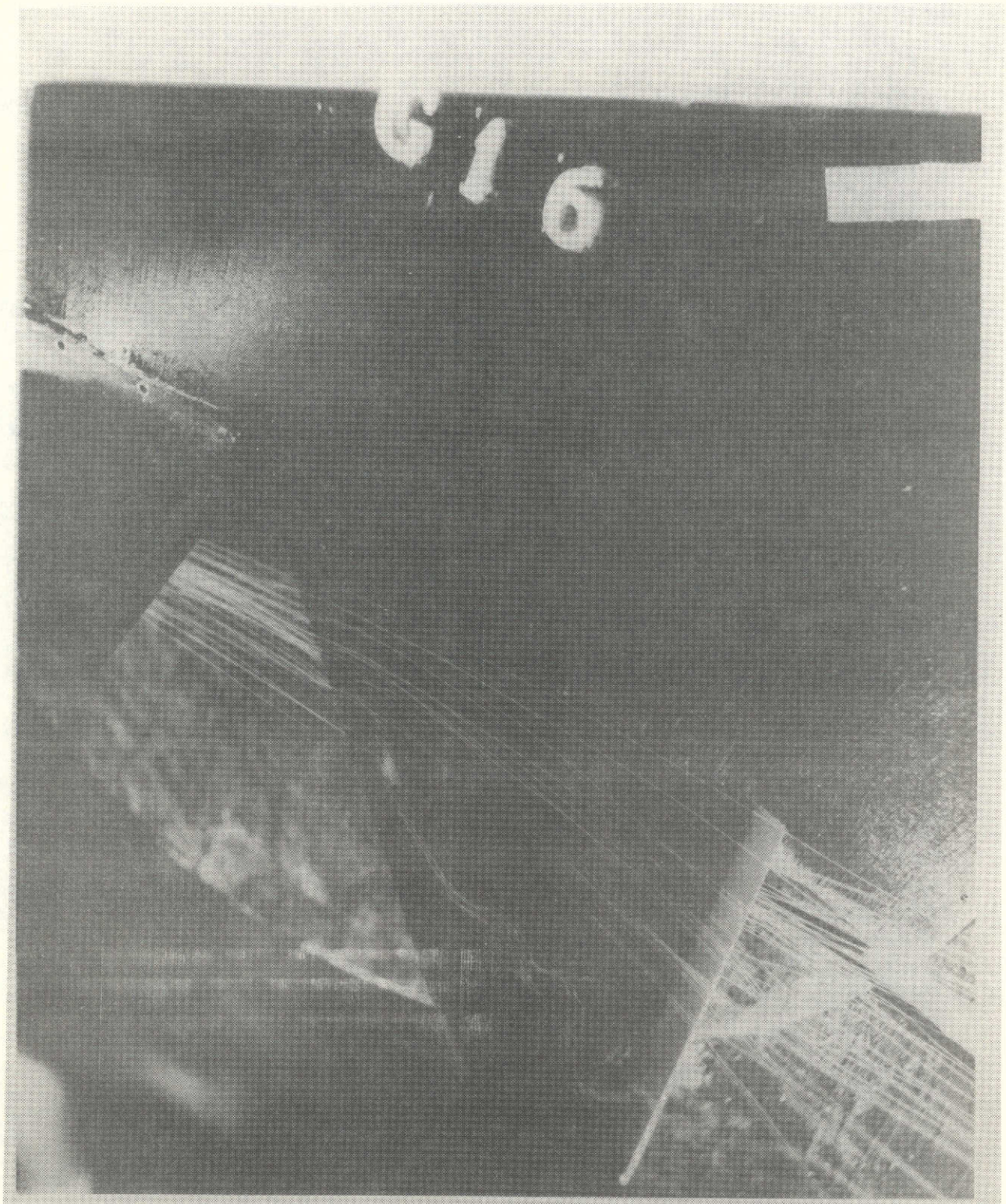

Figure 36. Wing in the presence of the mid canard at 15^{0} angle of attack.

Figure 37. Low canard at 15° angle of attack.

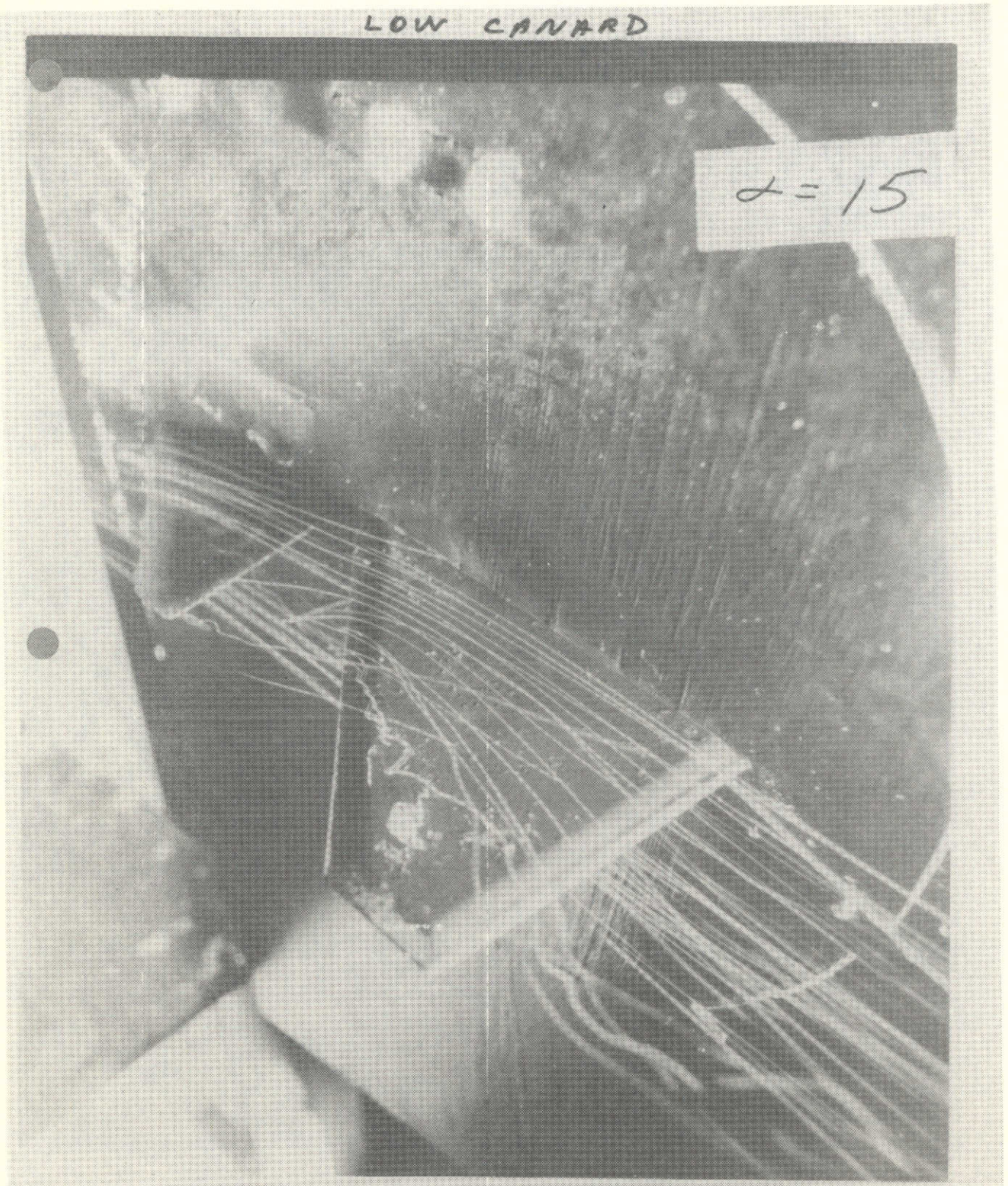

Figure 38. Wing in the presence of the low canard at 15^{0} angle of attack.

Figure 39. Side view of the low canard configuration at 15° angle of attack.

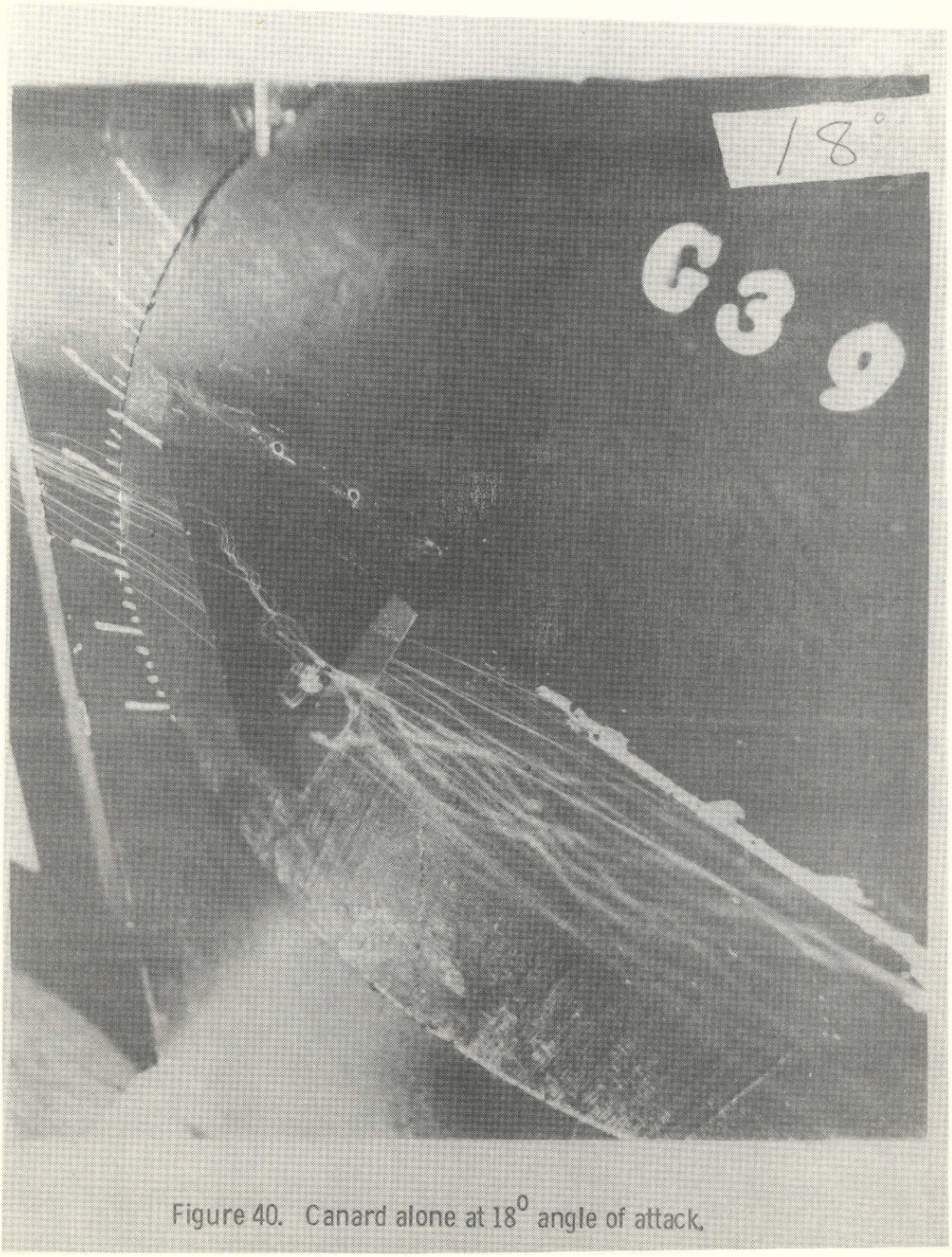

Figure 40. Canard alone at 18^{0} angle of attack.

Figure 41. Wing in the presence of the high canard at 18° angle of attack.

Figure 42. Mid canard at 18^{0} angle of attack.

Figure 43. Wing in the presence of the low canard at 18^{0} angle of attack.

Figure 44. Canard alone at 20^{0} angle of attack.

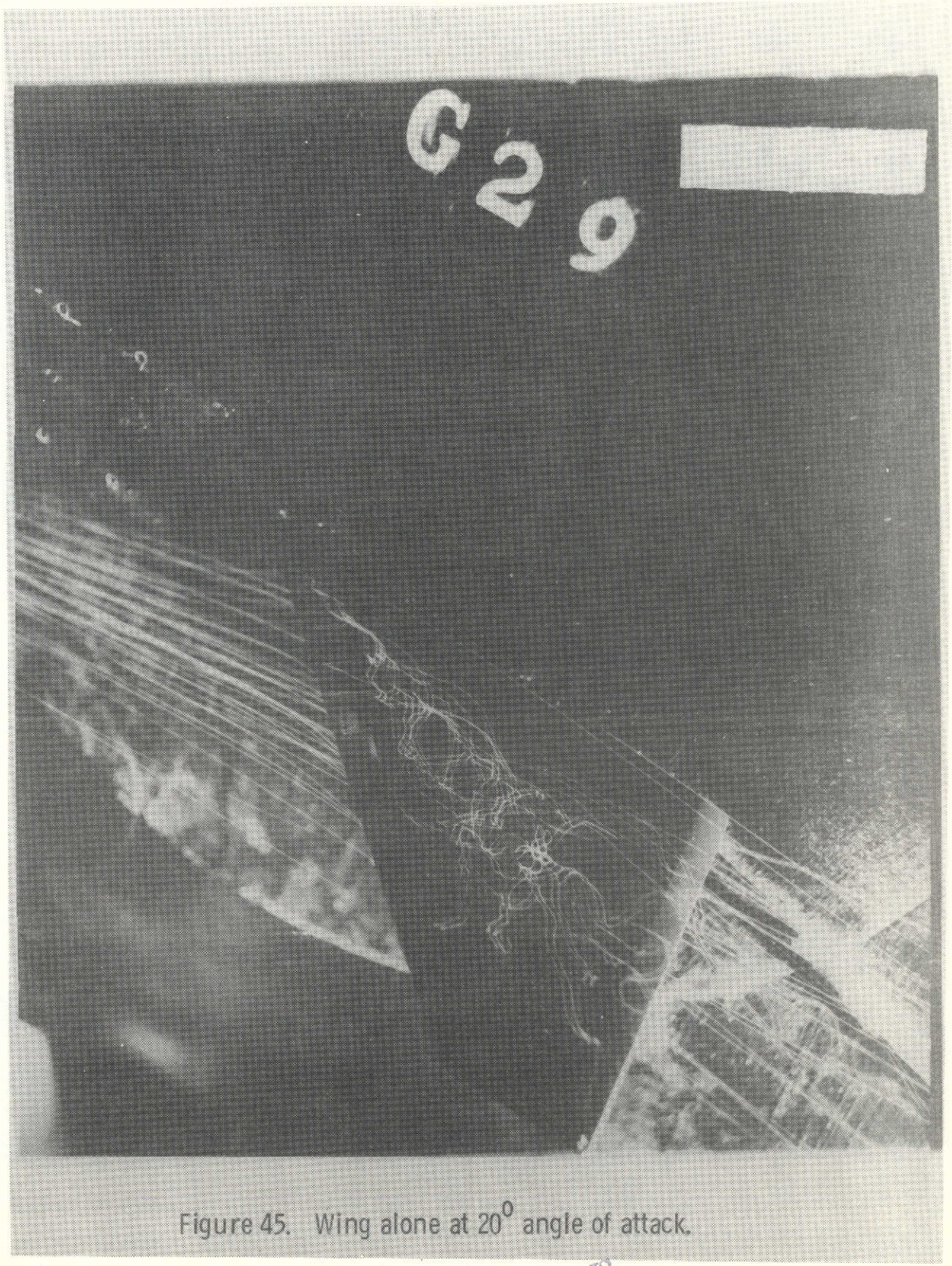

Figure 45. Wing alone at 20° angle of attack.

Figure 46. High canard at 20^{o} angle of attack.

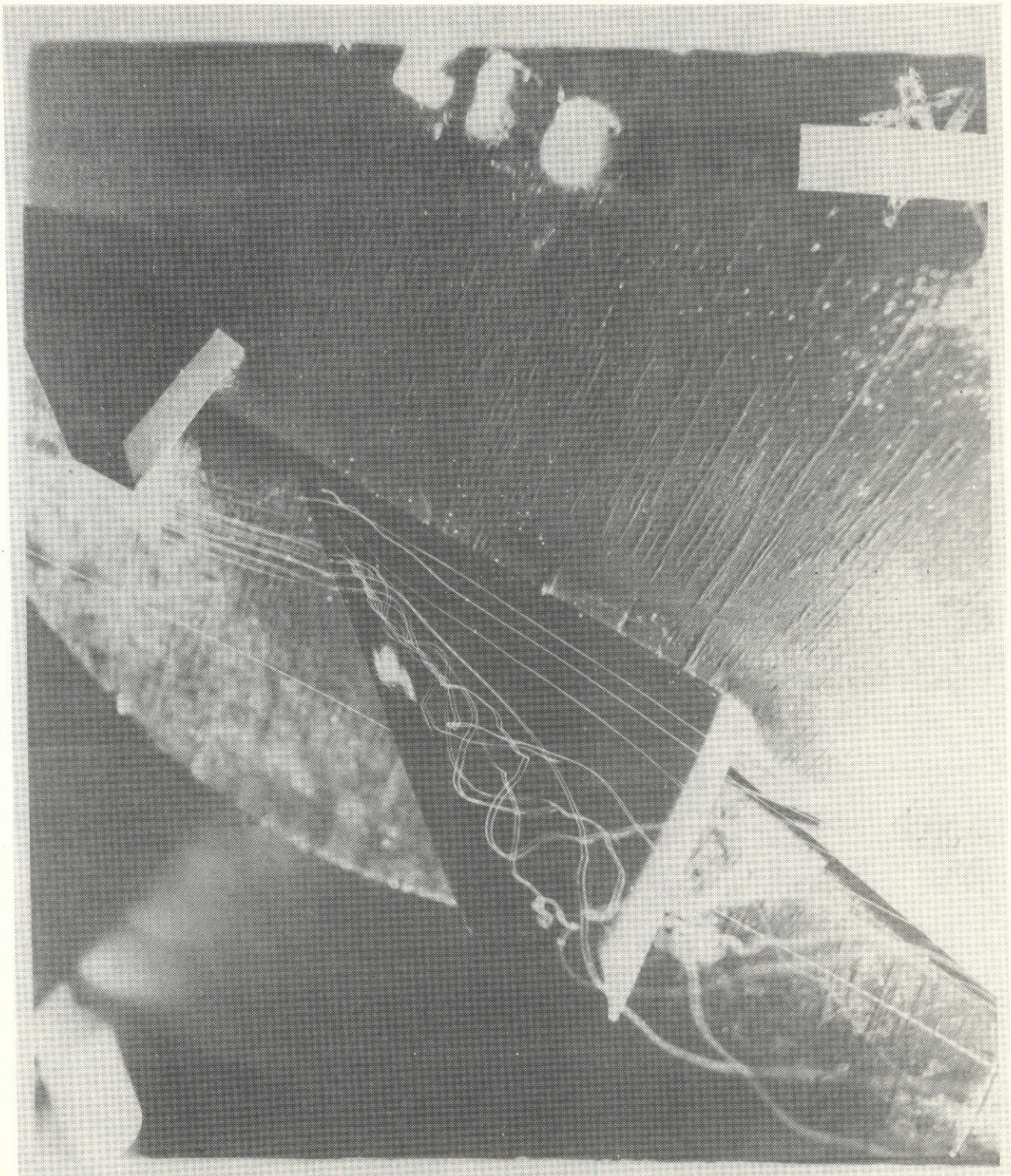

Figure 47. Wing the presence of the high canard at 20^{0} angle of attack.

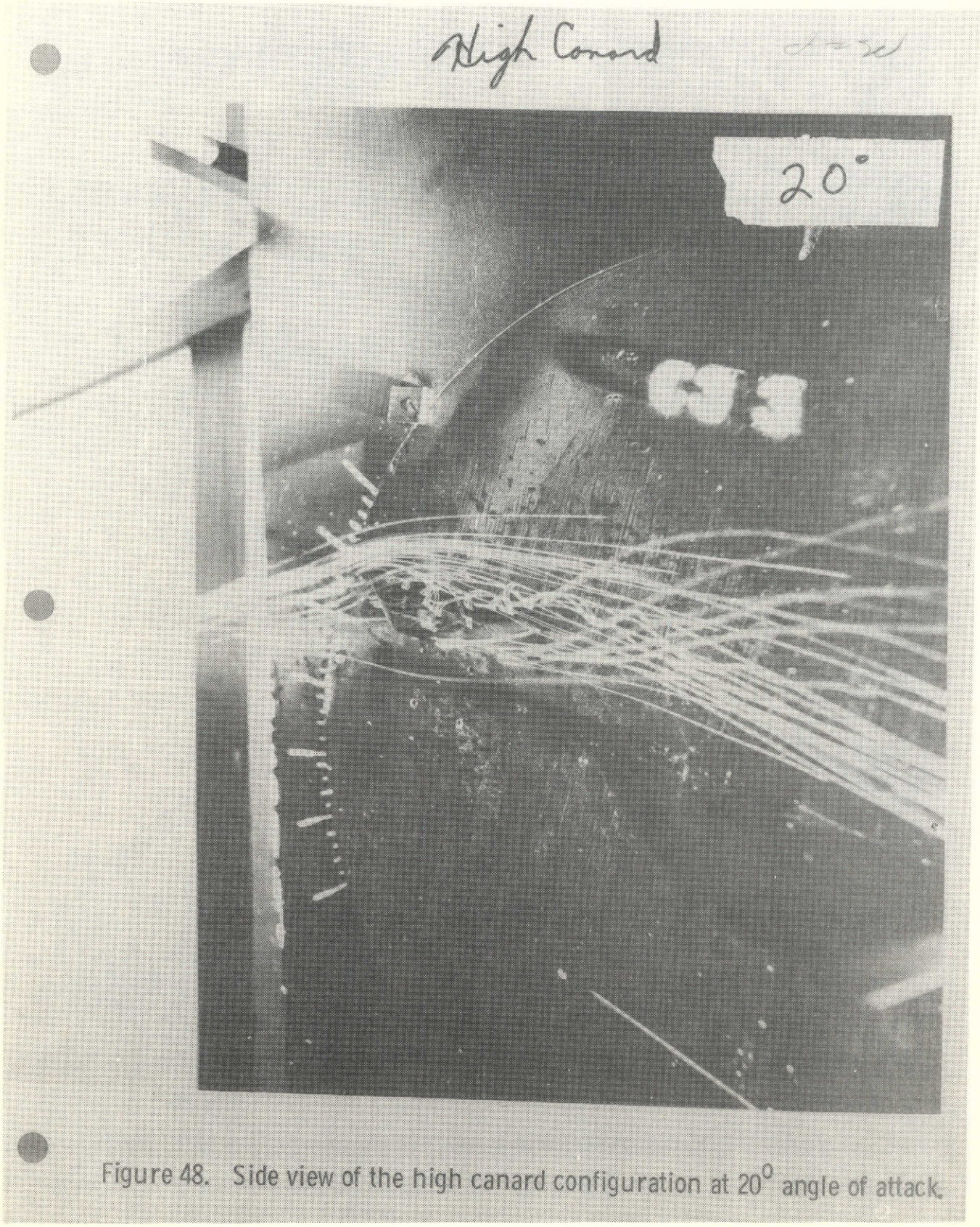

Figure 48. Side view of the high canard configuration at 20° angle of attack.

Figure 49. Mid canard at 20° angle of attack.

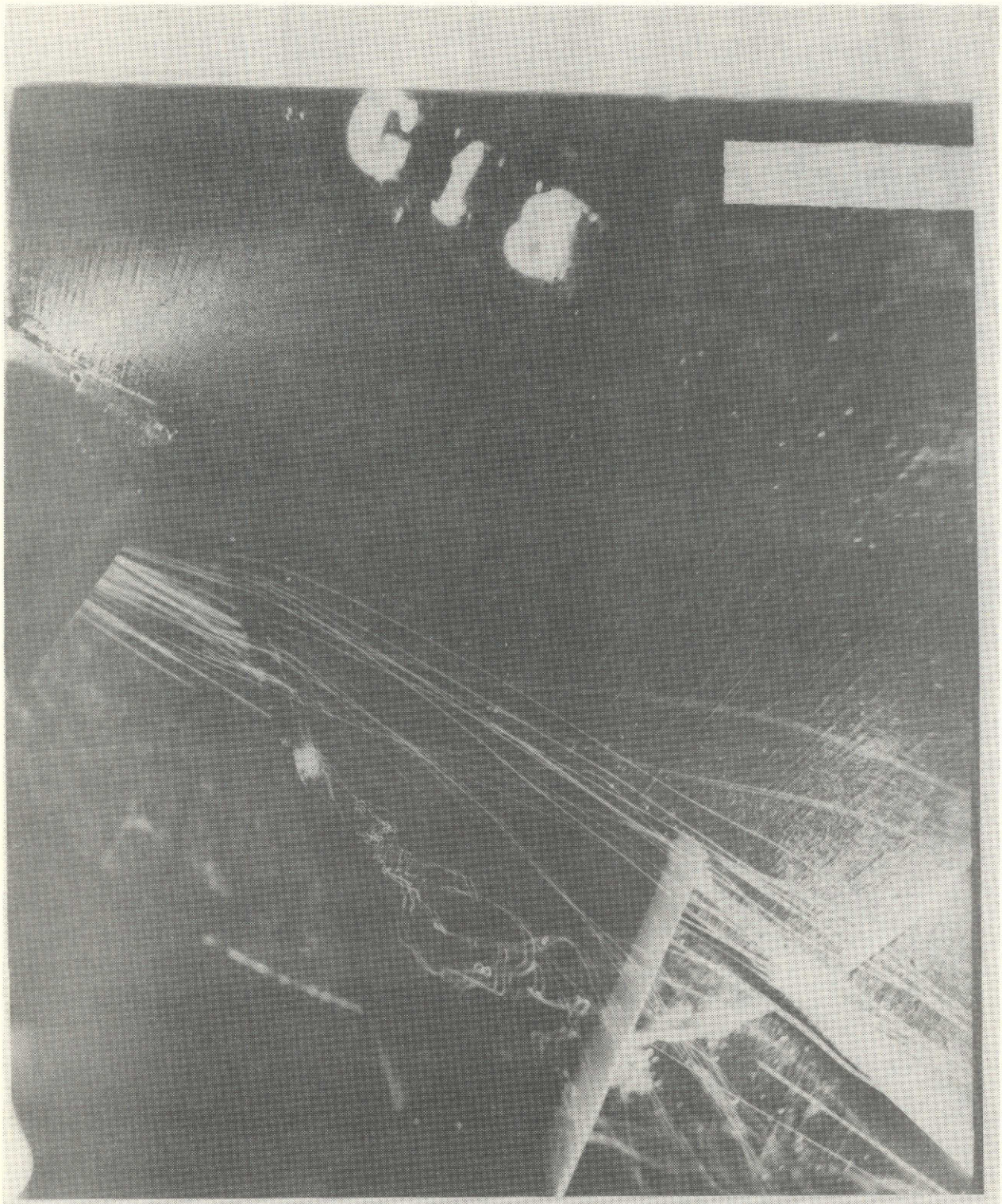

Figure 50. Wing in the presence the mid canard at 20^{o} angle of attack.

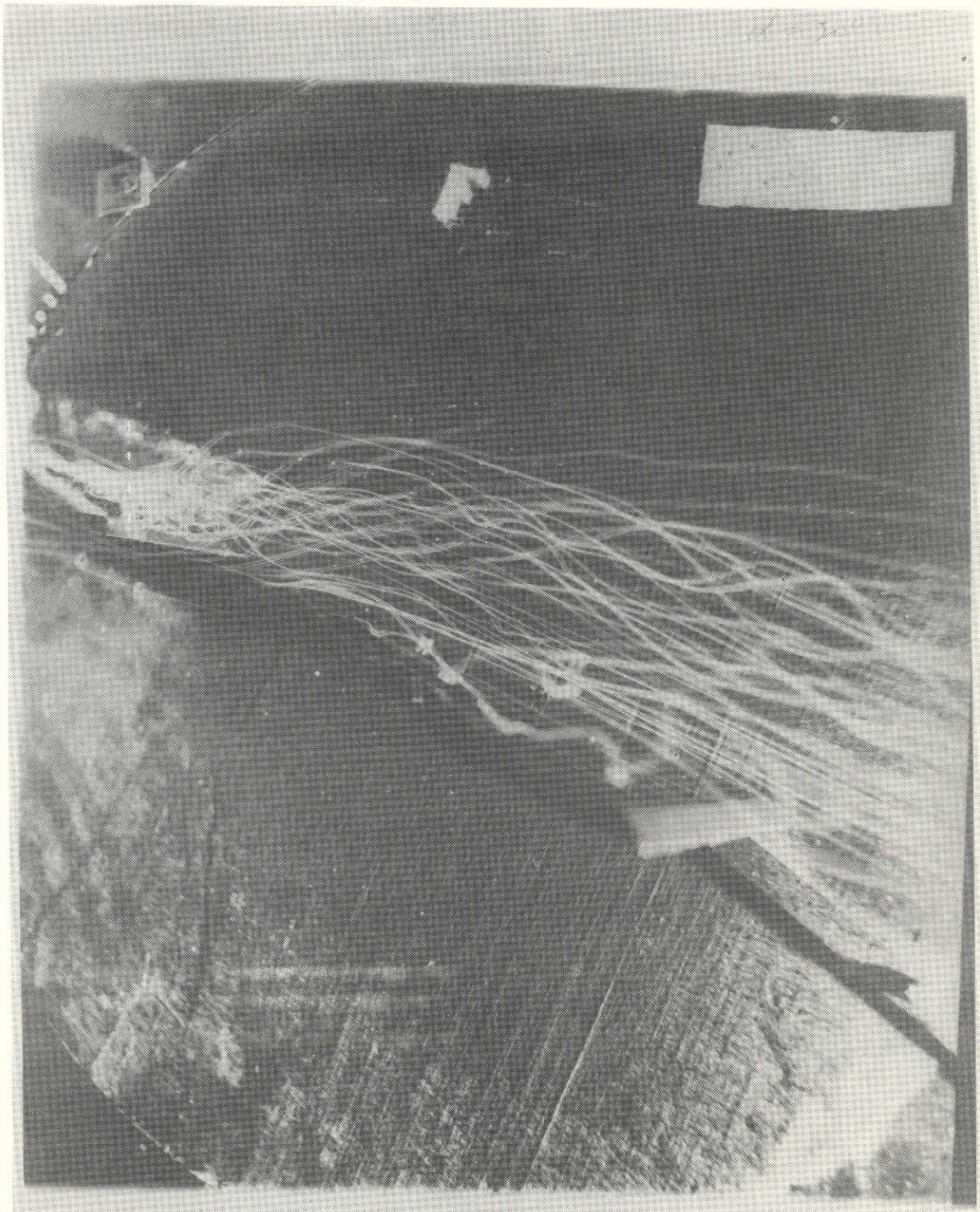

Figure 51. Side view of the mid canard configuration at 20^{o} angle of attack.

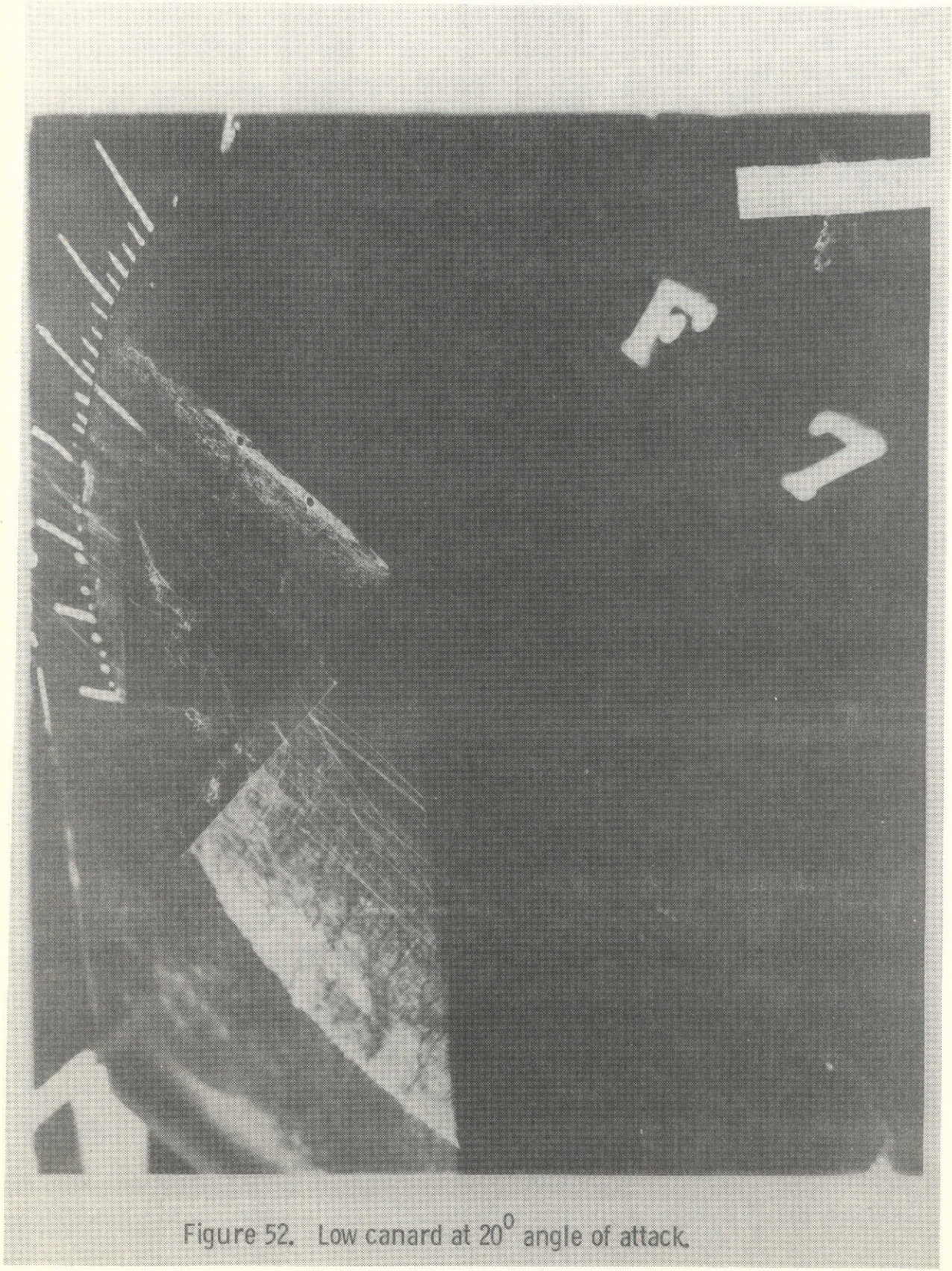

Figure 52. Low canard at 20^{0} angle of attack.

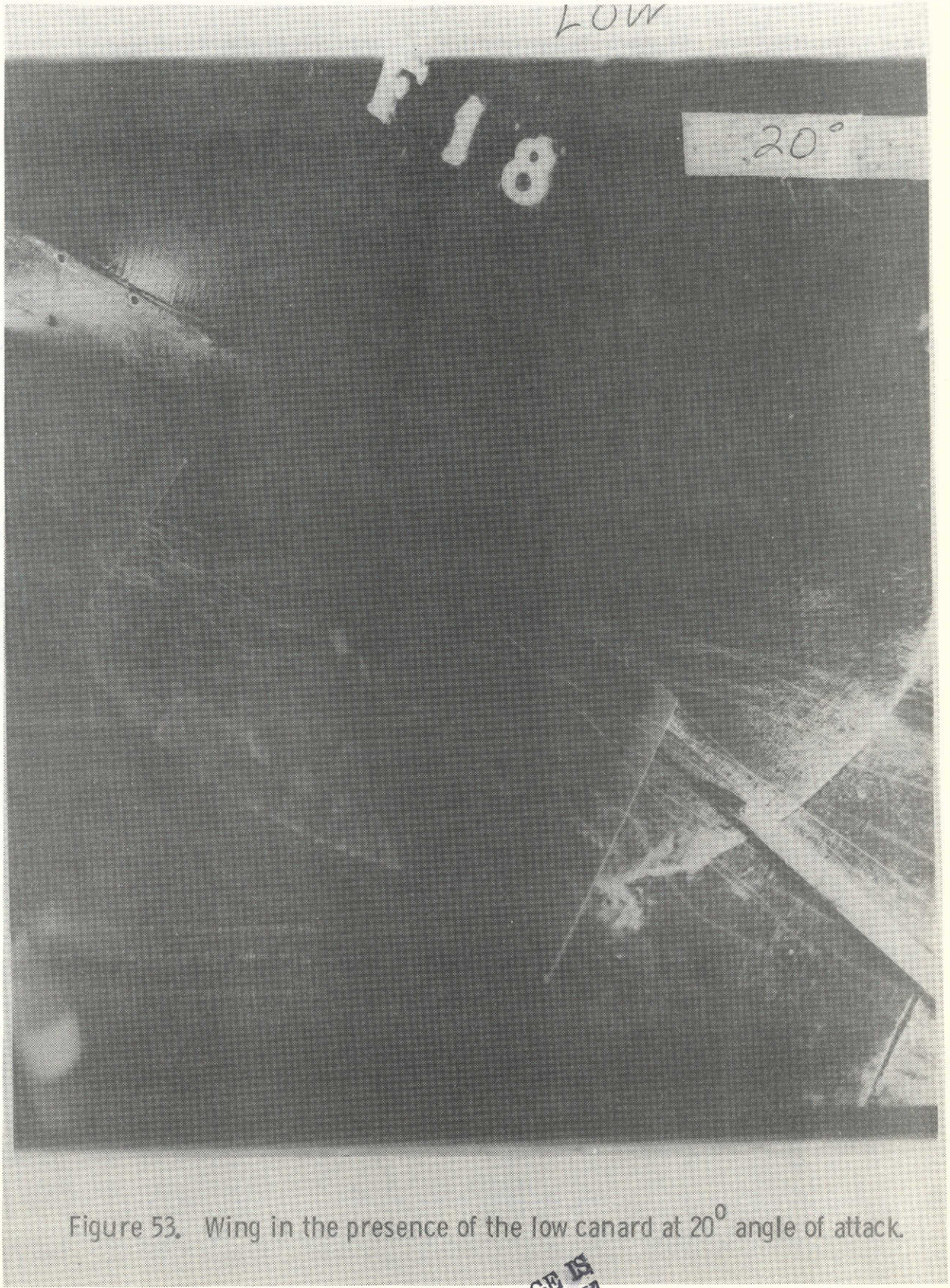

Figure 53. Wing in the presence of the low canard at 20° angle of attack.

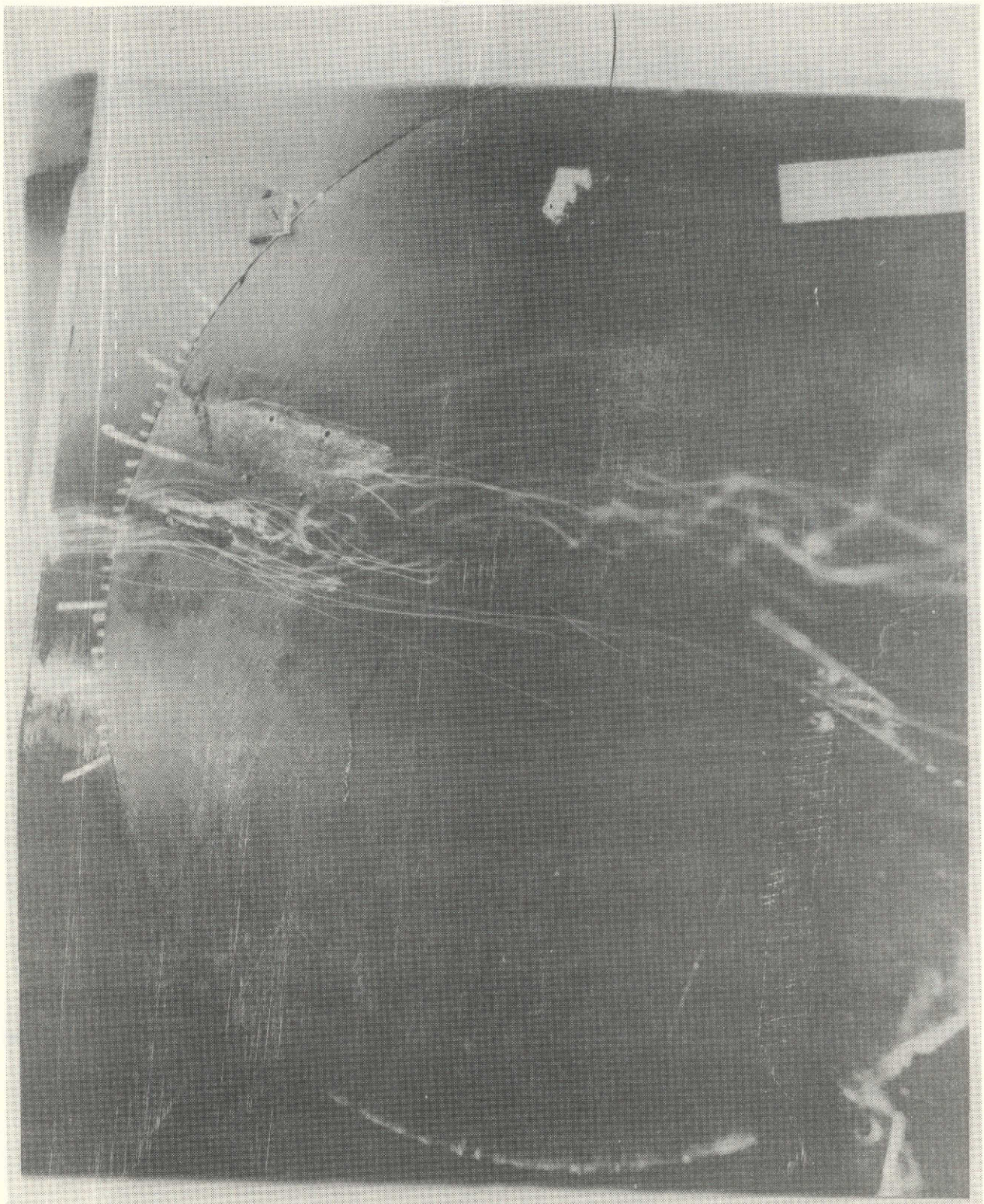

Figure 54. Side view of the low canard configuration at 20° angle of attack.

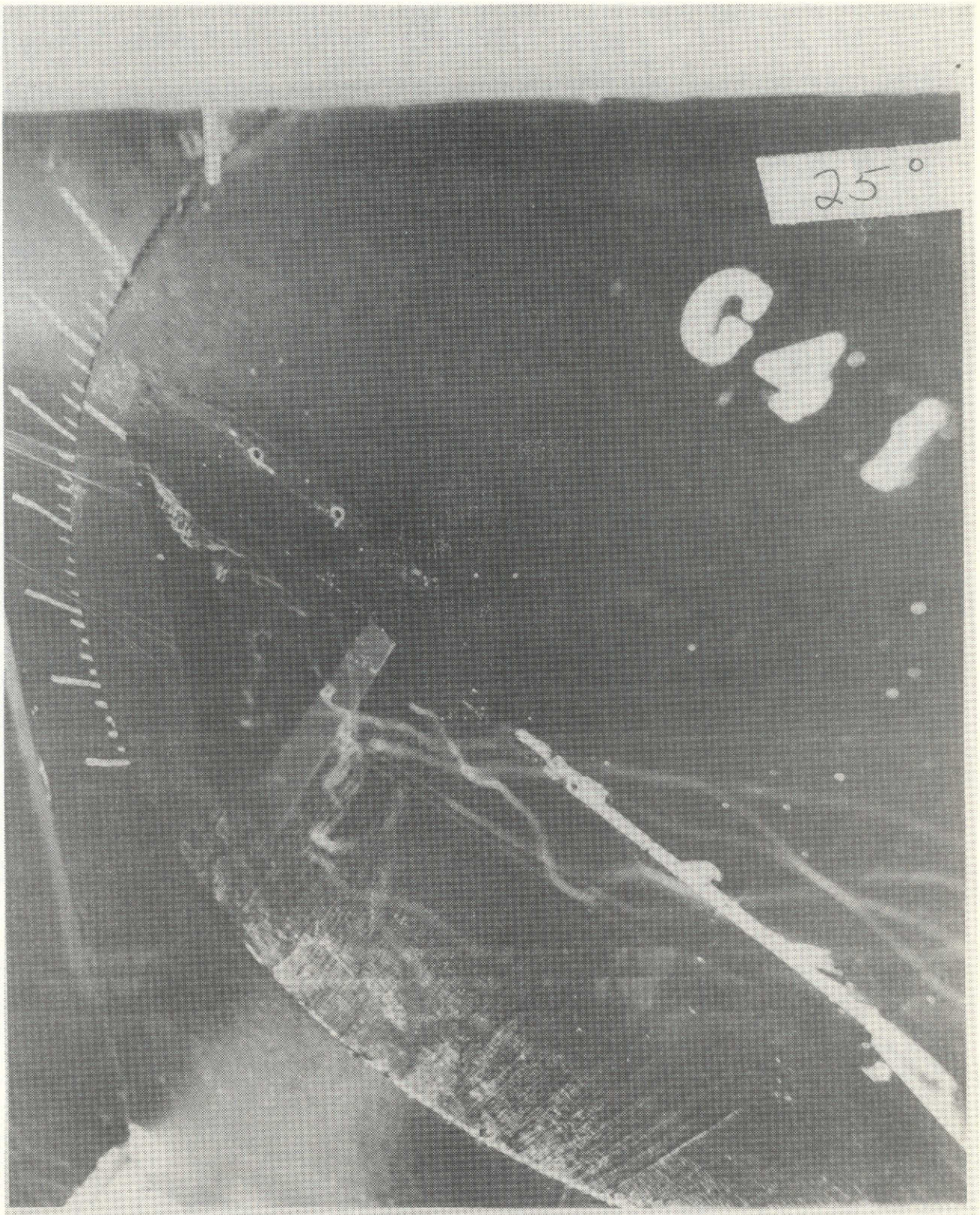

Figure 55. Canard alone at 25° angle of attack.

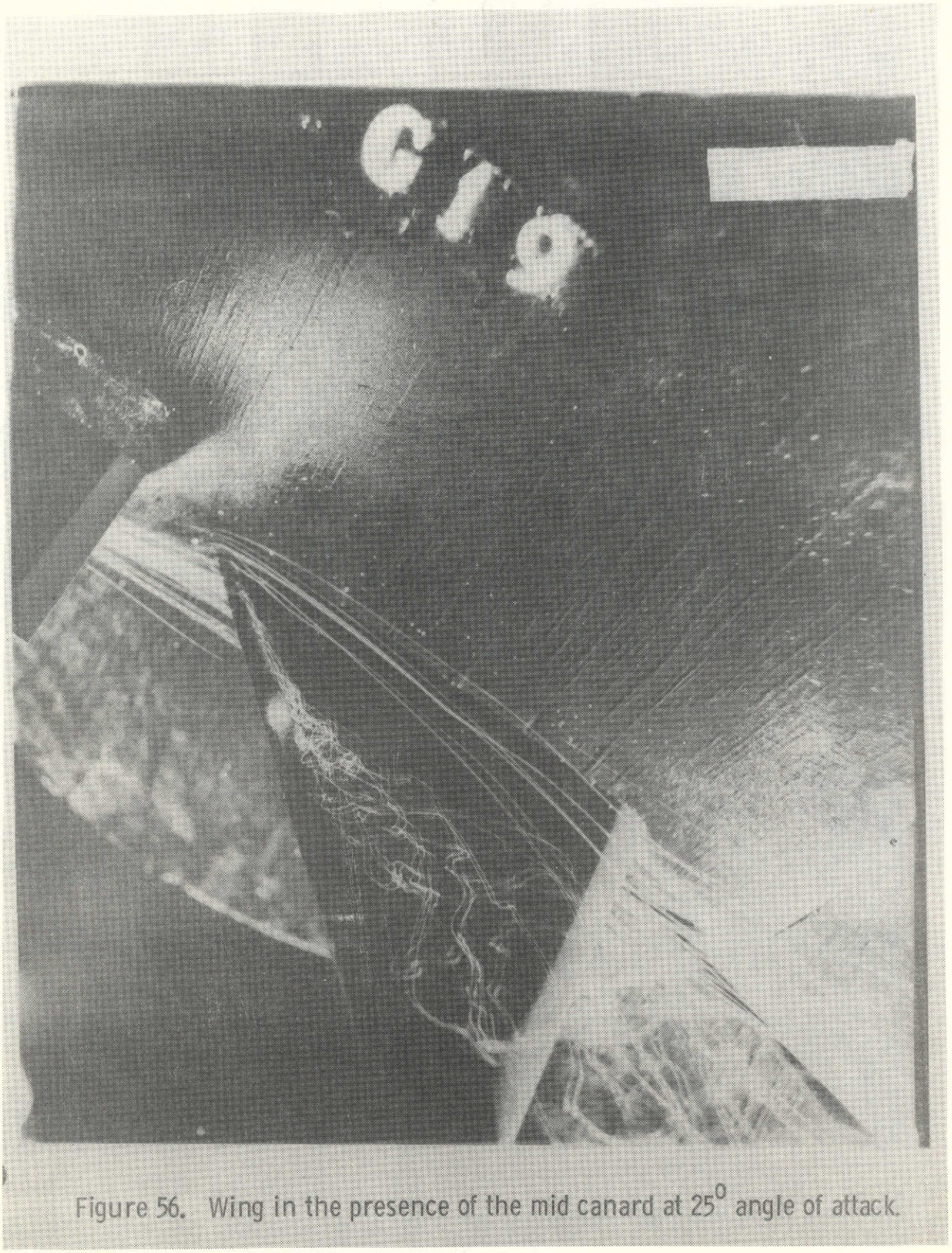

Figure 56. Wing in the presence of the mid canard at 25° angle of attack.

Figure 57. Canard alone at 30° angle of attack.

Figure 58. Wing alone at 30^{0} angle of attack.

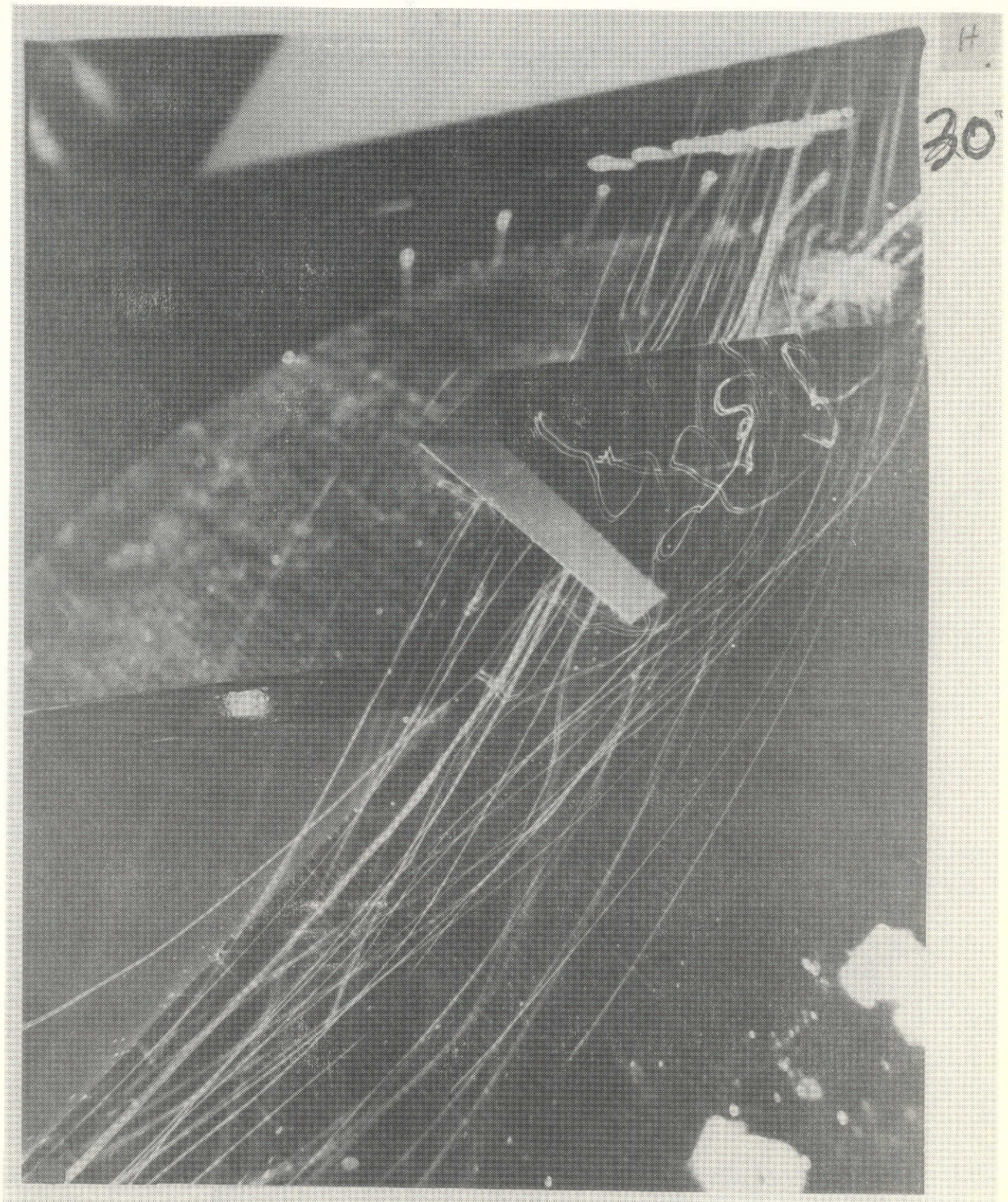

Figure 59. High canard at 30^{0} angle of attack.

Figure 60. Wing in the presence of the high canard at 30^{o} angle of attack.

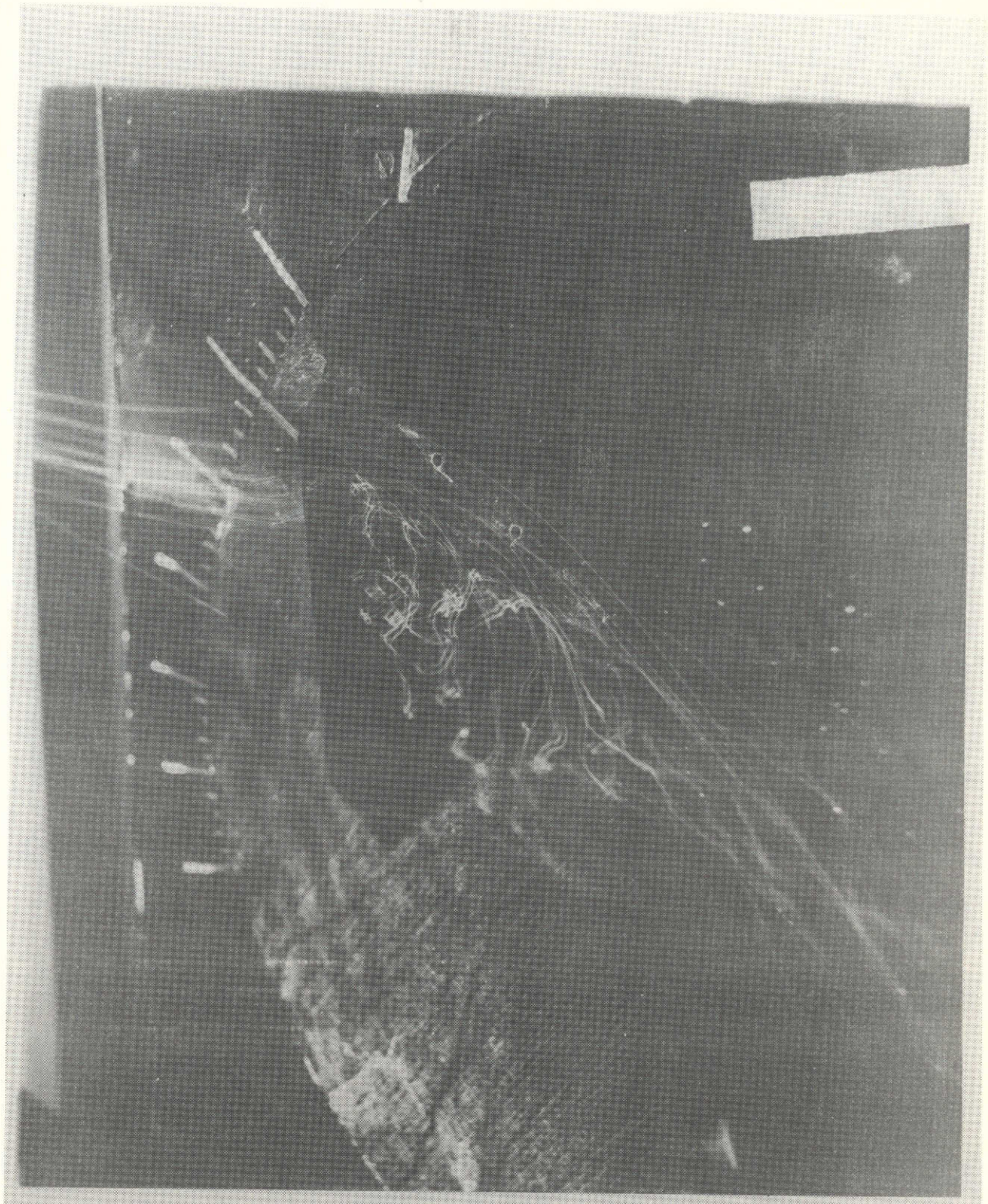

Figure 61. Mid canard at 30^{o} angle of attack.

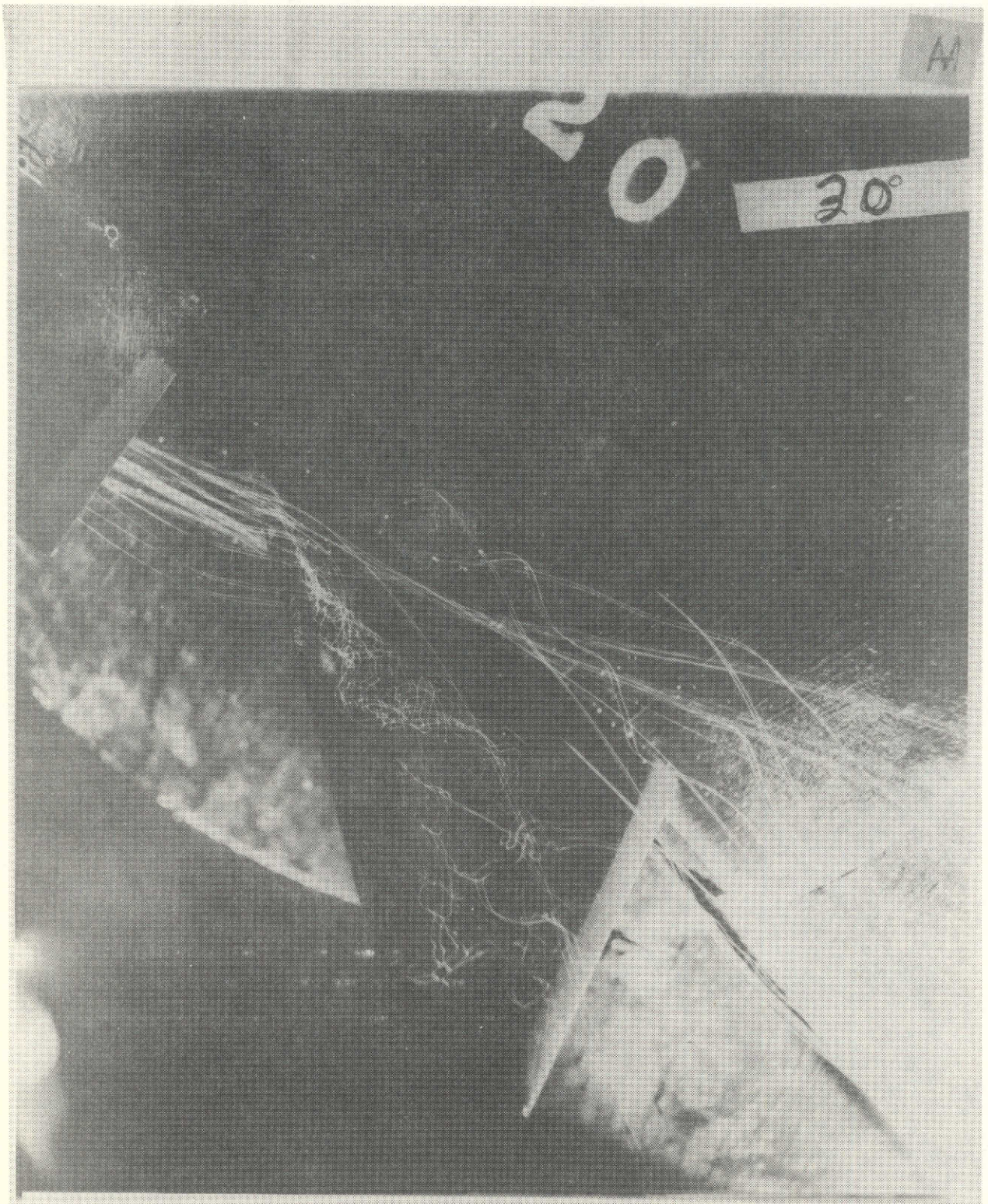

Figure 62. Wing in the presence of the mid canard at 30^{0} angle of attack.

Figure 63. Low canard at 30^{0} angle of attack.

Figure 64. Wing in the presence of the low canard at 30^{0} angle of attack.

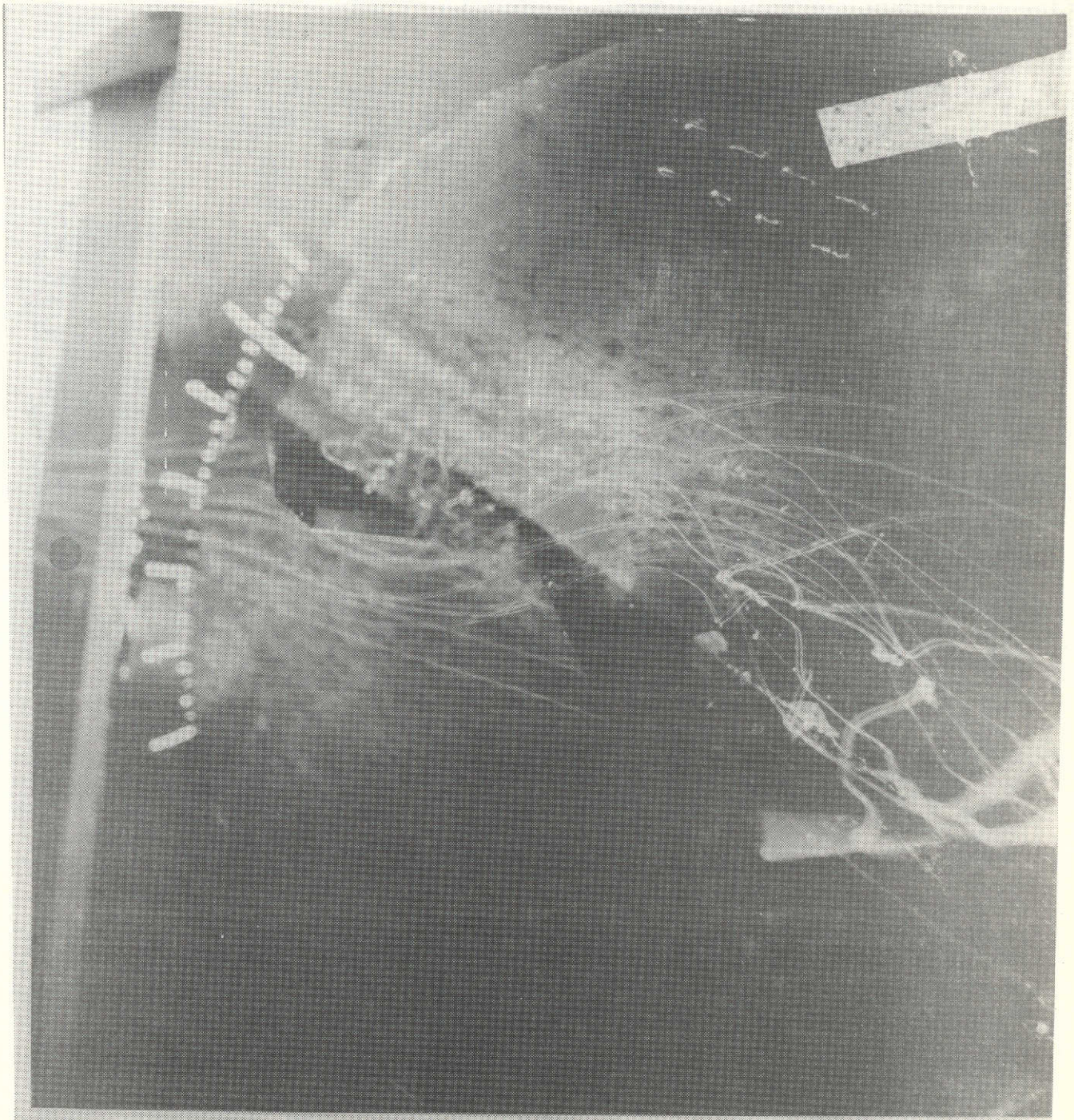

Figure 65. Side view of the low canard configuration at 30^{0} angle of attack.

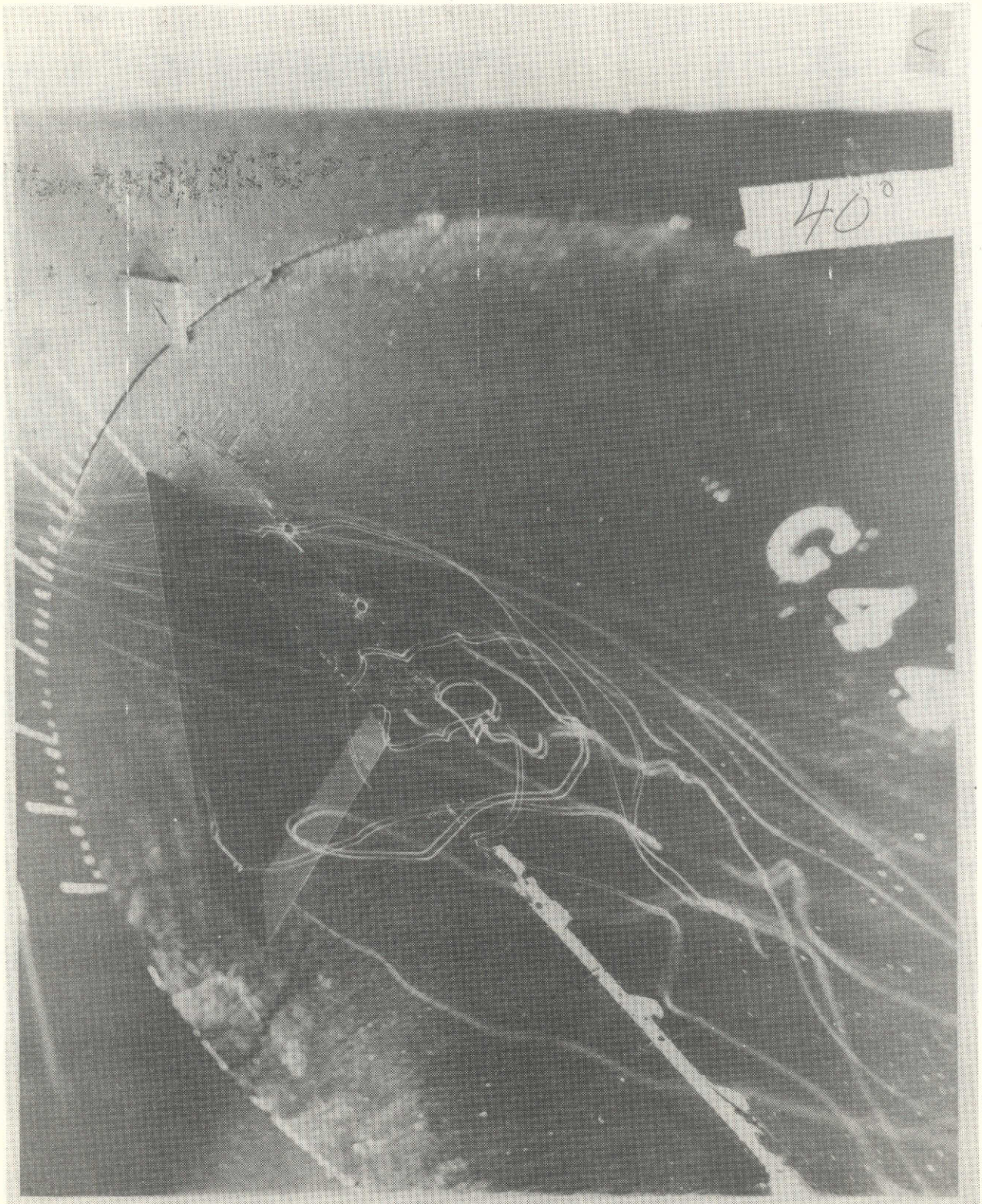

Figure 66. Canard alone at 40^{0} angle of attack.

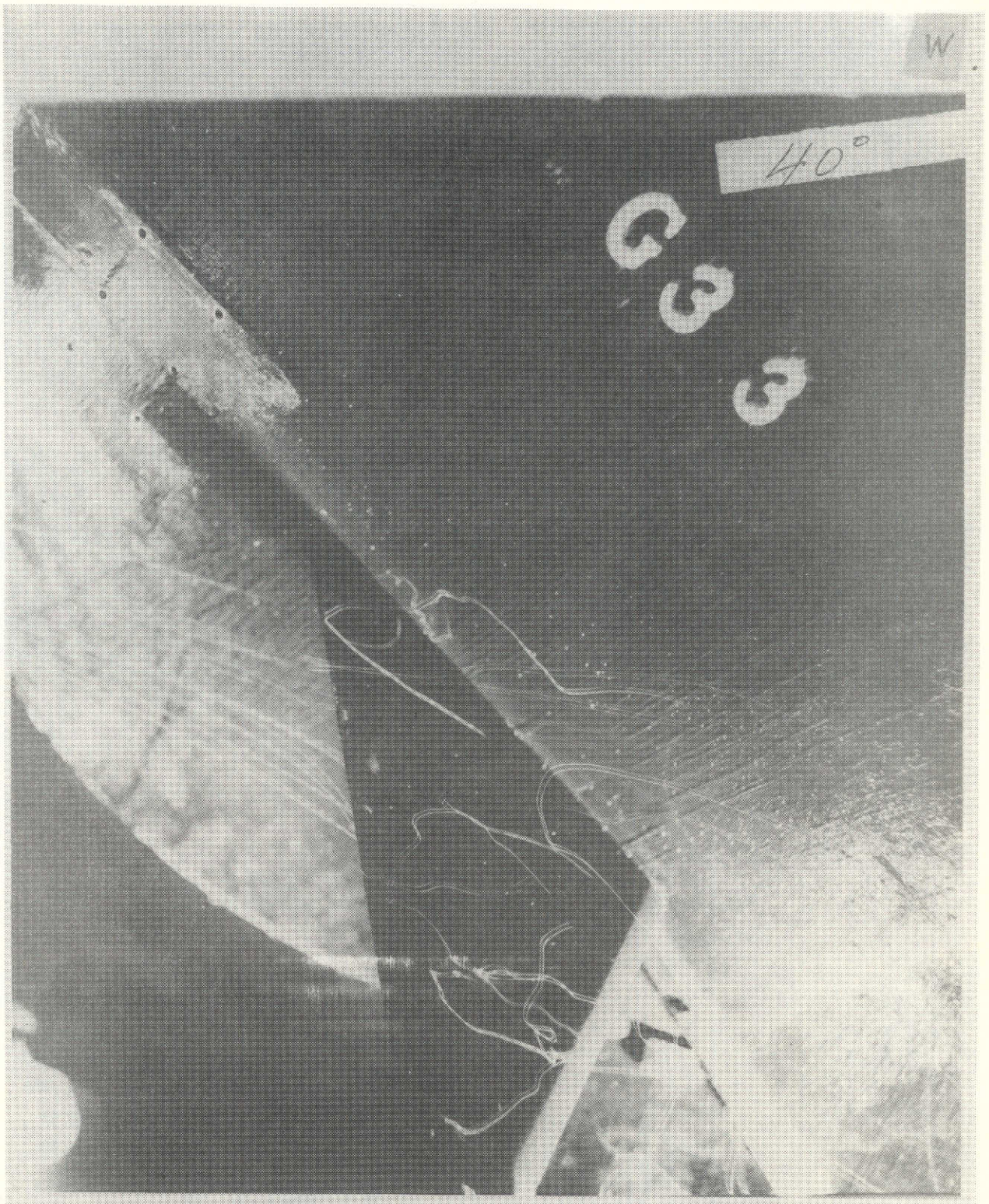

Figure 67. Wing alone at 40° angle of attack.

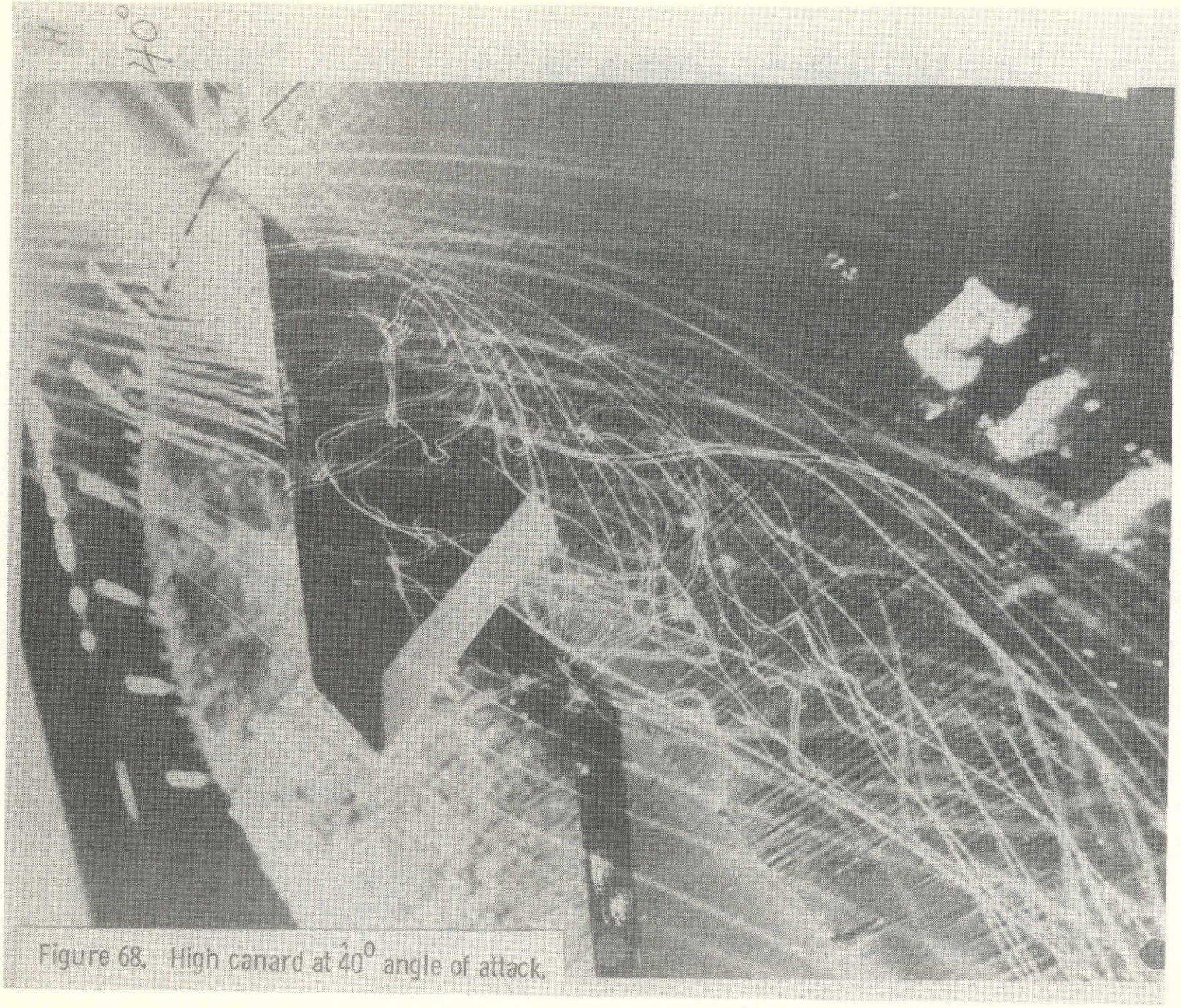

Figure 68. High canard at 40° angle of attack.

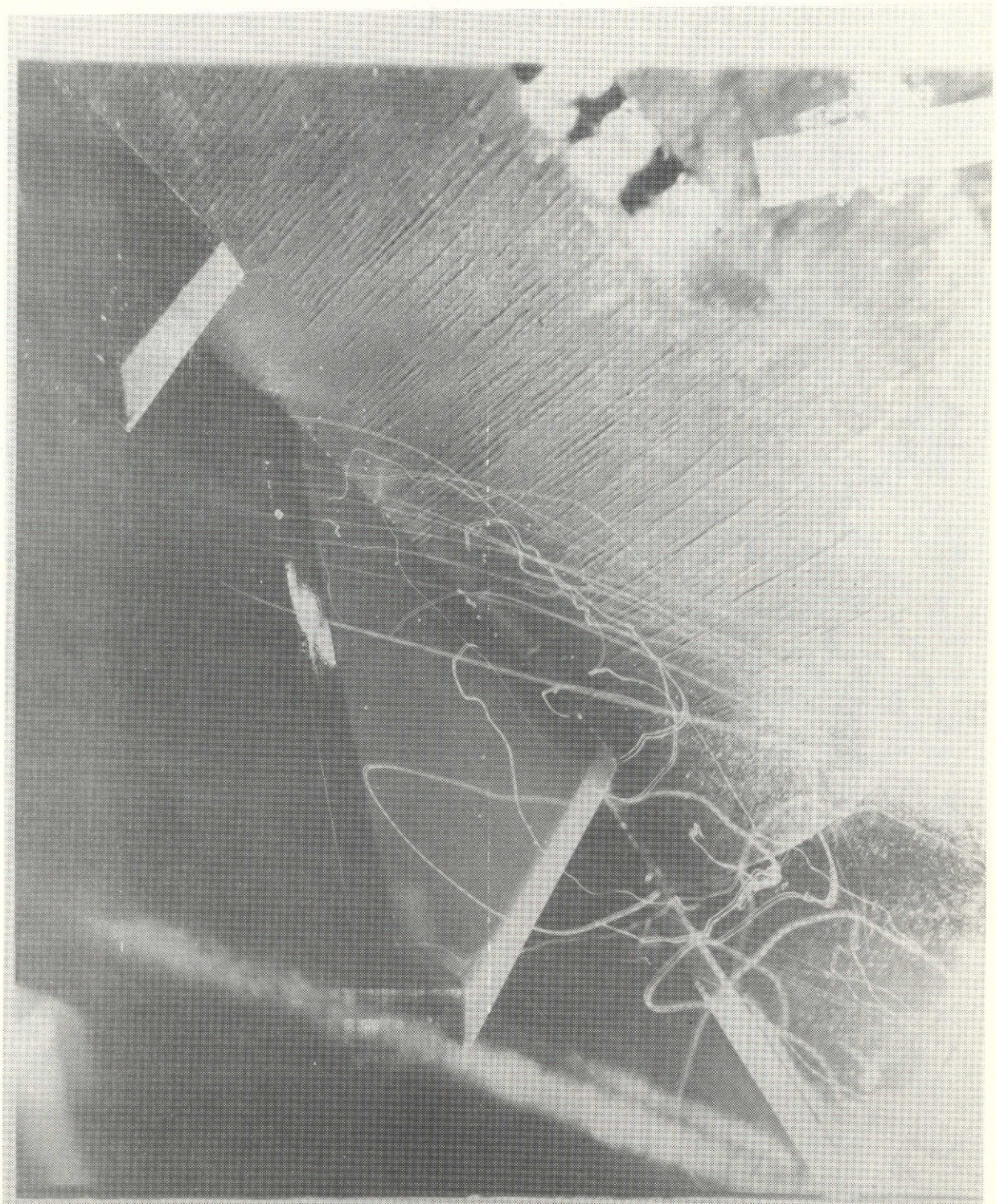

Figure 69. Wing in the presence of the high canard at 40^{0} angle of attack.

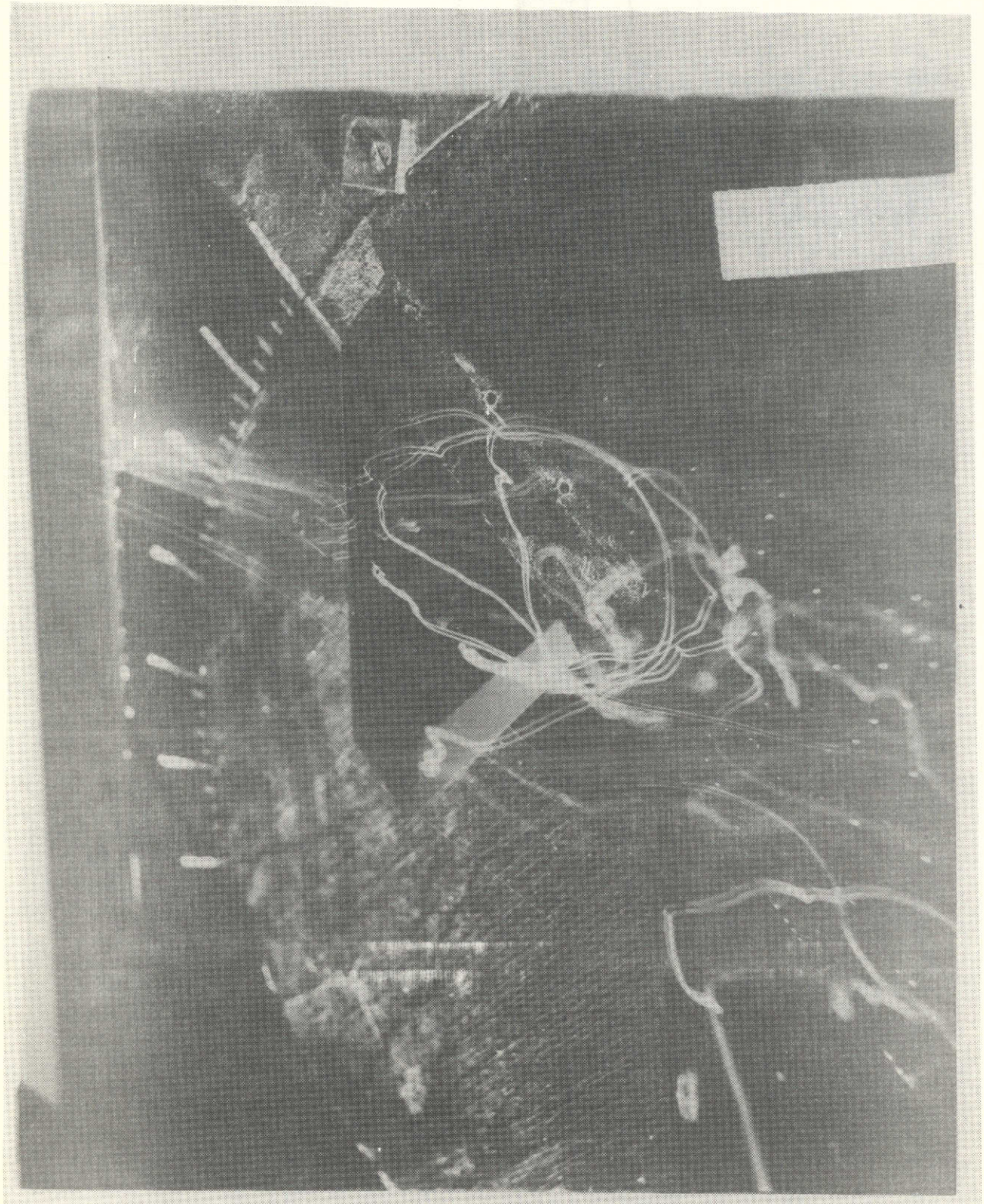

Figure 70. Mid canard at 40^{o} angle of attack.

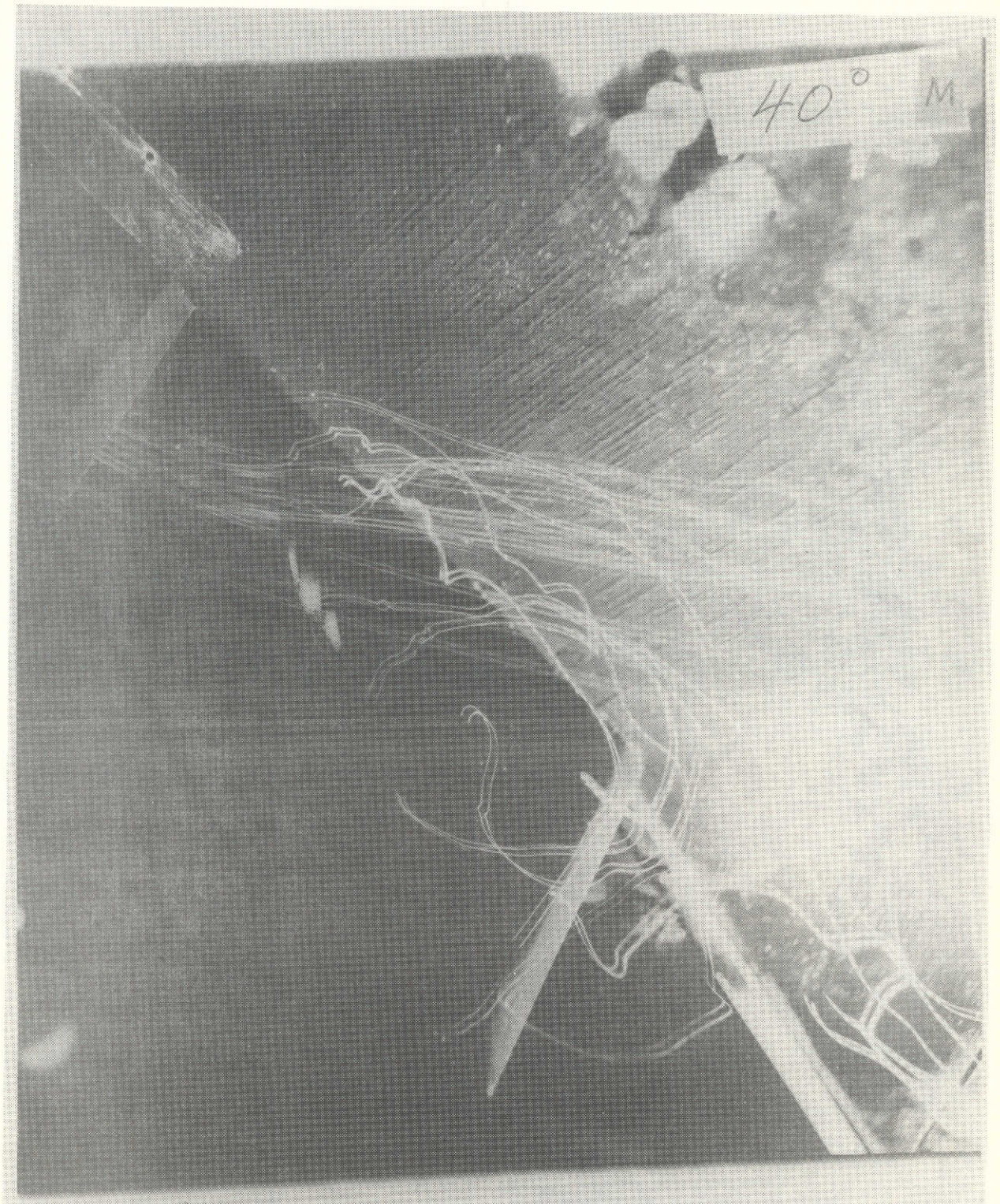

Figure 71. Wing in the presence of the mid canard at 40° angle of attack.

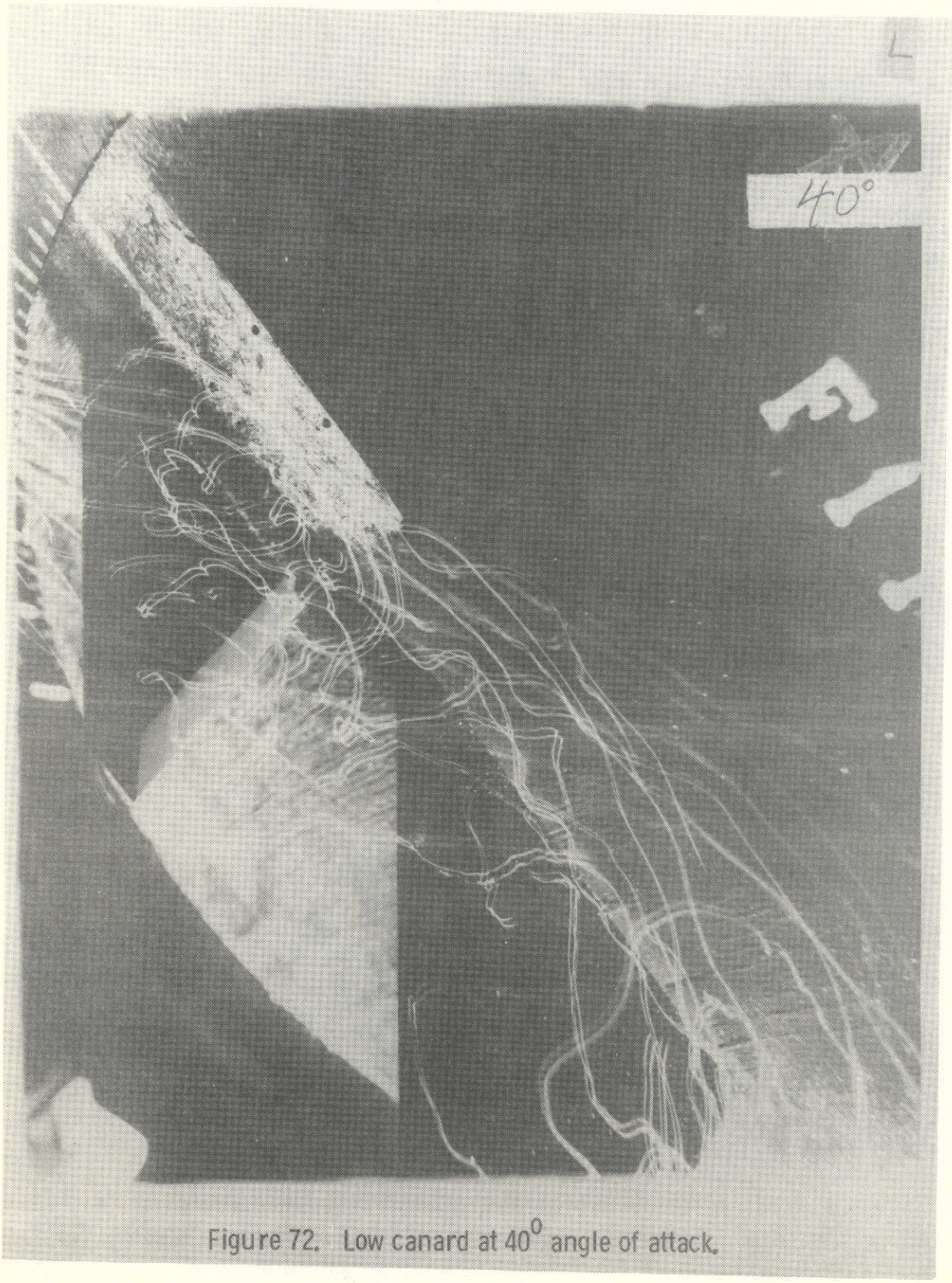

Figure 72. Low canard at 40^{0} angle of attack.

Figure 73. Wing in the presence of the low canard at 40° angle of attack.

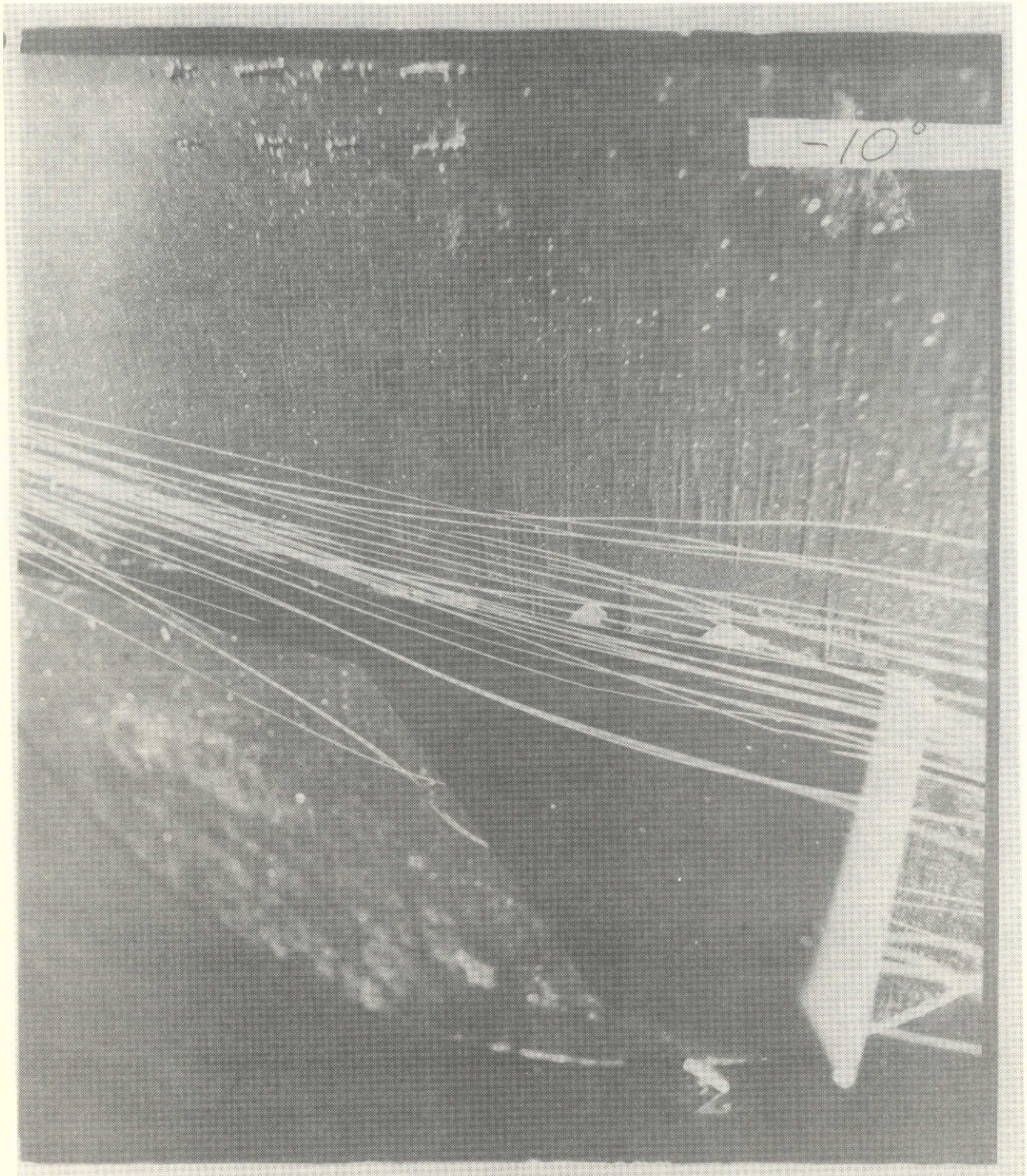

Figure 74. Strake-wing at an angle of attack of -10^{0}.

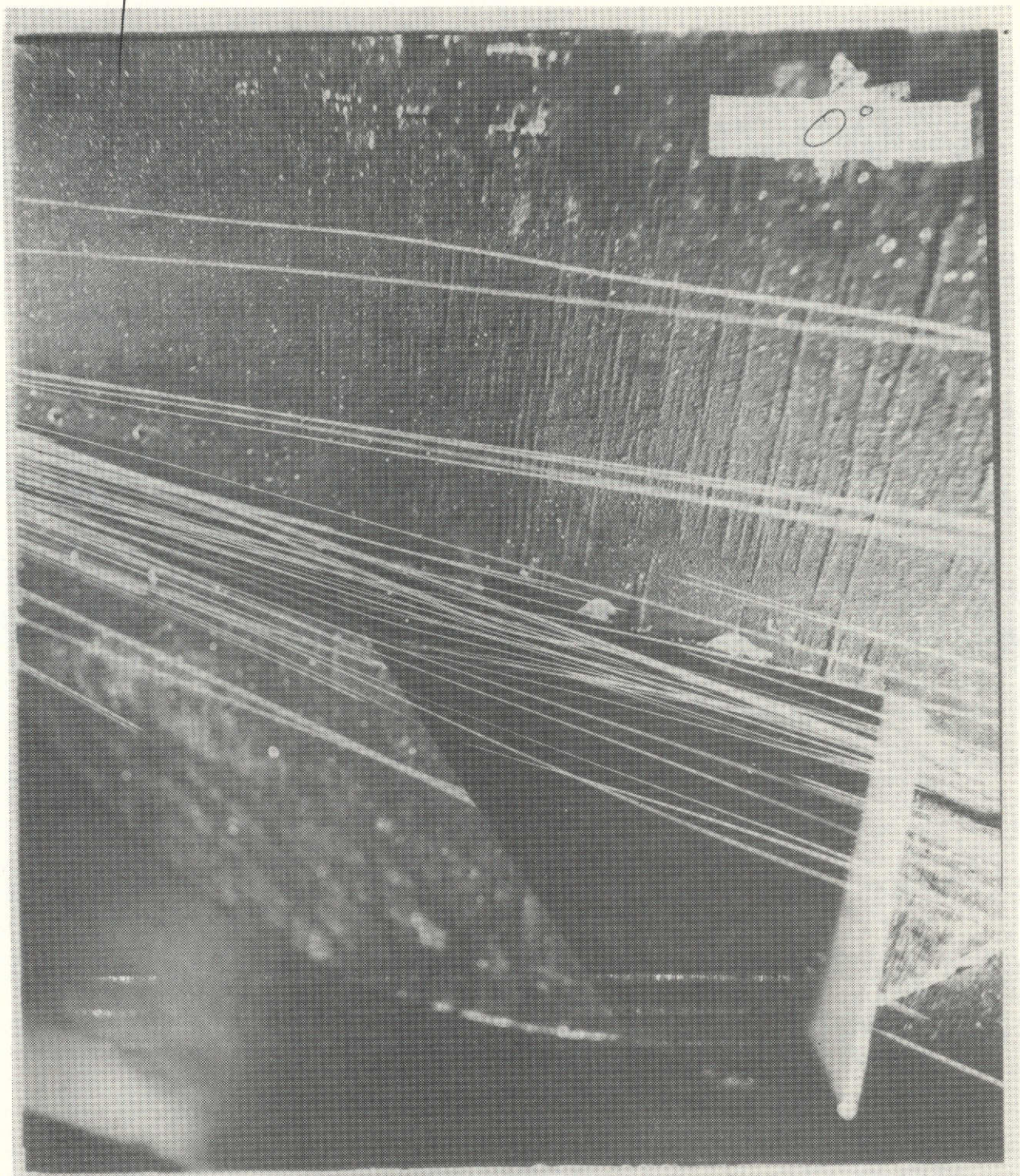

Figure 75. Strake-wing at an angle of attack of 0°.

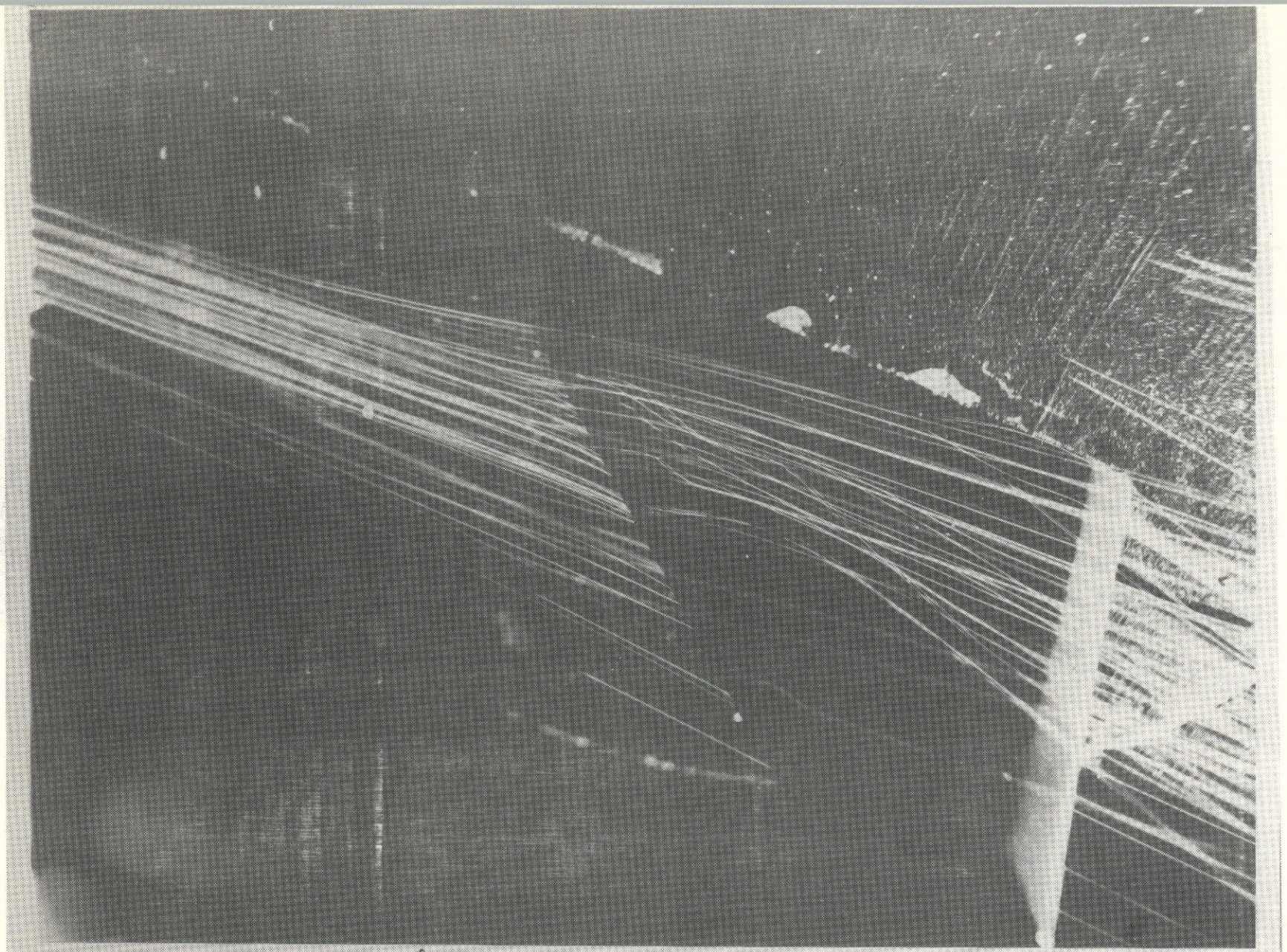

Figure 76. Strake-wing at an angle of attack of 10^{0}.

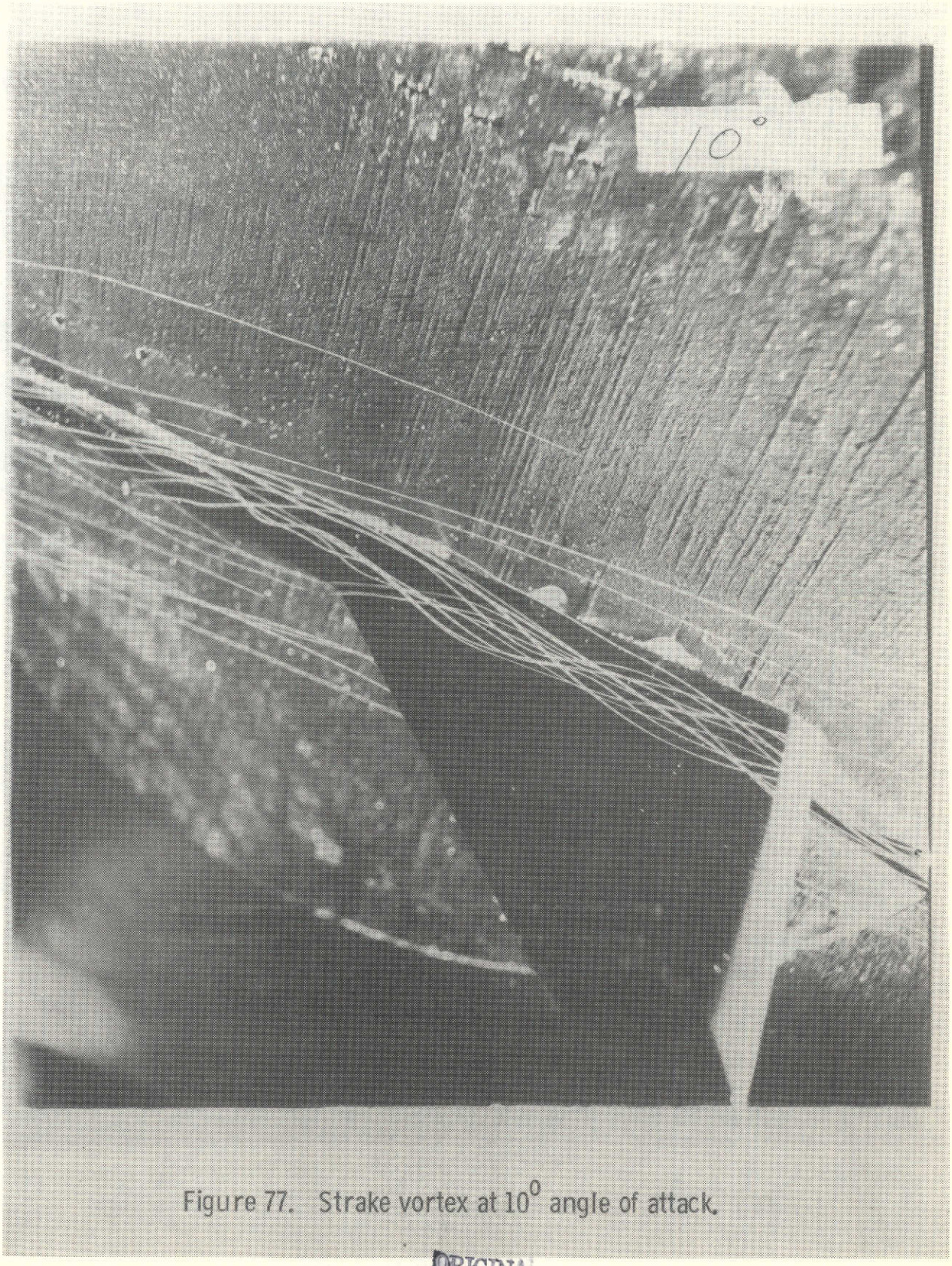

Figure 77. Strake vortex at 10^{0} angle of attack.

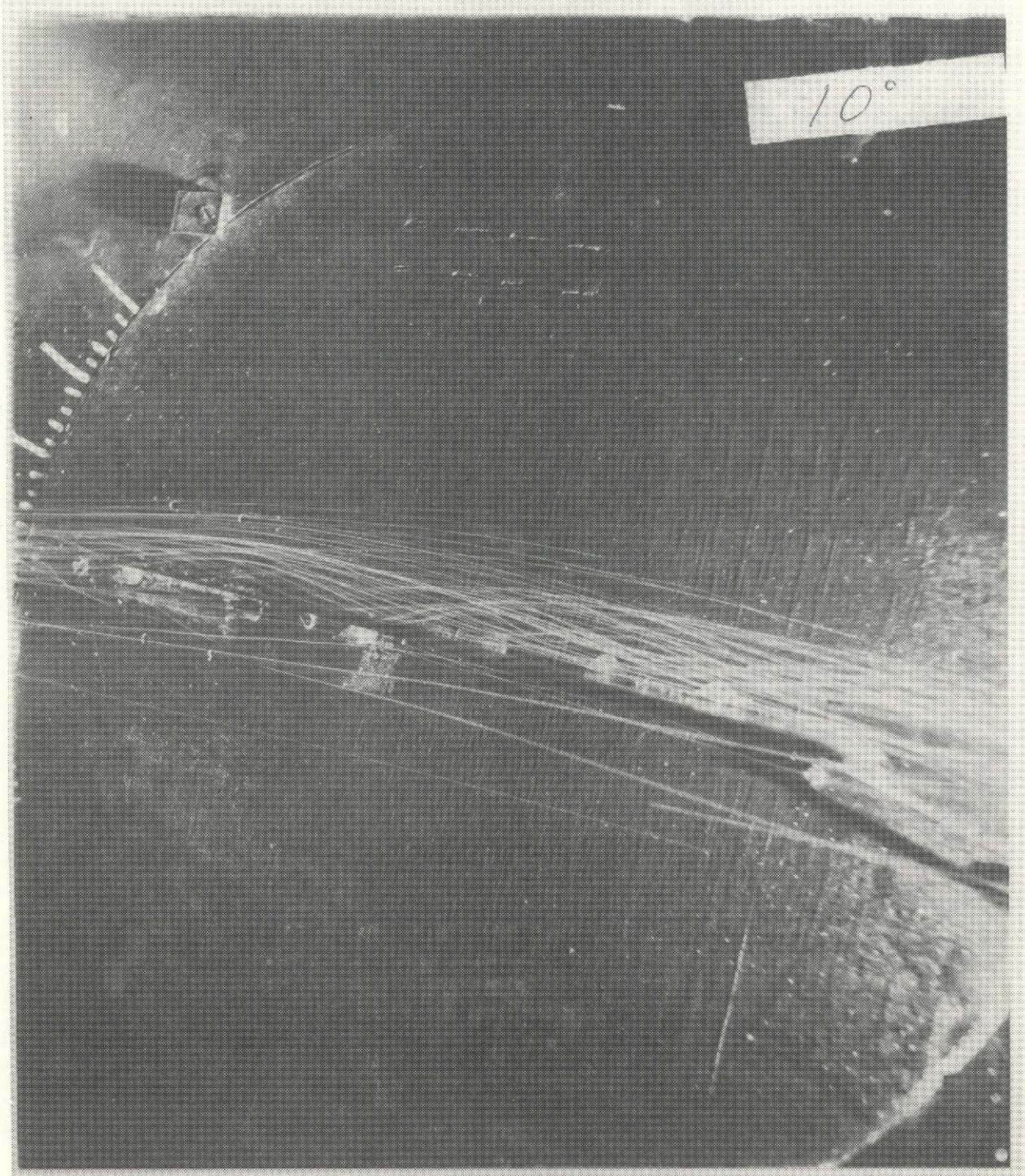

Figure 78. Side view of the strake vortex at 10^{0} angle of attack.

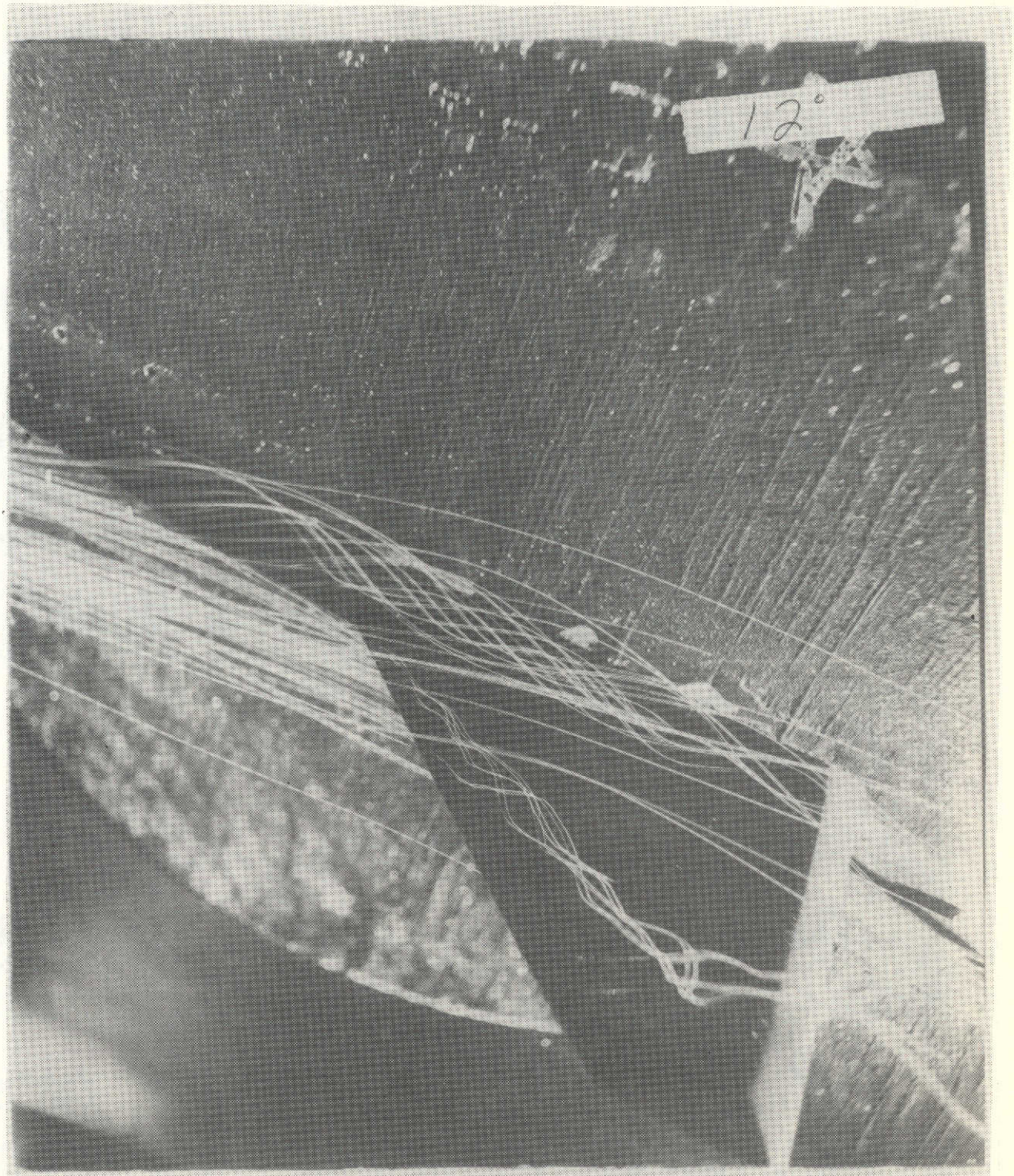

Figure 79. Strake-wing at an angle of attack of 12^{0}.

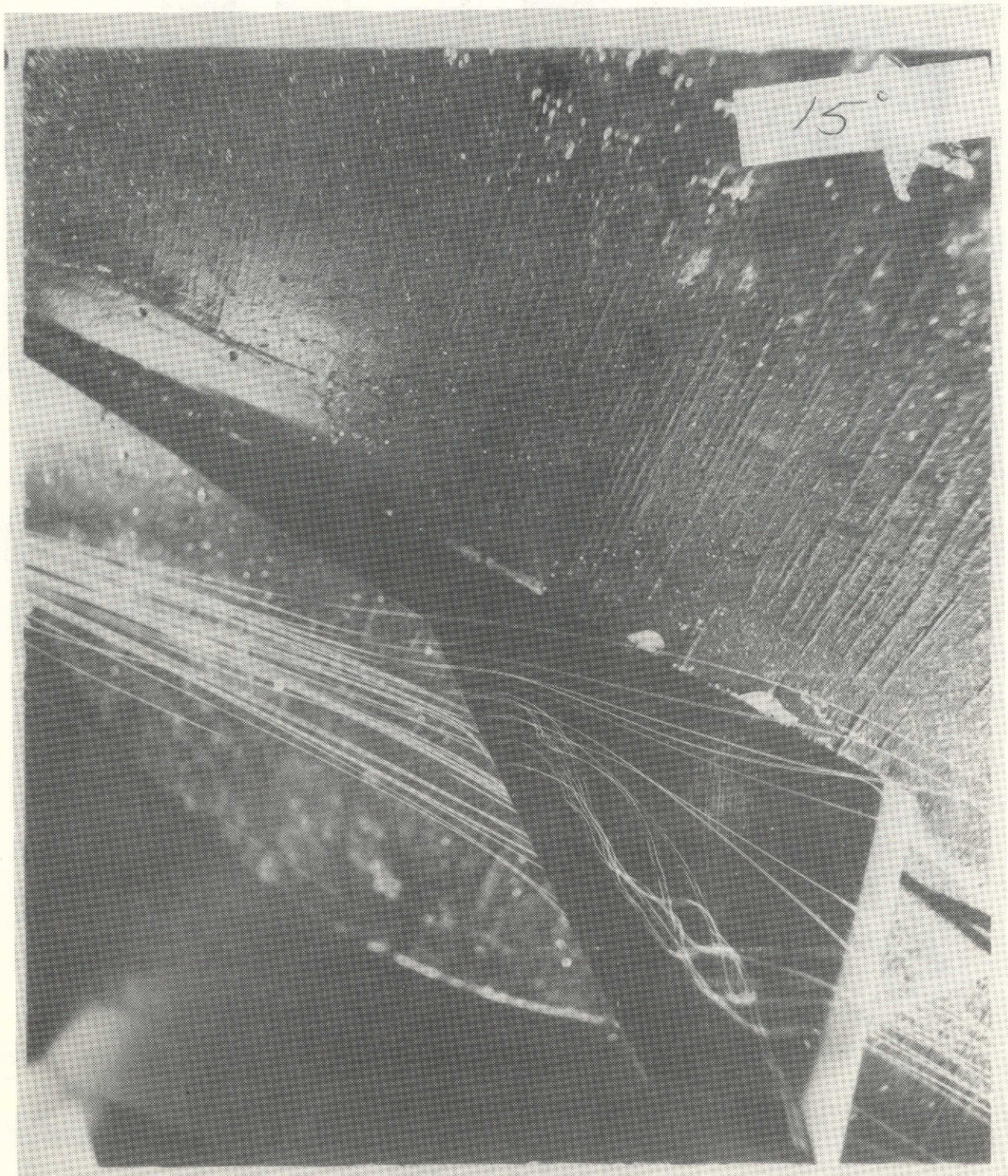

Figure 80. Strake-wing at an angle of attack of 15^{0}.

Figure 81.- Strake vortex at 15^{0} angle of attack.

Figure 82. Strake-wing at an angle of attack of 18^{0}.

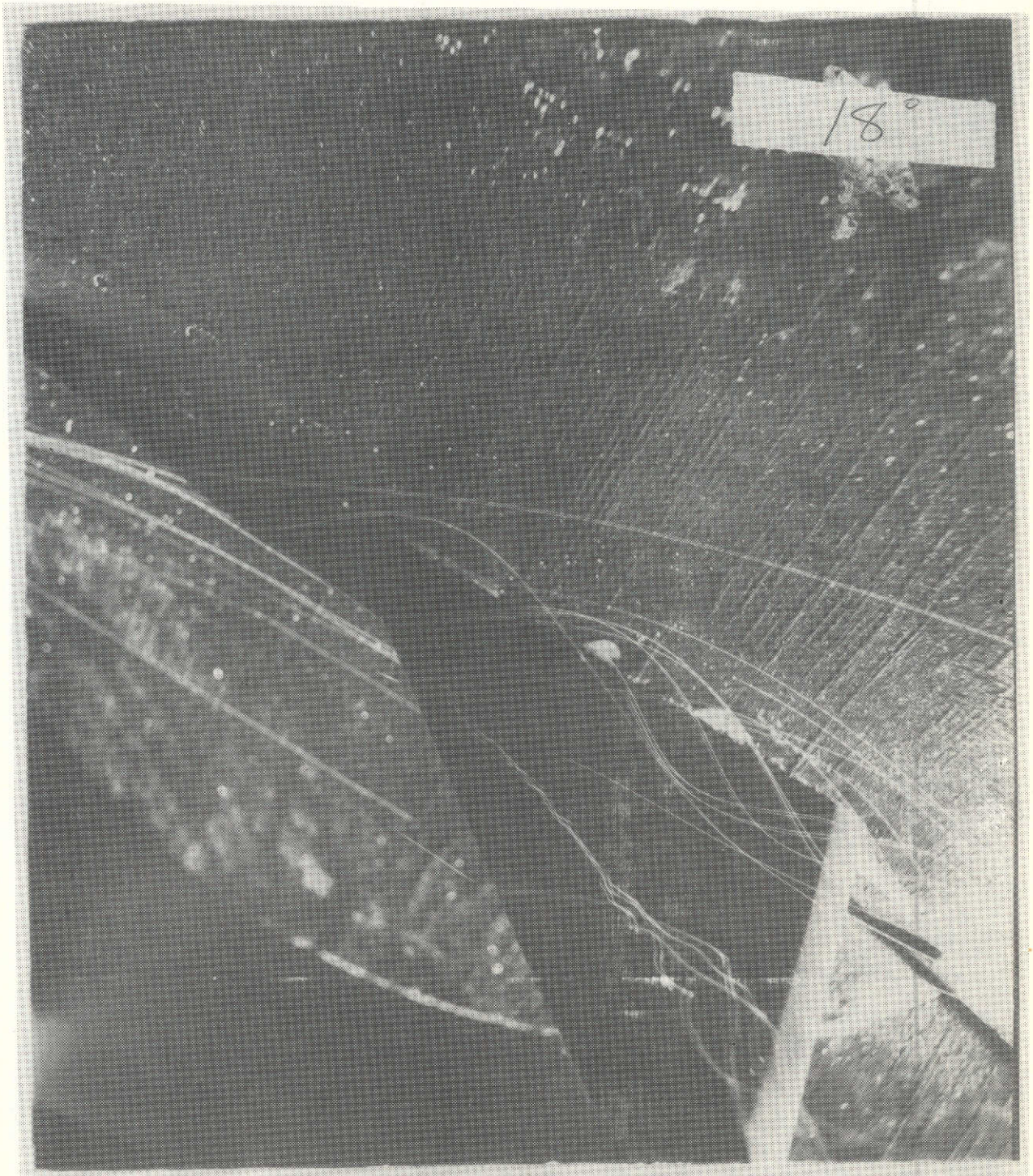

Figure 83. Strake-wing at an angle of attack of 18^{o}.

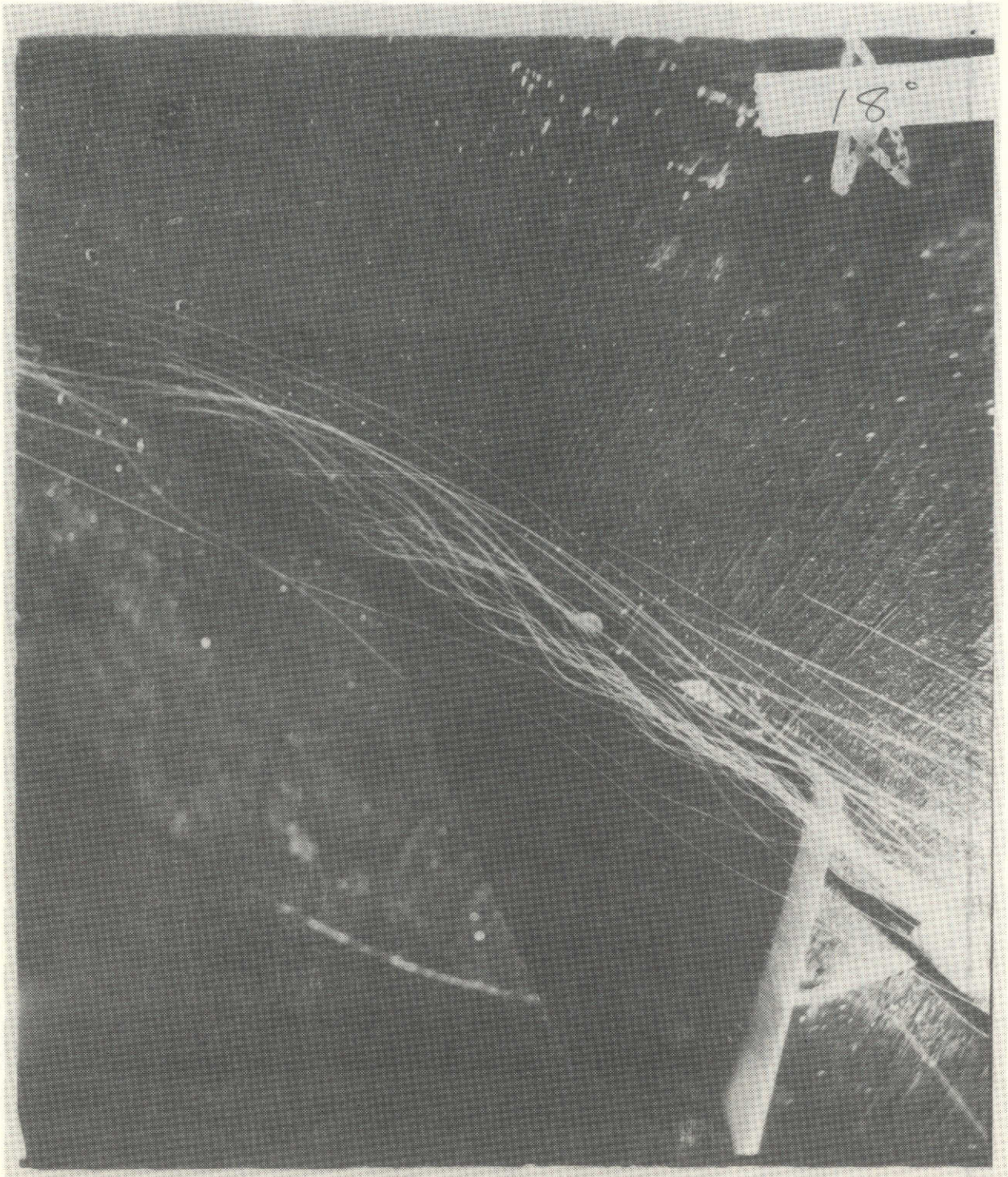

Figure 84. Strake vortex at 18° angle of attack.

Figure 85. Side view of the strake vortex at 18° angle of attack.

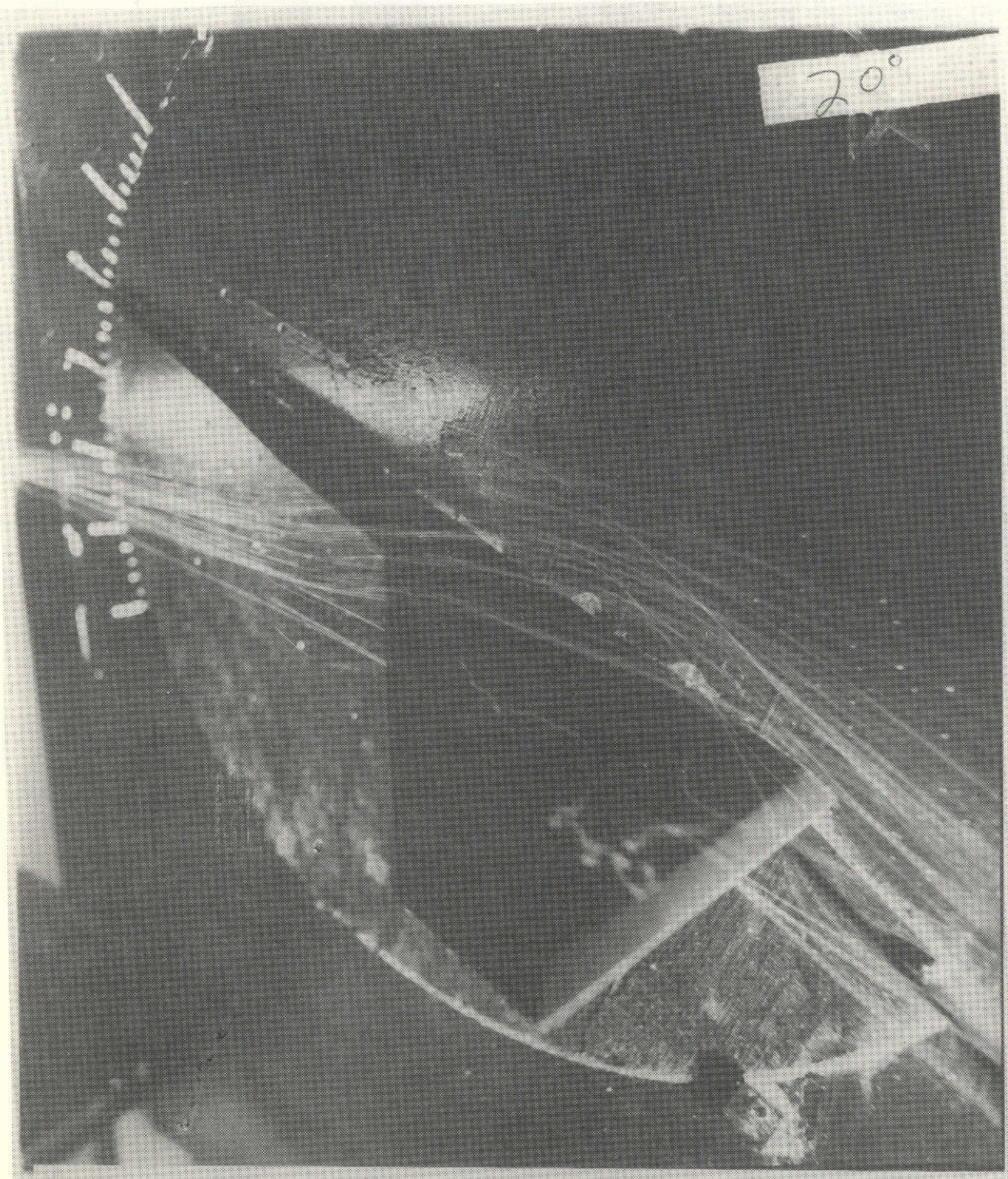

Figure 86. Strake wing at an angle of attack of 20^{o}.

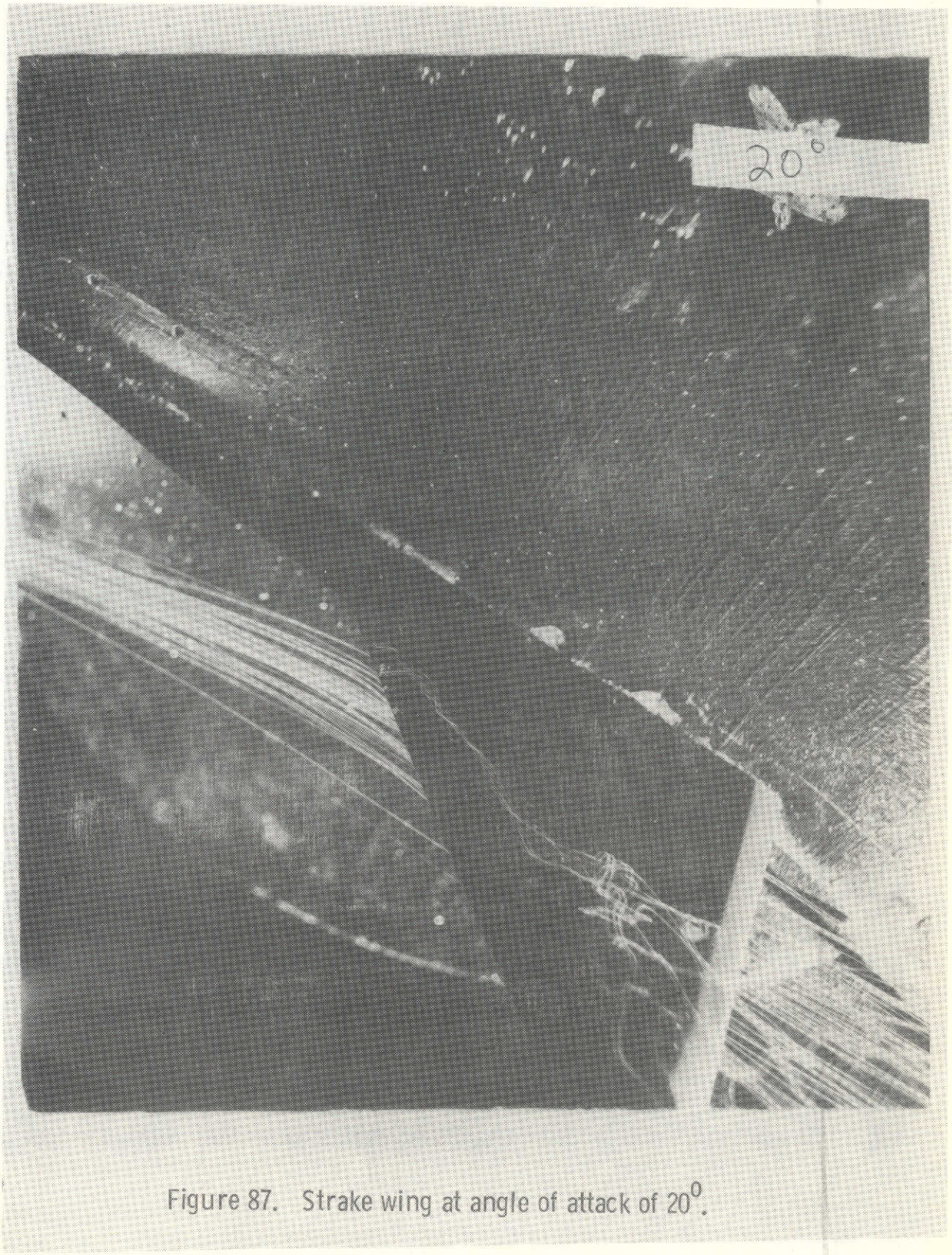

Figure 87. Strake wing at angle of attack of 20^{0}.

Figure 88. Strake wing at angle of attack of 20^{o}.

Figure 89. Strake wing at angle of attack of 20^{0}.

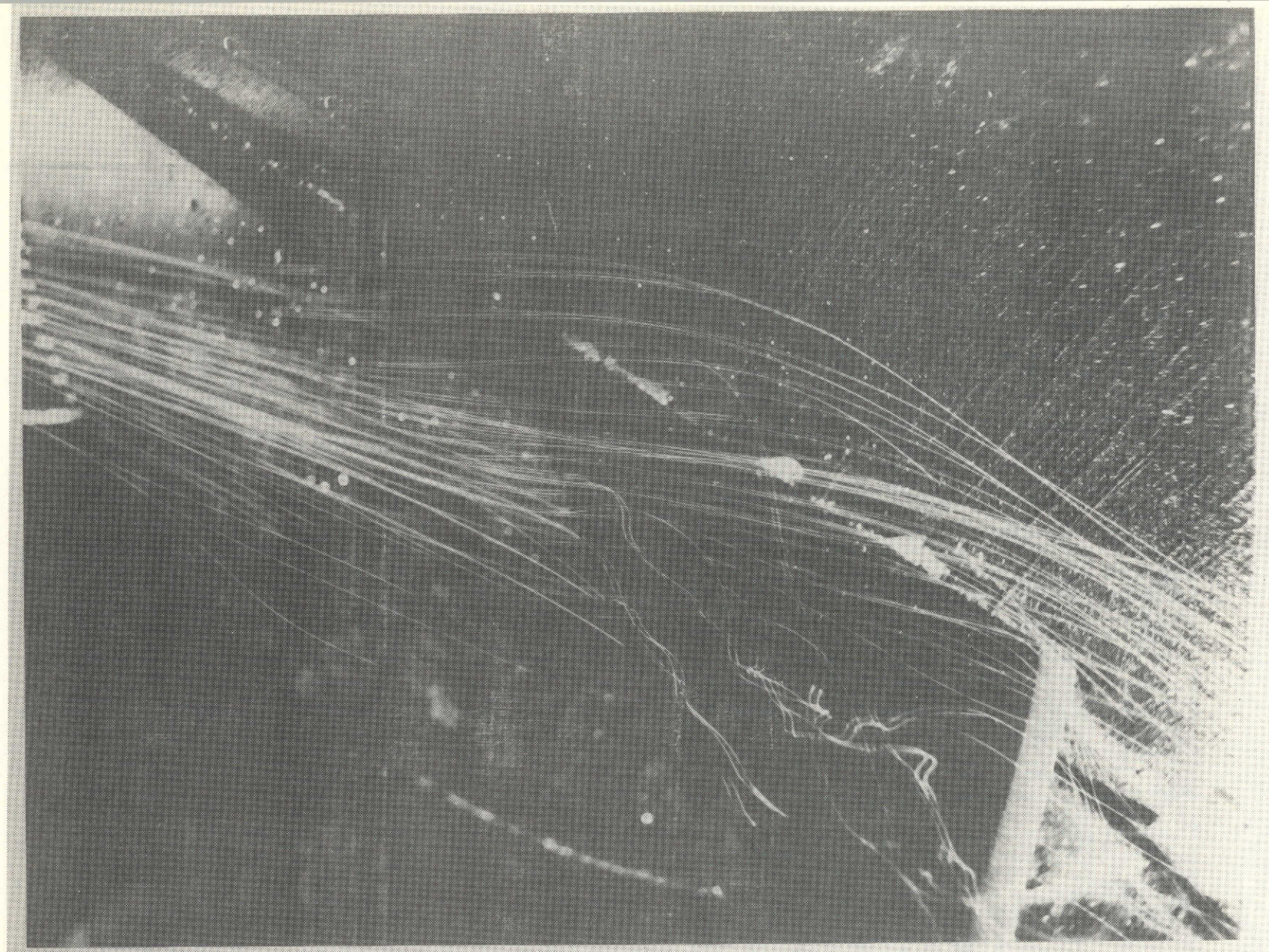

Figure 90. Strake-wing at an angle of attack of 20^{o}.

Figure 91. Strake-wing at an angle of attack of 25^{0}.

Figure 92. Strake-wing at an angle of attack of 25^{0}.

Figure 93. Strake-wing at an angle of attack of 25^{0}.

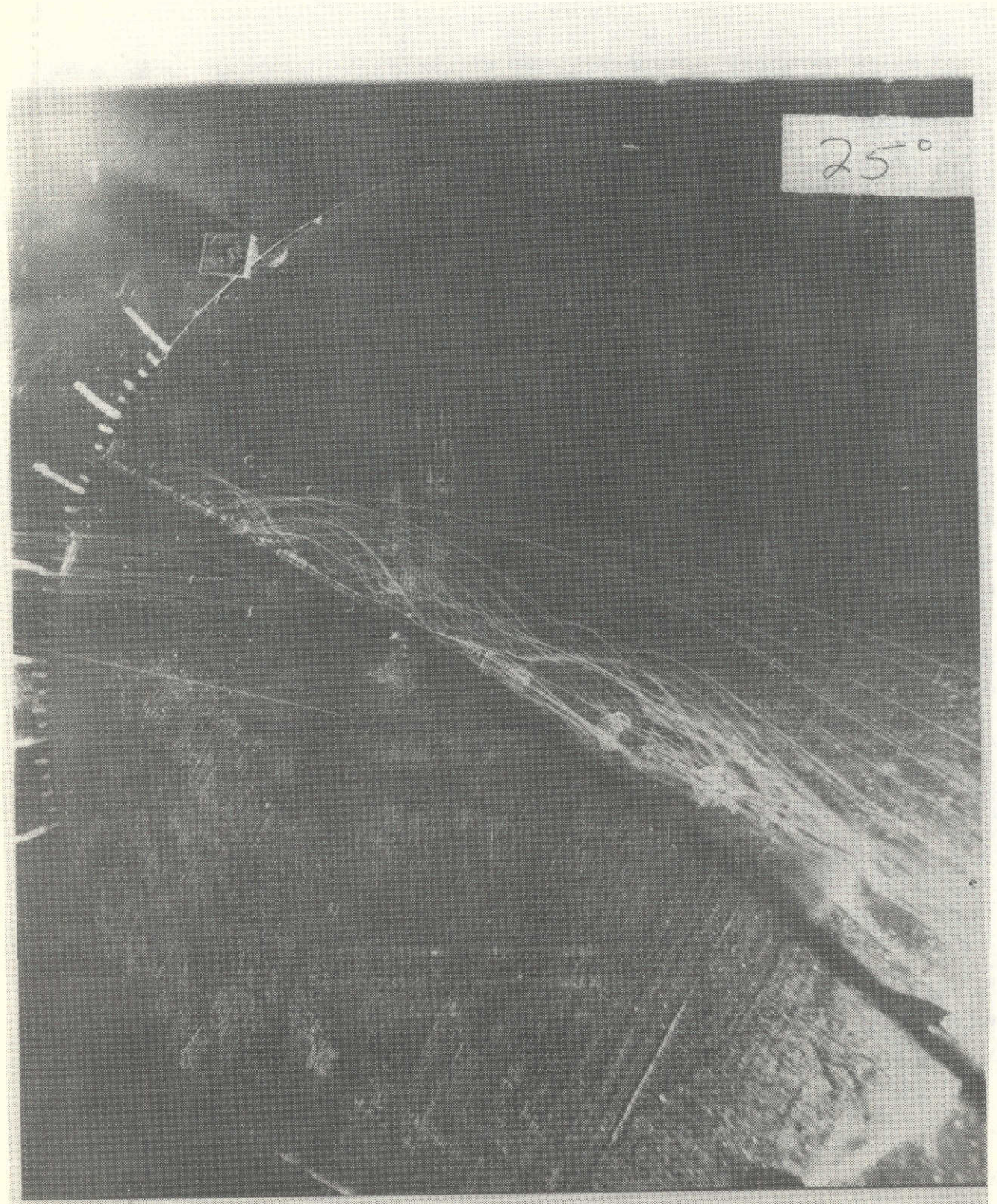

Figure 94. Side view of the strake vortex at an angle of attack of 25^{o}.

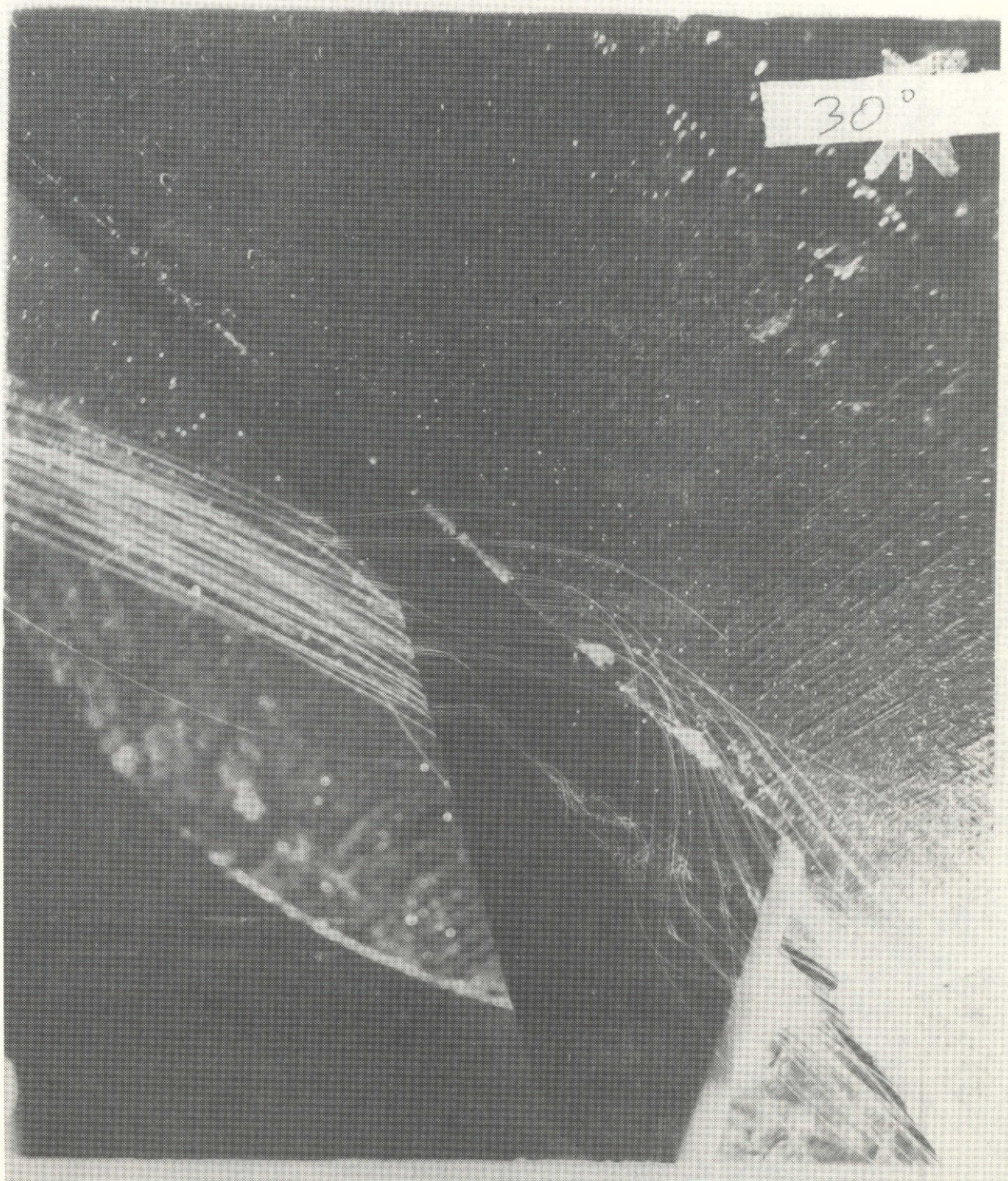

Figure 95. Strake-wing at an angle of attack of 30^{0}.

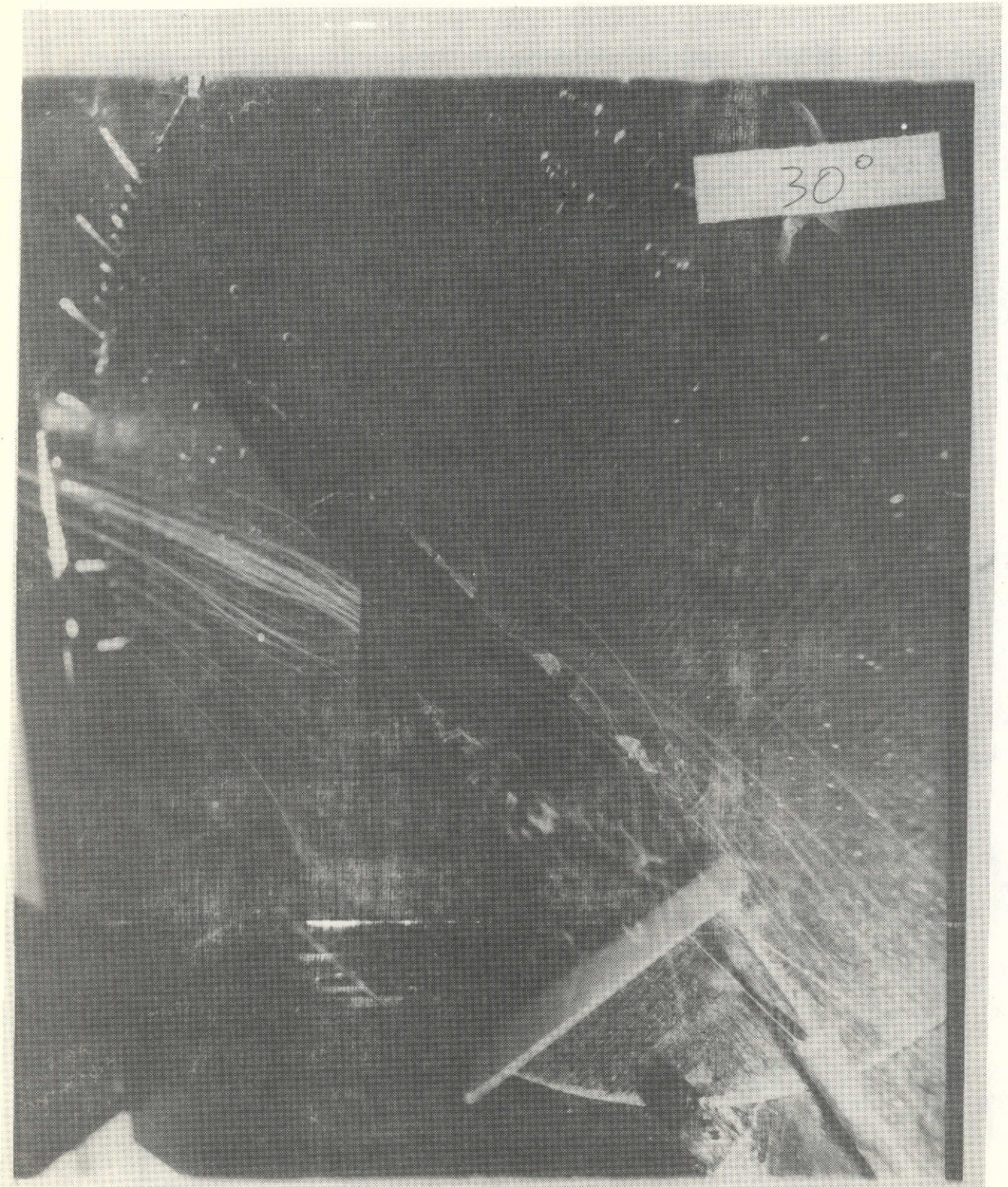

Figure 96. Strake-wing at an angle of attack of 30^{o}.

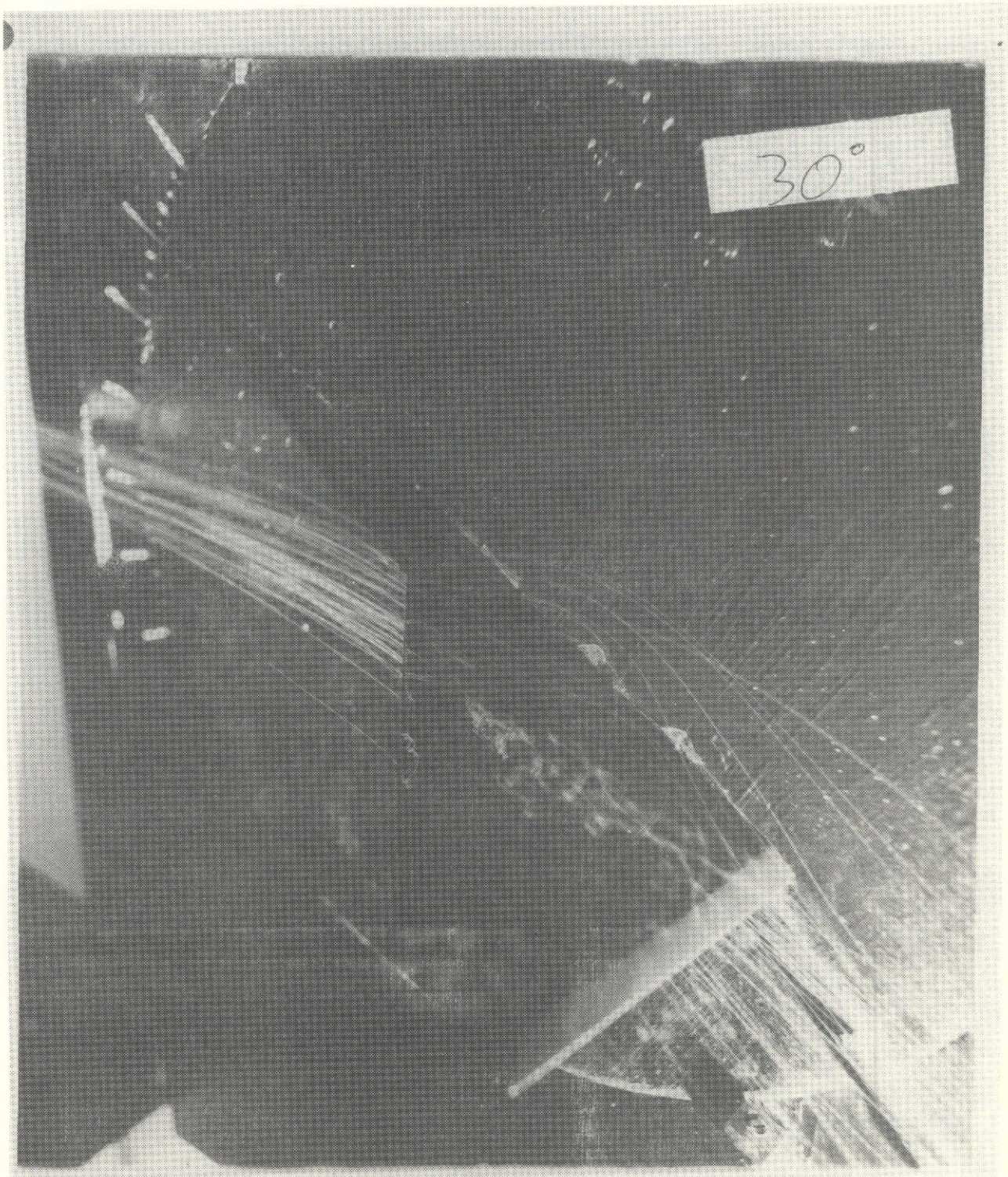

Figure 97. Strake-wing at an angle of attack of 30^{0}.

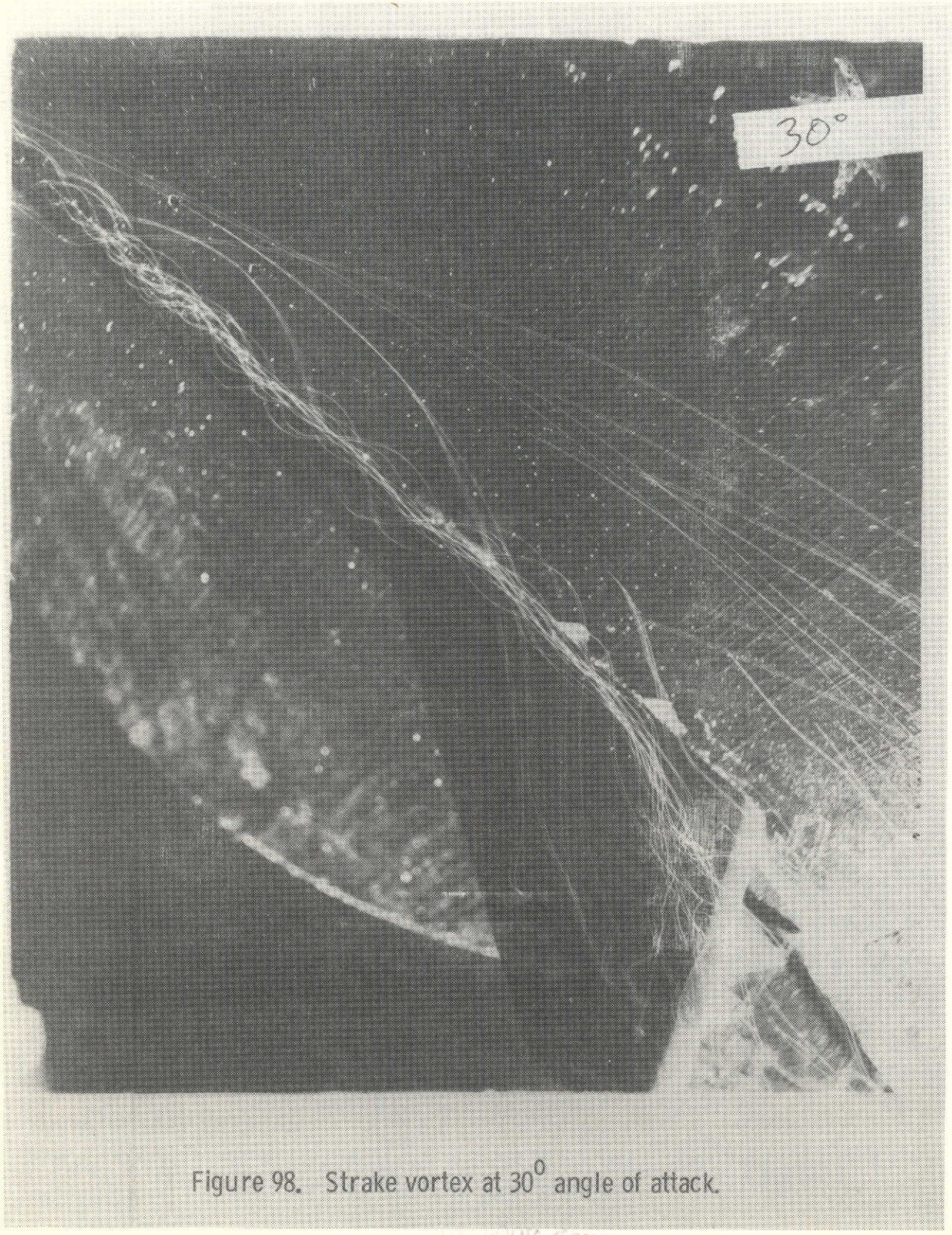

Figure 98. Strake vortex at 30^{0} angle of attack.

Figure 99. Side view of the strake vortex at 30^{0} angle of attack.

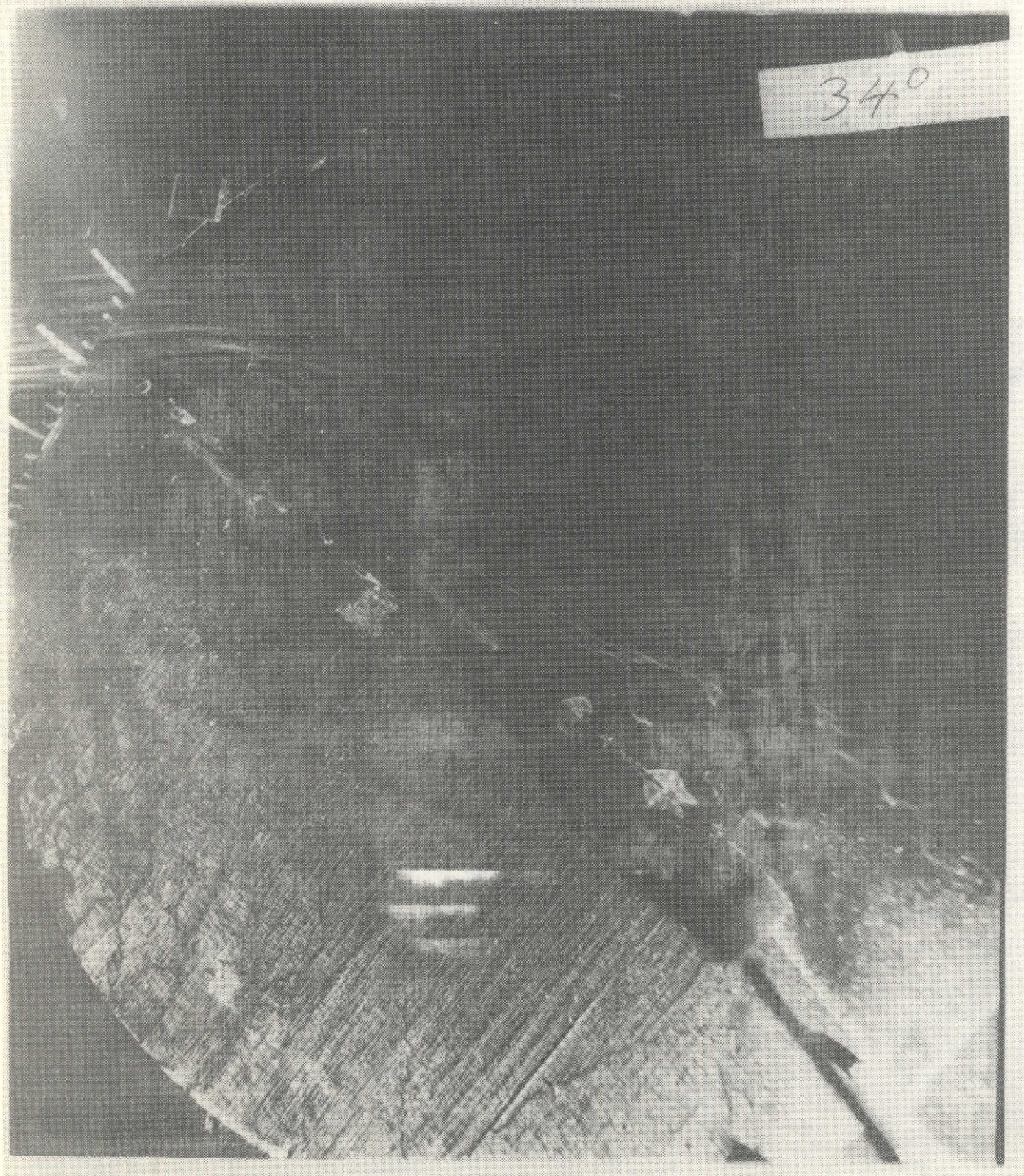

Figure 100. Side view of the strake vortex at 34° angle of attack.

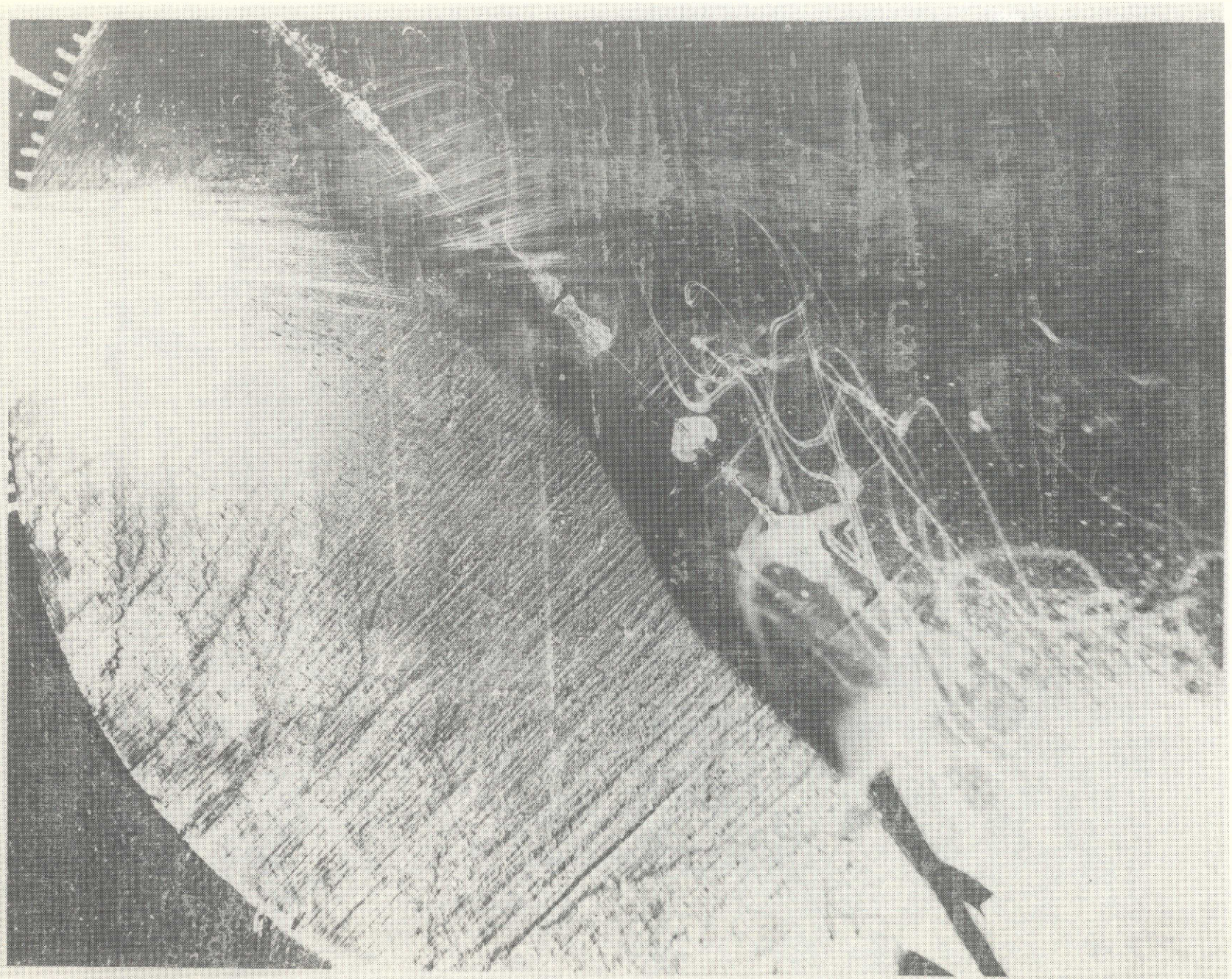

Figure 101. Strake-wing at an angle of attack of 40^{0}.

Figure 102. Side view of the strake vortex at 40^{o} angle of attack.